# Effects of α/β/γ-Synuclein overexpression on the mitochondria and viability of neurons, examined using genetically encoded fluorescent sensors

Dissertation

for the award of the degree

*Doctor of Philosophy (Ph.D.)*

Faculty of Biology

Georg-August-Universität Göttingen

submitted by

Johan Tolö

born in

Gothenburg, Sweden

Göttingen 2013

Reviewer: Dr. Sebastian Kügler
Dept. of Neurology, University Medical Center Göttingen

Reviewer: P.D. Dr. Mironov
Dept. Neuro- and Sensory Physiology, University Medical Center Göttingen

Prof. Dr. Tobias Moser
Department of Otolaryngology, University Medical Center Göttingen

Date of the oral examination: January 27, 2014

## Declaration

I hereby declare that the thesis:

"Effects of α/β/γ-Synuclein overexpression on the mitochondria and viability of neurons, examined using genetically encoded fluorescent sensors"

has been written independently by me and with no other sources and aids than those quoted.

Göttingen, November 2013

Johan Tolö

# Contents

# List of Figures

# List of Tables

# 1 Introduction

## 1.1 Age-related neurodegenerative disorders

In the aging population of the western world, an increasingly common cause of disability is the degeneration of the central nervous system. Age-related neurodegenerative disease is the common term for a set of diseases that affects the elderly, that progresses with advanced age and in which a loss of function, structure or death of neurons occurs. The most common include Alzheimer's disease (AD) and Parkinson's disease (PD). In both of these diseases the causes and mechanisms are still not well understood and only in a low number of cases is there a known inherited genetic mutation behind the pathology. Nevertheless, shared themes such as protein aggregation and neuronal loss through common programmed cell death (PCD) pathways occur in both of these diseases as well as in others such as adult onset Huntington's disease (Rubinsztein, 2006; Bredesen et al., 2006). This suggests the possibility of common mechanisms that when discovered, could lead to progress in treating many if not all neurodegenerative disorders.

### 1.1.1 Parkinson's disease

#### History and symptoms

In 1817 the British physician James Parkinson published "An essay on the shaking palsey" (Parkinson, 2002) where he characterized the symptoms of Parkinson's disease (PD). In 1919 the loss of neurons in the substantia nigra pars compacta (SNpc) had been described and in 1959, the hypothesis that PD patients experience their symptoms because of a lack of dopamine. This was confirmed when trials in treating the symptoms by administration of the dopamine pre-cursor L-dopa were successful some years later (Fahn, 2008). Today, PD is recognized as the second most common neurodegenerative disorder after AD and it affects between 1 and 2% of the population over 65 years of age. The incidence increases to between

3 and 5% in people over 85 (Nuytemans et al., 2010). The common symptoms of PD include: tremors at rest, rigidity, bradykinesia and posture instability. The clinical diagnosis of PD is based on the verification of two out of these four symptoms and of the positive response to L-dopa treatment. Before or after the onset of these motor symptoms, nonmotor symptoms such as olfactory dysfunction, sleep abnormalities and depression might be observed (Jankovic, 2008; O'Sullivan et al., 2008). The average age of onset for idiopathic PD is ~70 years and it has been observed that motor symptoms start to become apparent when ~70% of dopaminergic neurons in the SNpc are degenerated. At birth, the total number of dopaminergic neurons in the SNpc is approximately 400000 and a "healthy" brain loses these at a rate of ~2400 per year (Uversky and Eliezer, 2009). That means that a person who lives to be 120 years old would acquire PD related motor symptoms from normal loss of neurons.

### Lewy bodies and Lewy neurites

Another hallmark of PD which is not required for diagnosis is the formation of intracellular inclusions called Lewy bodies (LBs) and Lewy neurites (LNs). These inclusions are present in the cell bodies and neurites of neurons throughout the brain, including surviving neurons of the SNpc (Braak et al., 2003). As the disease progresses the region of the brain with the highest concentration of inclusions changes according to the stages laid out by Braak et al. (2003). The major component of LBs and LNs is aggregated α-Synuclein (αS) (Spillantini et al., 1997).

### Causes

Most cases of PD are classified as idiopathic but genetic mutations have been found in some patients. So far, 18 genes, called PARK genes, have been linked to PD (Eschbach and Danzer, 2013). The connection to PD for some of these genes were inconclusive in follow up studies but evidence for a causal relation have been shown for at least five of the genes (Nuytemans et al., 2010). These are SNCA (PARK1), parkin (PARK2), P-TEN-induced putative kinase 1 (PINK1), leucine-rich repeat kinase 2 (LRRK2) and DJ-1 (PARK7).

SNCA is the gene coding for αS. Mutations in SNCA are rare but several point mutations and gene duplications and triplications are known to cause autosomal dominant forms of PD (Polymeropoulos et al., 1997; Nuytemans et al., 2010). Because αS is the main topic of this thesis, the known properties of αS are further described in section 1.2.

Another gene with known mutations that cause autosomal dominant PD is LRRK2. It codes for the very large (2527 amino acid (aa)) protein lrrk2. LRRK2 was the second gene with a causal relationship with PD to be discovered after that of SNCA. Multiple mutations in LRRK2 have been associated with PD with G2019S being the most common (Singleton et al., 2013). Loss of dopaminergic neurons in the SNpc as well as the appearance of LBs are common features in the pathology associated with LRRK2 mutations (Singleton et al., 2013). The lrrk2 protein is expressed in various brain regions including cortex, cerebellum and hippocampus (Mandemakers et al., 2012) and in many other tissues although at lower levels (Paisán-Ruíz et al., 2004). The transcript has 51 exons containing several different functional protein domains suggesting both GTPase and kinase activity as well as protein protein interactions (Nuytemans et al., 2010; Singleton et al., 2013). Physiological function and pathological mechanisms of LRRK2 are still mostly unknown.

Homozygous or compound heterozygous mutations in the parkin gene causes up to half of the known familial PD cases with recessive inheritance and early onset. Early onset is a typical feature in patients with mutations in parkin as well as good response to treatment with L-dopa and otherwise benign disease development. Parkin disease causing mutations are usually not associated with the appearance of LB however, suggesting a different mechanism or action at a later point in the pathway of pathology compared to classical PD (Singleton et al., 2013). The Parkin gene codes for parkin, a 456 aa large protein with four major functional domains. These corresponds to parkins role as a E3 ubiquitin ligase (Shimura et al., 2000). It has been demonstrated that parkins role in the ubiquitin proteasome system (UPS) is that of targeting no longer functional or excessive proteins for proteasome degradation.

Homozygous mutations associated with early-onset PD have also been found in the PINK1 gene. Mutations in PINK1 are so far rarer than parkin mutations (Puschmann, 2013). The gene consists of eight exons and encodes a 581 aa protein. It is ubiquitously expressed in tissues (Unoki and Y Nakamura, 2001).

Another gene that is found with mutations in very rare cases of recessive PD is DJ-1. Most patients with mutations in DJ-1 have early-onset PD (Puschmann, 2013). DJ-1 has been demonstrated as acting as an antioxidant (Mitsumoto and Nakagawa, 2001) in response to oxidative stress and has been shown to readily oxidize in cultured cells (Canet-Aviles et al., 2004).

In the beginning of the 1980s, it was discovered that drug users from Northern California had developed an acute state of akinesia. The drug they had injected was 1-methyl-4-phenyl-4-propionoxypiperidine (MPPP), an analog of the synthetic opioid meperidine. It

was eventually recognized that the preparation of MPPP was contaminated by 1-methyl-4-phenyl-1,2,3,6-tetrahydropyridine (MPTP), which had been inadvertently produced during the clandestine manufacture (Langston et al., 1983). MPTP has since been used in a variety of mammalian species to model PD (Bove et al., 2005). The symptoms produced by MPTP in humans correspond to those of PD. This includes tremors at rest, rigidity, bradykinesia and posture instability (Bove et al., 2005). However, LBs does not appear in MPTP induced parkinsonism (Forno et al., 1993). After administration, MPTP crosses the blood brain barrier. In the brain, it is metabolized by monoamine oxidase (MAO) by non-dopaminergic cells to 1-methyl-4-phenyl-2,3-dihydropyridinium ($MPDP^+$) and then further to the toxic species 1-methyl-4-phenylpyridinium ($MPP^+$) through spontaneous oxidation. $MPP^+$ is then released into the extracellular space through an unknown mechanism (Przedborski and Vila, 2001). Due to its strong polarity $MPP^+$ can not freely cross the plasma membrane. However, $MPP^+$ shows high affinity for the dopamine active transporter (DAT) located in the plasma membrane of dopaminergic neurons (Mayer et al., 1986). Inside dopaminergic neurons, $MPP^+$ can either stay within the cytosol, enter synaptic vesicles through vesicular monoamine transporter (VMAT) transport (Y Liu et al., 1992) or concentrate within mitochondria (Ramsay and Singer, 1986). Neurons transfected to overexpress VMAT become $MPP^+$ toxicity resistant (Y Liu et al., 1992) and conversely, mutant mice with lower expression are more sensitive to MPTP induced toxicity (N Takahashi et al., 1997), suggesting toxicity from MPTP to occur when it remains in the cytosol or is taken up by the mitochondria. In the mitochondria, $MPP^+$ will inhibit complex I of the electron transport chain (ETC) at or near the same binding site as another inhibitor, rotenone (Przedborski and Vila, 2001).

Rotenone, commonly used as a pesticide, is another complex I inhibitor which is routinely used as a mitochondrial poison in cell culture and *in vivo* research (Bove et al., 2005). Rotenone rapidly breaks down by exposure to sunlight and in soil and water and has a half-life of about 1-3 days (Hisata, 2001). Thus it seems unlikely for environmental exposure to rotenone from its use as a pesticide to be a major cause of PD. However, systemic administration of rotenone in rats and mice have been used as a model for PD. Stereotaxic injection of rotenone into the median forebrain bundle of rats depletes both striatal dopamine and serotonin (Heikkila et al., 1985) and rotenone causes dopaminergic cell loss in rats treated with rotenone by intravenous infusion (Bove et al., 2005). Rotenone administered this way has also been shown to cause proteinaceous inclusions that stain positive for αS in some of the remaining substantia nigra dopaminergic neurons (Sherer et al., 2003). Behavioral symptoms also match those of PD, such as reduced mobility. This has however been reported for rats without nigrostriatal dopaminergic lesion as well, thus it is not clear that they occur because of nigrostriatal dam-

age, casting doubt on the validity of rotenone as a model for PD in these experiments (Bove et al., 2005).

Evidence suggests that the common pathway for the toxicity or pathological mechanism behind all of these causes for PD involves the mitochondria. What is known about the role that mitochondria plays in the generation of PD is summarized in section 1.3.

## 1.2 The synuclein family of proteins

### 1.2.1 History, identification and classification

The first isolation and characterization of a synuclein protein was done by Maroteaux et al. (1988). They used antiserum raised against purified cholinergic synaptic vesicles from the pacific electric ray (*Torpedo californica*) to identify a 143 aa protein. They found this protein to localize both to presynaptic nerve terminals and to a portion of the nuclear envelope. Because of this they named the protein synuclein (SY-NUCLEin). Later examinations of the composition of amyloid-beta (Aβ) plaques from AD patients found a peptide that was unrelated to Aβ and hence got the name non-Aβ component (NAC). Later studies have questioned whether NAC is actually a part of Aβ plaques (Culvenor et al., 1999) but the precursor for this peptide, NAC protein (NACP), was found to be homologous with rat α-Synuclein (αS) (Uéda et al., 1993). NACP is therefor referred to as human αS. A little later, another synuclein protein, initially described as a 14 kDa phosphoneuroprotein, was identified in cattle (Nakajo et al., 1990). This protein was also found to have a human ortholog, distinct in structure from NACP. NACP and this protein are since referred to as human αS and β-Synuclein (βS) respectively (Jakes et al., 1994). Since then, a third member of the human synuclein protein family has been identified. It was first characterized from human breast carcinoma as the expression product of the BCSG1 gene (Ji et al., 1997). Shortly thereafter this protein was identified as being highly homologous to human αS and was named ɣ-Synuclein (γS) (Lavedan et al., 1998). As it turned out, the synuclein originally isolated from *Torpedo californica* is actually most closely related to γS (Lavedan, 1998).

Synucleins have since been identified in other organisms but so far only in vertebrates (George, 2002; Surguchov, 2013). Synelfin is the αS ortholog in the Atlantic Canary (*Serinus canaria*) and PNP14, the phosphoneuroprotein mentioned above, is the βS ortholog in Cattle (*Bos taurus*). All characterized synuclein proteins so far can be assigned to one of

the three protein groups, αS, βS or γS (Lavedan, 1998; Surguchov, 2013). The human genes coding for these proteins are called SNCA, SNCB and SNCG for αS, βS and γS respectively.

### 1.2.2 Structure, conformation and interactions

All three members of the synuclein family of proteins, α-, β- and γS, are small ~127-140 aa proteins. The N-terminal region is highly conserved both between species and between the different members of the synuclein family. The C-terminal region contains many highly charged and acidic residues and shows high variability between the different family members. Another common feature of all characterized synucleins is their complete lack of cysteine and tryptophan residues.

The aa sequence of αS comprises 140 residues and it can be divided into three regions. Residues 1-60 contains four repeats of 11-aa with a KTKEGV consensus sequence. Residues 61-95 contains the hydrophobic NAC region plus another two repeats. Residues 96-140 contains a highly charged acidic region with low sequence similarity to β- and γS (George, 2002; Uversky and Eliezer, 2009).

Early attempts at characterizing the structure of αS found it to lack secondary structure but to have an elongated shape. It was also found that its structure did not change in response to treatments such as different concentrations, boiling, changes in pH, salt and other chemical denaturants and it was suggested that the conformation of αS is unfolded in solution (Weinreb et al., 1996). Later studies confirmed αS to be mostly disordered. However, it was found to be more compact than that predicted of a completely random coil, suggesting the possibility for conformational changes and placing it in the class of proteins called natively unfolded proteins (Uversky et al., 2001). Assuming that the unfolded conformation of αS is due to its low hydrophobicity and high net charge, changes in these two environmental factors could induce structure in the protein. This was confirmed by Uversky et al. (2001) in experiments were they neutralized the charge by lowering the pH and increasing the hydrophobicity by increasing the temperature. Both of these factors were found to introduce secondary structure to αS and make it more compact suggesting the folding into β-structure. The structure introduced was reversed by going back to physiological pH and temperature (Uversky et al., 2001).

The A30P, E46K and A53T mutations have also been studied for their impact on the structure of αS. Very small to no differences compared to the wild type (WT) protein in terms of the unfolded structure have been observed (J Li et al., 2001; Fredenburg et al., 2007). The A30P

mutant however, as can be expected from the steric hindrance introduced by proline, reduces the propensity for α-helical structure (Bussell and Eliezer, 2001).

That parts of αS can assume α-helical structure was observed in studies of membrane affinity. The binding to synthetic vesicles containing negatively charged acidic phospholipids produced large conformational changes and the formation of two bent antiparallel α-helices (Davidson et al., 1998; Chandra et al., 2003). These changes were localized to the N-terminal region with repeated aa sequence whereas the acidic C-terminal region remained unstructured (Jao et al., 2004). The helical structure induced by membrane binding has been shown to be dependent on lipid particle size (Borbat et al., 2006) and in the most extreme case a single linear α-helical conformation of the N-terminal region have been described (Jao et al., 2004; Georgieva et al., 2008).

The periodicity demonstrated by the stretches of 11-aa repeats in the N-terminal region of αS is characteristic of another group of proteins namely the apolipoproteins. These proteins have the same 11-aa repeat periodicity in their amphipathic lipid binding α-helical domains. The rules that have been developed for determining the secondary structure of apolipoproteins predict four consecutive class A2 helices in αS. In apolipoproteins this helix class mediates exchangeable lipid binding, suggesting that membrane binding is a physiological property of αS. αS have in comparison to apolipoproteins a highly conserved sequence that might indicate conserved specificity for a particular type of membrane (Clayton and George, 1998).

In general, the structure of αS seems to be able to take on many different conformations and be sensitive to modification by many different kind of factors. Metal ions, salts, pesticides and simple and fluorinated alcohols are some of the stimuli that has been shown to confer changes in conformation to αS and it can also undergo spontaneous oligomerization (Uversky and Eliezer, 2009).

Recently the notion that αS exists as a natively unfolded protein in solution has been challenged. Instead, a conformation as a helically folded soluble tetramer that resist aggregation has been suggested (Bartels et al., 2011; W Wang et al., 2011). This has proven controversial however and other groups have published data showing αS to exist predominantly as a unfolded monomer (Fauvet et al., 2012).

### 1.2.3 Physiological function

The physiological function(s) of αS is so far not well understood. Nevertheless, several ideas have been put forth based on findings made during the last ~20 years of αS research. Since αS was initially described as a presynaptic protein (Maroteaux et al., 1988), its function has often been assumed to be involved in synaptic vesicle handling. However, αS is not only found in the brain and a large fraction of it is located throughout the cytosol and not only at the synapse, suggesting a broader role. αS has been reported to make up as much as 0.5-1% of cytosolic protein in the brain (Iwai et al., 1995). This figure was different for different areas, with cortex, hippocampus and striatum reported as having the highest levels of αS.

In support of the idea that αS plays a role in synaptic regulation is the property of αS to bind and interact with membranes. In the presence of membranes with acidic phospholipids, the N-terminal domain of αS undergoes conformational changes and folds into a α-helical structure (Davidson et al., 1998; Chandra et al., 2003). This seemed to go well in hand with the finding that αS could inhibit phospholipases, something which was suggested to play a role in synaptic vesicle cycling (Jenco et al., 1998). Later studies were unable to find a direct role of αS in inhibiting phospholipases however, casting doubt on this function for αS (Rappley et al., 2009). Nevertheless, other studies have found other interactions of αS with synaptic vesicle handling. Experiments on αS knock out (KO) mice, demonstrated that these mice have enhanced dopamine release at nigrostriatal terminals as well as reduced total dopamine content compared to WT mice, the effects were small however (Abeliovich et al., 2000). Other experiments using antisense oligonucleotides to deplete αS led to reduced synaptic vesicle pool at the presynapse as observed in electron micrographs (Murphy et al., 2000). Cysteine string protein α (CSPα) is another synaptic protein with largely unknown function. A connection to αS was made with the observation that the rapidly neurodegenerative phenotype of CSPα KO mice was rescued by αS overexpression (Chandra et al., 2005). Chandra et al. (2005) also showed that deletion of CSPα inhibits soluble N-ethylmaleimide sensitive fusion protein (NSF) attachment protein (SNAP) receptor (SNARE) complex assembly. In another paper they later examined the effects of αS on the SNARE complex and found that αS too was required for proper maintenance and assembly. Removal of 44 residues from the C-terminal of αS abolished this ability. This suggests that αS and CSPα have complementary or redundant roles in the assembly of the SNARE complex. The ability of αS to rescue the phenotype of CSPα KO mice has since been observed by another group who also found that γS lacks this ability (Ninkina et al., 2012). More recently, overexpression of αS was shown to inhibit neurotransmitter release through a reduction in size of the synaptic vesicle pool due to inhibition

of synaptic vesicle reclustering after endocytosis (Nemani et al., 2010). Strangely enough, this effect of αS was not dependent on the C-terminal part of the protein, suggesting a different mechanism to that of SNARE complex assembly. It did require the full α-helix forming ability however, as evident by the lack of inhibition of synaptic transmission from the A30P mutant. It seems reasonable to assume that αS plays a role in some type of vesicle regulation considering these reports and its established ability to associate with membranes.

George et al. (1995) observed changes in the expression of ribonucleic acid (RNA) for αS during song learning in the Zebra finch songbird. Based on their findings, they suggested that αS is involved in vertebrate neural plasticity.

αS has been shown to interact with other proteins. Synphilin-1, a protein with unknown function, was initially described after it was found to interact with αS in a yeast two-hybrid screen (Engelender et al., 1999).
The 14–3-3 protein family shares some sequence homology with synucleins and has been suggested to interact with αS (Ostrerova et al., 1999). 14–3-3 proteins are cytoplasmic chaperones with known interactions with Bcl-2-associated death promoter (BAD) and Bcl-2-associated X protein (BAX), proteins involved in the regulation of apoptosis (Datta et al., 2000; Lim et al., 2013) and this suggests a possible connection between αS and PCD.

αS has been demonstrated to be able to be phosphorylated at residues S87, S129, Y125, Y133 and Y136 (Okochi et al., 2000; Pronin et al., 2000; Negro et al., 2001; Fujiwara et al., 2002). Phosphorylation of αS in normal brain tissue occurs at low levels and has only been demonstrated at S87, S129 and Y125. In LBs, αS is found to be hyperphosphorylated at S129 (Fujiwara et al., 2002; Anderson et al., 2006). Regulation occurs by polo-like kinases (PLKs) *in vivo* and possibly casein kinase 1 (CK-1), casein kinase 2 (CK-2) and G protein-coupled receptor (GPCR) kinases (GRKs) (Braithwaite et al., 2012). Interestingly, the N-terminal region is essential for phosphorylation of S129 by PLKs and only PLK2 is able to phosphorylate βS (Mbefo et al., 2010). None of the PLKs are able to phosphorylate γS. The residue most often found to be phosphorylated *in vivo*, S129, is located in the C-terminal region of αS. It would therefor not be expected to interfere with membrane binding and this has been confirmed for the WT form of αS (Visanji et al., 2011). However, both the A30P and A53T mutants showed increased membrane association upon phosphorylation.

### 1.2.4 Relation to Parkinson's disease

#### α-Synuclein

LBs are, as mentioned above, a hallmark in brains of PD patients and these intracellular protein aggregates consist to a major extent of αS (Spillantini et al., 1997). Also, several point mutations as well as duplications and triplications in SNCA have been found in patients with PD.

In 1996 a point mutation, A53T was found in members of a large Italian-American family (Golbe et al., 1996) as well as in three families from Greece (Polymeropoulos et al., 1997). These patients show similar symptoms to patients with idiopathic PD except for lower prevalence of tremors. Average age of onset is lower at ~46 years of age but the progression is not generally faster (Polymeropoulos et al., 1997; Papapetropoulos et al., 2003).

A year after that, another point mutation, A30P was described in a German family (Krüger et al., 1998). Age of onset ~54 years and fast progression with bradykinesia and rigidity were reported for mutation carrying members of this family. Recently, the first brain of a diseased patient carrying the A30P mutation have been studied. Neuronal loss in the substantia nigra, locus coeruleus and dorsal motor vagal nucleus as well as occurrences of αS immunopositive LBs, LNs and glial aggregates throughout the brain was observed. In general, the neuropathology was more severe than in a typical brain from a patient with idiopathic PD (Seidel et al., 2010).

Later, in 2004, a E46K mutation was found among members of a large family from the Basque region in northern Spain (Zarranz et al., 2004). These patients have shifting impairment of frontal lobe function, memory dysfunction, tremors, bradykinesia and postural abnormalities. Average age of onset is reported as ~60 years of age. Later they develop severe dementia. Analysis of brains for diseased patients carrying the E46K mutation revealed neuronal loss in the substantia nigra and numerous cortical and subcortical LBs that stained positive for αS (Somme et al., 2011).

In 2003, triplications of the SNCA genomic locus was reported for the first time (Singleton et al., 2003) and one year later duplications (Chartier-Harlin et al., 2004; Ibáñez et al., 2004). The patients with a triplication had symptoms ranging from those typical of PD to typical dementia with Lewy bodies (DLB) and a very early average age of onset at ~34 years. Analysis of brains from diseased patients revealed profound pathology and extensive LBs (Singleton et al., 2003). The patients with duplications, had symptoms more closely resembling those of

idiopathic PD and an average age of onset of ~50 years. Because of this, a relation between disease onset and severity of progression and gene dosage has been suggested (Chartier-Harlin et al., 2004; Ibáñez et al., 2004).

### β- and γ-Synuclein

In contrast to αS, no genetic connection between βS or γS and PD has been described so far. And neither βS nor γS is detectable in LBs or LNs. Wild type βS has been shown to act as a scavenger for αS aggregation and neurotoxicity in a variety of experimental systems *in vitro* and *in vivo* (Hashimoto et al., 2001; Uversky et al., 2002; Hashimoto et al., 2004; Fan et al., 2006). Since both βS and γS are present in axonal lesions in the hippocampus in PD and in DLB (Galvin et al., 1999), their possible contribution to neurodegenerative disease should not be ignored. Also, the DLB-linked mutation P123H in SNCB, the gene coding for βS, have been demonstrated to produce progressive neurodegenerative symptoms such as axonal swelling, astrogliosis and behavioral abnormalities in transgenic (TG) mice. And when these mice were cross-bred with αS TG, but not αS KO mice, these symptoms were aggravated (Fujita et al., 2010). Thus it seems likely that βS can play a role in the pathogenesis of neurodegenerative disease. In fact, in a recent publication by our group (Taschenberger et al., 2013), we demonstrate that βS is neurotoxic for primary neuronal culture and produces aggregates as well as neuronal degeneration in rats *in vivo*.

### Pathological mechanism

The pathological mechanism that leads to the development of symptoms in PD is, just like the physiological function of αS so far not well understood. Due to the presence of αS in LBs and LNs, it has been extensively studied as an agent in the pathology of the disease. Since the αS found in LBs is of a fibrillar form, major focus of these studies has been on the properties of its aggregation. In general, aggregation is thought to occur when hydrophobic patches present themselves during folding of a protein. These patches would prefer other such patches because of the hydrophobic effect and thus lead to dimeric, oligomeric and larger aggregates that eventually become insoluble (Fink, 1998). This predicts that conditions or interacting agents that favors a partially folded intermediate state where the patches are present, also favors aggregation. Since αS is most probably a natively unfolded protein in solution, it is highly influenced by its environment and the range of conditions that favors such aggregation prone intermediate states should be wide (Uversky and Eliezer, 2009). This

model fits with *in vitro* examinations of fibril formation in αS where conditions such as agitation, increased concentration and certain anions and cations among other factors are able to accelerate the fibril formation (Uversky and Eliezer, 2009). An increase in concentration would increase the probability for the partially folded state and the probability for interaction with another protein in such a state. This fits with the dose relationship of αS and the severity of PD seen with gene duplications and triplications (Polymeropoulos et al., 1997; Nuytemans et al., 2010).

Several findings already mentioned point to aggregation being important in the pathology of PD. Early onset PD is caused by higher expression of αS due to duplication or triplication of the gene, the familial point mutations increase the propensity for aggregation (Fink, 1998) and αS is present in aggregated form within LBs. The aggregation of αS follows a sigmoidal curve with an initial lag phase which is followed by exponential growth and finally a plateau. During the lag phase, transient soluble oligomeric forms of αS forms (Fink, 2006) and it is some set of these, called protofibrils, that are proposed to be the neurotoxic species (Stefanis, 2012) and there is some experimental support for this idea. The A53T and A30P mutants form more protofibrils and at a faster rate than WT *in vitro* (Conway et al., 2000). And experiments with artificial mutants that favors the formation of soluble oligomers over fibrils in neuronal cell culture and invertebrate models showed higher toxicity for these mutants compared to WT (Karpinar et al., 2009; Winner et al., 2011). What exact specie of oligomer is toxic and whether monomeric αS can become toxic without aggregation through some gain-of-function is still under debate however. It also seems likely that over time, the presence of large intracellular aggregates, especially in neurites where they might block trafficking, would be detrimental to the normal functioning of the cell as well.

Some studies have been made on the interaction of αS with the cytoskeleton and possible effects on trafficking within cells. It has been demonstrated that αS negatively influences tubulin polymerization (Lee et al., 2006; L Chen et al., 2007; Zhou et al., 2010). And genome-wide association studies (GWASs) have linked both tau and αS as major risk factors for developing PD (Nalls et al., 2011). Phosphorylation of tau has been demonstrated to be facilitated by αS (Jensen et al., 1999; Haggerty et al., 2011) and tau and αS can seed the aggregation of each other (Giasson et al., 2003).

In section 1.2.3 a possible function for αS in the regulation of the synapse was described. It is also possible that these functions are active in causing disease symptoms. The inhibition of synaptic vesicle recycling shown by Nemani et al. (2010) or changes in the levels of several critical presynaptic proteins which precedes neuronal degeneration in rats overexpressing

αS demonstrated by (Chung et al., 2009) could both be explanations for decreased synaptic transmission and the symptoms associated with PD. However, they are not explanations for the aggregation or destruction of neurons and might therefor contribute to disease in its early stages but is unlikely to be the major toxic mechanisms.

In solution, evidence suggest that αS is a natively unfolded protein. However, as was discussed in section 1.2.2, αS acquires secondary structure upon association with membranes. Together with the idea that it is a oligomeric, "protofibril" (page 12) conformation of αS and not mature fibrils that are toxic and the fact that these protofibrils take on pore like appearance in atomic force microscopy (AFM) and electron microscopy (EM) images (Ding et al., 2002; Lashuel et al., 2002) that resemble the structures of pore forming bacterial toxins (Wallace et al., 2000), led researchers to examine the effect of these oligomers on membranes. Several groups have observed membrane permeability due to these oligomers. Early on, permeability was observed *in vitro* by the leakage of fluorescent dyes from vesicles formed from different phospholipids after the addition of αS oligomers (Volles et al., 2001; Volles and Lansbury, 2002). Later, permeability was also demonstrated in intact cells using both electrophysiology and fluorescent techniques (Furukawa et al., 2006; Tsigelny et al., 2012). Most groups report that the A53T and A30P mutants both produce similar membrane permeability but greater than WT αS (Volles and Lansbury, 2002; Furukawa et al., 2006).

A consequence of membrane permeability would be increased ion conductance and this has been demonstrated both in phospholipid vesicles (Volles et al., 2001) and in intact cells (Furukawa et al., 2006). Calcium would be one ion that might pass through such pores and this could have detrimental effects if it means that calcium homeostasis is affected. Not only is calcium influx important in the release of synaptic vesicles but prolonged elevated calcium levels within cells can cause apoptosis (Weiss, 2011). Elevated calcium levels have been observed in cell lines overexpressing αS as well as in cell lines that are exposed to preformed oligomeric αS. Furukawa et al. (2006) found increased basal $Ca^{2+}$ levels and increased levels after high potassium depolarization for the A53T mutant and to a lesser degree the A30P mutant in SH-SY5Y cells. In the same cell line, Hettiarachchi et al. (2009) confirmed the effect of increased peak calcium from high potassium depolarization but found the opposite situation in regards to the mutant A53T which they found was significantly less affected than WT. They also show the increased calcium uptake to be inhibited by blocking L-type voltage-dependent $Ca^{2+}$ channels. This suggests a different effect on calcium uptake by αS, one that is mediated by $Ca^{2+}$ channels and not directly due to influx of $Ca^{2+}$ through αS pores. A third study found elevated cytosolic calcium levels upon extracellular addition of prefibrillar

oligomeric αS to both SH-SY5Y and primary cortical neurons. The response was as fast and with similar amplitude as when they added ionomycin, a known ionophore (Danzer et al., 2007).

In addition to its localization in the cytosol and at the synapses, a portion of the αS is present also at the mitochondria, as evident in EM images with immunogold stained αS as well as in western blots from purified mitochondria (Perez et al., 2002; Martin et al., 2006; Devi et al., 2008; K Nakamura et al., 2008; G Liu et al., 2009; Loeb et al., 2010). The distribution of αS in mitochondria seem to be different depending on brain region with higher levels present in mitochondria from striatum (G Liu et al., 2009). αS can associate with the outside of the outer mitochondrial membrane (OMM) but has also been found to be present both in the intermembrane space and the matrix. This localization seems to be variable however, with αS found in the intermembrane space in mice and HEK293 cells (WW Li et al., 2007; Parihar et al., 2008) and in both the intermembrane space and matrix in human and rat neurons and SH-SY5Y cells (WW Li et al., 2007; Parihar et al., 2008; G Liu et al., 2009). Devi et al. (2008) found that uptake of αS into purified mitochondria was energy dependent and could be blocked by antibodies (ABs) against the mitochondrial import channel.

MPTP is a potent complex I inhibitor and is used in PD research for its ability to induce parkinsonian symptoms and dopaminergic cell loss. Studies have found the dopaminergic cell loss from MPTP administration to be reduced in αS KO animals (Dauer et al., 2002; Robertson et al., 2004; Klivenyi et al., 2006), suggesting the interaction of αS with MPTP. Conflicting reports are available for the opposite case, increased presence of αS however. Some reports suggest no increase in toxicity (Rathke-Hartlieb et al., 2001; Dong et al., 2002) or even protective effect (Pérez-Sánchez et al., 2010), while others suggest increased toxicity (Song et al., 2004; Nieto et al., 2006; Yu et al., 2008). Qian et al. (2008) found that αS WT was protective against MPTP toxicity in PC12 cells but that the A30P and A53T mutants both increased the toxicity. It might be that αS is protective by preventing MPTP from binding to complex I but that the mutant forms and possibly higher levels of the WT protein eventually acquires the same inhibitory effect as MPTP itself. In fact, αS was found to impair complex I activity (Devi et al., 2008; G Liu et al., 2009; Chinta et al., 2010) and increase reactive oxygen species (ROS) levels (Hsu et al., 2000; Junn and Mouradian, 2002) in several studies. Elevated ROS levels are in turn linked to apoptosis (Sinha et al., 2013).

αS also alters mitochondrial morphology. Enlarged and rounded mitochondria in αS TG mice treated with MPTP was initially described by (Song et al., 2004). Later, Martin et al. (2006) observed degenerating mitochondria in A53T TG mice. In SH-SY5Y cells transfected with

a plasmid coding for the expression of αS, which presumably produced higher expression levels than those in TG mice, αS was found to produce fragmented mitochondria (Kamp et al., 2010). K Nakamura et al. (2011) later confirmed fragmentation of mitochondria to occur also in HeLa cells and primary hippocampal rat neurons. Both groups found the fragmentation to occur independent of the mitochondrial fission protein dynamin related protein 1 (Drp1), suggesting that it is not occuring through the normal fission/fusion processes of the mitochondria but as a direct effect of αS. The effects of mitochondrial fragmentation by αS is not clear but the normal processes of mitochondrial fusion and fission is important in the regulation of PCD by the mitochondria (Westermann, 2010; Chan, 2012), suggesting another possible mechanism for how αS might contribute to toxicity.

## 1.3 Mitochondria, the common link behind Parkinson's disease

### 1.3.1 Mitochondrial dynamics

Mitochondria are dynamic structures that move and change shape in response to their environment and the needs of the cell. Their shape is regulated by the rate of fission and fusion and this is controlled by proteins of the Dynamin family with GTPase domains (Bliek et al., 2013). Drp1 is responsible for fission of mitochondria by self-assembly into spirals and association with constriction sites on mitochondrial membranes (Knott et al., 2008). The reverse, fusion, is mediated by mitofusins, of which there are two homologs in mammals, mitofusin 1 (Mfn1) and mitofusin 2 (Mfn2). A suggested mechanism for their action is binding to opposing sides of OMM and pulling them together in a SNARE like mechanism (Koshiba et al., 2004). Fusion of mitochondria serves to increase the efficiency of energy distribution throughout cells (Skulachev, 2001) and motility is necessary for redistribution along neurites in neurons (MacAskill and Kittler, 2010). Increased intracellular calcium levels and calcium uptake by the mitochondria are both associated with mitochondrial fission (Szabadkai and Duchen, 2008). For example, Drp1 has been shown to translocate to the OMM in response to elevated cytoplasmic $Ca^{2+}$ levels (Cribbs and S Strack, 2007). Regulation of fission/fusion is also important in the regulation of PCD pathways involving the mitochondria (Westermann, 2010; Chan, 2012).

Another aspect of mitochondria is their motility. In cells such as neurons, that are polarized

and have long processes, and where high energy requirements are needed in localized regions i.e. synapses, the proper movement of mitochondria can be assumed to be especially important. Most mitochondria moves along microtubules using the kinesin/dynein motor proteins (Hollenbeck and Saxton, 2005). This occurs through the Miro1 and Miro2 adapter proteins on the OMM (Reis et al., 2009). Also, mitochondrial movement is inhibited by increased calcium levels (Rintoul et al., 2003). This is facilitated through the EF-hand motifs of the miro proteins and this sequesters the mitochondria at locations of increased need for ATP (X Wang and Schwarz, 2009).

All of this indicates a complicated interplay between mitochondrial fission/fusion, movement, energy metabolism, calcium signaling and PCD.

### 1.3.2 Toxins, the mitochondria and apoptosis

Pore formation of mitochondrial membranes is important in apoptosis. When the intrinsic apoptotic pathway is activated, pro-apoptotic members of the BCL-2 class of proteins (BAX, BAK, BOK) inserts into the OMM and oligomerizes, permeabilizing the membrane (Venderova and Park, 2012). This leads to the release of cytochrome *c* from the intermembrane space. Cytochrome *c* release in turn leads to the formation of the apoptosome and activation of caspase-9 (Ott et al., 2007). Another mechanism for initiation of apoptosis in the mitochondria is that of the mitochondrial permeability transition (MPT), this causes a pore opening in the inner mitochondrial membrane (IMM) causing swelling, loss of mitochondrial membrane potential and release of cytochrome *c*, causing apoptosis (Petit et al., 1998; Büki et al., 2000).

The connection between αS and the mitochondria was established on page 14. However, αS is not the only suspected cause of PD that are linked to the mitochondria. In fact, all of the causes described in section 1.1.1 are believed to interact with some part of the mitochondria either directly or indirectly. For two of the toxins used to model PD symptoms, rotenone and MPTP the direct mode of toxicity is through inhibition of complex I of the ETC (Przedborski and Vila, 2001; Bove et al., 2005). This is also one possible mechanism behind αS toxicity (Devi et al., 2008; G Liu et al., 2009; Chinta et al., 2010). Inhibition of complex I leads to reduced ATP production, but it is elevated ROS levels that are believed to be responsible for toxicity since only a transient 20% reduction in ATP levels have been observed *in vivo* (Przedborski and Vila, 2001). Increased ROS production in the mitochondria is in turn believed to cause apoptosis but the mechanism behind it is still a matter of discussion. Oxidation/damage of

mitochondrial deoxyribonucleic acid (DNA) (Ricci et al., 2008) and oxidation of the phospholipid cardiolipin in the OMM (Ott et al., 2007) have been suggested as mediators that will lead to formation of the MPT pore and release of cytochrome *c* and subsequent formation of the apoptosome. For an up to date review on ROS in apoptosis, see Sinha et al. (2013).

### 1.3.3 The PARK genes and the mitochondria

PINK1 has a predicted mitochondrial targeting sequence in its first 34 aa and a conserved protein kinase domain with high homology to serine/threonine kinases of the calmodulin family (Valente et al., 2004) and a mechanism in the mitochondrial response to cellular and oxidative stress have been proposed (Valente et al., 2004). Gandhi et al. (2009) found that PINK1 deficient cultured neurons exhibit lowered mitochondrial calcium capacity. They also found these neurons to have increased ROS production and a lower threshold for opening of the MPT pore and apoptosis. Recent studies have suggested a common pathway for parkin and PINK1 in the regulation of mitophagy (Narendra et al., 2010; Lazarou et al., 2013). This regulation is proposed to work as follows. Damaged mitochondria undergo fission mediated by Drp1. Lowered mitochondrial membrane potential leads to accumulation of PINK1 which recruits parkin to the mitochondria. Parkin then ubiquitinates proteins in the OMM and targets the mitochondria for removal by the autophagosome. The healthy part of the mitochondria from the previous fission step can then undergo mitofusin mediated fusion (Kubli and Gustafsson, 2012).

DJ-1 is found in the cytosol as well as both the intermembrane space and the matrix of mitochondria. It has been proposed to translocate to the mitochondria in response to oxidative stress (AHV Schapira and Gegg, 2011). Another suggested role for DJ-1 is as part of a complex with parkin and PINK1. This complex would promote ubiquitination of parkin substrates including parkin itself and synphilin-1 (sph1) (Xiong et al., 2009).

LRRK2 is found primarily in the cytosol but has also been shown to associate with the OMM (West et al., 2005). An interaction between LRRK2 and parkin has been described (Smith et al., 2005) and expression of parkin in *Drosophila melanogaster* protected dopaminergic neurons from LRRK2 G2019S mutant induced neurodegeneration.

### 1.3.4 Mitochondrial impairment in Parkinson's disease patients

The most convincing evidence for a role of the mitochondria in PD comes from the described presence of mitochondrial dysfunction in cells from PD patients. A reduction in complex I protein as well as activity in neurons from the SNpc was found early on (Mizuno et al., 1989; A Schapira et al., 1989). Later, deficiency of mitochondria in other tissues including muscles and platelets has been described as well (Shoffner et al., 1991; Yoshino et al., 1992).

## 1.4 Genetically encoded sensors

To study physiological processes and the effects on those created by pathological conditions such as neurodegenerative diseases, tools are needed that can report on changes in physiological states within cells. Traditionally, cellular states and functions have been studied in a static way using biochemical or immuno-fluorescence and immuno-cytochemical methods. These methods have given great insight into the components of cells and in what ways the components can interact. What they lack however, is the ability to show the dynamics of a system. They work "retrospectively" on a frozen in time state of the cell or tissue. In other words, they can have great spatial resolution but lack temporal resolution. Live cell time-lapse microscopy on the other hand, works in real-time, showing dynamic changes of proteins as they occur in individual cells and compartments (Bunt and Wouters, 2004; Palmer et al., 2011). To accomplish this, tools are required that respond to changes in the state of the system being studied, and that provides an optical readout that can be sampled using a microscope. Fluorescence provides a high contrast signal that is suitable for live cell imaging and modifying either the intensity, spectral characteristics or life-time of the fluorescence provides a sensitive readout. Coupling such a change in the properties of the fluorescence to a state change within a physiological system of interest, provides a readout for information about that state change.

### 1.4.1 Fluorescent Proteins

The discovery of green fluorescent protein (GFP) in *Aequoria victoria* by Shimomura et al. (1962) and its subsequent cloning by Prasher et al. (1992) provided the necessary building

blocks for the creation of genetically encoded sensors (GESs). GFP exhibits bright fluorescence when fused to other proteins and can be expressed in a wide variety of cells and tissues (Tsien, 1998). The usefulness of GFP was furthered by engineering to provide increased brightness and spectrally modified variants ranging from blue in blue fluorescent protein (BFP) to yellow in yellow fluorescent protein (YFP) (Heim and Tsien, 1996). This made it possible to use different variants of GFP to label different cellular structures or cell types and record them simultaneously. Producing a red-shifted variant of GFP has so far not been successful but the discovery of fluorescent proteins (FPs) from a multitude of other marine animals such as anemones and corals (Shagin et al., 2004) have provided red variants.

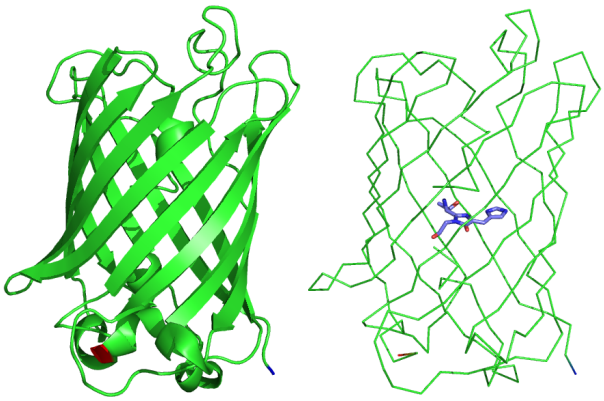

**Figure 1.1: Green Fluorescent Protein**
Cartoon (left) and ribbon rendering (right) of the crystal structure of enhanced green fluorescent protein (EGFP). The ribbon rendering shows the chromophore in the center of the β-barrel. The N- and C-terminals are colored red and blue respectively. Rendering is based on PDB entry 1KYS.

### 1.4.2 Single fluorescent protein based sensors

Two general approaches are available for constructing GESs based on a single FP. The first approach involves exploiting the sensitivity of GFP to its environment. Since the fluorescence of GFP is dependent on protonation, it is sensitive to changes in pH (Tsien, 1998) and sensors have been created that utilize this (Kneen et al., 1998; Miesenböck et al., 1998). The second approach is to move the N- and C-terminals of a FP to an position within the β-barrel. The result of such a transformation is referred to as "circular permutation" (cp). This new position for the N- and C-terminals are more sensitive to perturbations than the original and fusing a binding domain such as calmodulin to these positions have successfully generated GESs capable of reporting on changes in free-$Ca^{2+}$ concentrations (Baird et al., 1999; Nakai et al., 2001). The crystal structure for this type of sensor revealed that upon binding of $Ca^{2+}$, the

binding domain (calmodulin and M13) undergoes a conformational change such that solvent is blocked from the inner side of the β-barrel and the chromophore is effectively deprotonated (Akerboom et al., 2009). This means that the second approach also exploits the dependence of GFP on protonation, leaving these types of sensors sensitive to large shifts in pH, limiting or complicating their use in certain applications. Further developments on this theme has produced genetically encoded calcium indicator (GECI) with high affinity and fast kinetics, allowing the resolution of $Ca^{2+}$ influx from single action potentials *in vivo* (Hires et al., 2008; Akerboom et al., 2012). A schematic representation of this type of sensor can be seen in figure 1.2a. These single FP GESs have several advantages over GESs incorporating two FPs. They are smaller, meaning that they are less bulky when fused with other proteins and thus less likely to interfere with the properties of the fusion protein. They also show high dynamic range and because of their narrower spectra can be easier to use together with other FPs or labels. They come with some disadvantages as well however. As already mentioned, they are sensitive to pH, and since this stems from an exposed chromophore, they are sensitive to other changes in their environment as well, such as oxidation. Most variants are not ratiometric due to the difficulty in creating a single FP sensor that will switch between fluorescent states as opposed to fluorescent/non-fluorescent in response to induced changes. However, ratiometric single FP GECI and pH sensitive sensors are available, proving that the concept is viable Miesenböck et al. (1998) and Baird et al. (1999).

### 1.4.3 FRET based sensors

Another type of GESs exploits the phenomenon of Förster resonance energy transfer (FRET) between two FPs with overlapping spectra. FRET occurs when an excited donor fluorophore is in close proximity to a suitable acceptor. This leads to a reduction in the donor fluorescence and increase in acceptor fluorescence. The efficiency of FRET is steeply dependent on the distance between the donor and acceptor according to the following relationship first laid out by Főrster (1959):

$$E = \frac{1}{1 + (R/R_0)^6}$$

where $E$ is the FRET efficiency, $R$ the current distance and $R_0$ the distance at which half of the energy is transferred from the donor, a constant which is unique for each donor/acceptor pair and strongly dependent on their relative orientation (Selvin, 2000). The most common FRET pair in GESs are cyan fluorescent protein (CFP) and YFP or variants thereof. Figure 1.2b shows a schematic representation of a FRET based GESs that responds to changes

in free-$Ca^{2+}$. The same binding domain consisting of calmodulin and the M13 peptide as are used for many single FP GECIs are attached as a linker between CFP (donor) and YFP (acceptor). Binding of $Ca^{2+}$ to calmodulin facilitates the binding to M13 which decreases the distance between the FPs, increasing the FRET efficiency which can be read out as the ratio of the fluorescence between the acceptor and the donor. Another example for how FRET between two FPs can be exploited in a GESs is given in figure 1.2c. A short peptide cleavage sequence linker connects the donor with the acceptor and upon activation of the enzyme that cleaves the linker, FRET is abolished. The advantages of FRET sensors are their inherent ratiometric nature as well as being straight forward to construct. But due to their larger size, they can be difficult to target to subcellular locations and use as fusion constructs. Their broader spectra also limits the number of other sensors/FPs that can be used in the same experiment. Also, the equipment needed to measure signals from a FRET sensor is slightly more complicated than for single wavelength sensors. Acquisition requires either splitting the optical path to record two channels simultaneously or very fast switching of optical filters for fast sequential recording.

### 1.4.4 Advantages of genetically encoded sensors

Since GESs are genetically expressed and because of their relatively low toxicity, they can be used in experiments over long time spans. By substituting the promoter used for expression and by fusing targeting sequences or complete other proteins to the GESs, it is possible to have them expressed only in specific cell types and subcellular compartments. It is also possible to generate TG animals with constitutive or induced expression of the GESs of interest (Guerrero and Isacoff, 2001; Griesbeck, 2004). These features make them superior to traditional small molecule fluorescent indicators.

## 1.5 Hypothesis and aim of thesis

The evidence presented above shows how the mitochondria is involved in much of what is known about the pathology of PD. There are only few studies where the function of mitochondria have been directly studied in the presence of elevated levels of αS however and none of those dealt directly with ATP consumption, production and basal levels in intact neurons. With the role of βS and to some extent γS becoming more important in PD research, I wanted to examine the effects of αS on mitochondrial function and compare them

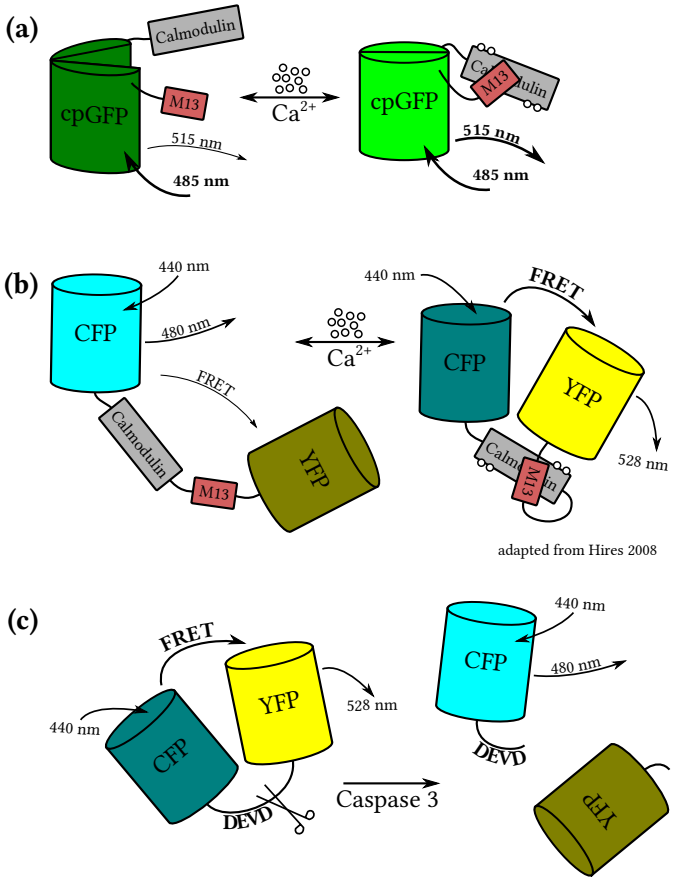


**Figure 1.2: Different types of genetically encoded sensors**
An overview showing different ways that FPs can be exploited to generate GESs. **(a)** Sensor based on a single FP where the N- and C- terminals have been moved from their original position through "circular permutation" (cp) which opens up the β-barrel. In the unbound state, the chromophore is exposed to and quenched by water and protons. When calmodulin binds $Ca^{2+}$, binding to M13 is facilitated and the β-barrel closes, promoting fluorescence which is registered as an increase in brightness. **(b)** A FRET based sensor in which two FPs with overlapping spectra are linked by a binding domain. Upon binding of $Ca^{2+}$ to calmodulin, binding to M13 is facilitated which induces a conformational change that reorients and decreases the distance between the two FP, increasing the FRET efficiency. **(c)** A variant of the FRET sensor in which the two FPs are linked by a peptide cleavage linker. When caspase-3 is activated during apoptosis, it cleaves the DEVD sequence and FRET between the two FPs is abolished.

to the possible effects of β- and γS. Because αS has been shown to impair complex I activity and this complex is part of the ETC which is responsible for generation of ATP in the mitochondria through the process of oxidative phosphorylation, the hypothesis when starting out was for a possible reduction in ATP levels or impairment in ATP production due to αS. The recent availability of a novel GESs for ATP dynamics provided additional rationale for these measurements in the form of reproducible measurements of ATP consumption, production and basal levels. Several studies of the possibility of membrane permeability by αS have been made, but none of those have examined the possibility of induced ion permeability on the mitochondrial membranes in intact neurons. The hypothesis was that if αS can enter the mitochondria and integrate or associate itself with the mitochondrial inner membrane in such a way that it becomes permeable to ions, this permeability might also induce the MPT. To test this hypothesis, it was decided to examine the properties of calcium handling in the mitochondria. If the mitochondrial inner membrane is permeable to calcium ions, an elevated calcium level in the cytosol should lead to increased uptake and impaired efflux of calcium by the mitochondria.

# 2 Materials and Methods

## 2.1 Buffers and reagents

**aCSF-H** 1x: 128 mM NaCl, 3 mM KCl, 1 mM $MgSO_4$, 1 mM $NaH_2PO_4$, 30 mM HEPES, 10 mM Glucose, sterile filtered. Prepared fresh every week from stock solutions.

**aCSF-H-$K^+$** As aCSF-H but with 128 mM KCl and 3 mM NaCl. Diluted with aCSF-H to make 64 mM KCl before use for depolarization of neurons.

**CMF** 50 mL 10x Hanks balanced salt solution (HBSS), 450 ml Ampuwa $H_2O$, pH 7.3 adjusted with sterile sodium bicarbonate.

**DNA loading buffer (6x)** 15% Ficoll 400 DL, 100 mM LiCl, 2% glycerol, 100 mM EDTA, pH 8.0; 0.6% SDS, 0.03% BPB in $H_2O$.

**FCS** fetal calf serum (FCS) was thawed, pre-warmed to 37 ℃ and incubated for 30 min at 56 ℃ (heat inactivation). Aliquots were stored at −20 ℃.

**HCN** 5 µg $mL^{-1}$ transferrin, PSN (Penicillin 50 µg $mL^{-1}$, Streptomycin 50 µg $mL^{-1}$, Neomycin 100 µg $mL^{-1}$), 2 mM L-Glutamin, 2% B-27 supplement in neurobasal medium (NBM).

**LB agar** 40 g LB agar dissolved in 1000 mL $H_2O$, autoclaved with appropriate antibiotic added during cooling shortly before pouring in Petri dishes. Stored at 4 ℃.

**LB media** 25 g of LB powder dissolved in 1000 mL $H_2O$. Stored at 4 ℃ (autoclaved).

**ligation buffer** 1x: 10 mM $MgCl_2$, 1 mM ATP, 10 mM DTT, 25 µg $ml^{-1}$ BSA, 50 mM Tris-HCl, pH 7.5.

**PBS** 9.55 g of PBS powder in 1 L millipore $H_2O$ (autoclaved).

**SOC$^{++}$** 2% bacto-tryptone, 0.5% yeast extract, 10 mM NaCl, 2.5 mM KCl, 10 mM $MgCl_2$, 10 mM $MgSO_4$, 20 mM glucose, pH 7.0. Glucose added after autoclaving.

**TBE** 42 mM Boric Acid, 10 mM EDTA, 50 mM Tris-HCl, pH 8.0 (autoclaved).

**TE** 10 mM Tris-HCl, 1 mM EDTA, pH 8.0.

## 2.2 Chemicals

**Applichem**: acrylamide, agarose for gel, ampicillin, boric acid, calcium chloride, chloroform, D-(+) glucose, dimethyl sulfoxide (DMSO), ethylenediaminetetraacetic acid (EDTA), ethanol absolute, Ficoll, glycerol, glycin, 4-(2-hydroxyethyl)-1-piperazineethanesulfonic acid (HEPES), isopropanol, kanamycin, potassium chloride (KCl), LB Agar, LB media, magnesium sulfate, methanol, modified Eagle's medium (DMEM), phosphate buffered saline (PBS), potassium chloride (KCl), phenol equilibrated stabilized, sodium azide, sodium chloride (NaCl), sodium dodecyl sulfate (SDS), sodium metabisulfite, sodium phosphate, sucrose, TRIS, Triton X
**Fermentas**: Hind III Lambda DNA
**Gibco**: B27 supplement, neurobasal medium (NBM), fat milk, hydrogen peroxide, magnesium chloride, perchloric acid, trichloroacetic acid, PS-N
**Life technologies**: Fura-2 AM, tetramethylrhodamine-methylester (TMRM), MitoTracker Red FM, MitoTracker Green FM
**New England Biolabs (NEB)**: 2-Log DNA marker, broad range protein marker, dNTPs, restriction enzymes and buffers, bovine serum albumin (BSA)
**PAA cell culture company**: FCS, PS (penicillin/streptomycin), trypsin for HEK 293 cells
**Macherey-Nagel**: NucleoBond PC2000 Mega Kit
**Sigma**: dithiothreitol (DTT), ethidium bromide, carbonyl cyanide 4-(trifluoromethoxy)phenylhydrazone (FCCP), kainate, laminin, poly-l-ornithine, transferrin, Triton X-100, trypsin for primary cell culture

## 2.3 Equipment

| *Equipment* | *Supplier* |
|---|---|
| Arduino Uno | Arduino, Italy |
| Autoclave | Systec, Germany |
| Axio Examiner microscope stage | Zeiss, Germany |
| Binocular microscope | Zeiss, Germany |
| Biophotometer | Eppendorf, Germany |
| CCD camera AxioCam MRm | Zeiss, Germany |
| Colibri LED illumination | Zeiss, Germany |
| Cell culture hood | HeraSafe HS18, Heraeus, Germany |
| DNA electrophoresis chambers | BioRad, Germany |
| Electrophoresis power supply | BioRad, Germany |
| Freezer −80 ℃ | Heraeus, Germany |
| Gene Pulser II | BioRad, Germany |
| Heat block | Eppendorf, Germany |
| Heating controller TC-344B | Warner Instruments, USA |
| Heating platforms PH-1, PH-3 | Warner Instruments, USA |
| Ice machine | Scotman, Italy |
| Imaging chambers RC-25, RC-26GLP | Warner Instruments, USA |
| Incubators | B. Braun, Germany |
| In line heater SHM-8 | Warner Instruments, USA |
| Instruments for dissection | Fine Science Tools, Germany |
| Objective W Plan-Apochromat 20x/1.0 DIC M27 75mm | Zeiss, Germany |
| Objective W Plan-Apochromat 63x/1.0 M27 | Zeiss, Germany |
| pH-meter | Sartorius, Germany |
| Perfusion system VC-8T | Warner Instruments, USA |
| Pipettes | Eppendorf, Germany |
| Pipetboy, accu-jet pro | Brand, Germany |
| Scales | Sartorius, Germany |
| Table centrifuge | Eppendorf, Germany |
| Thermocycler | MJ Research Biozym, Germany |
| Transluminator | Bio-Rad, Germany |
| Western blot Electrophoresis chambers | BioRad, Germany |

## 2.4 Vectors

### AAV6-s-SEWB

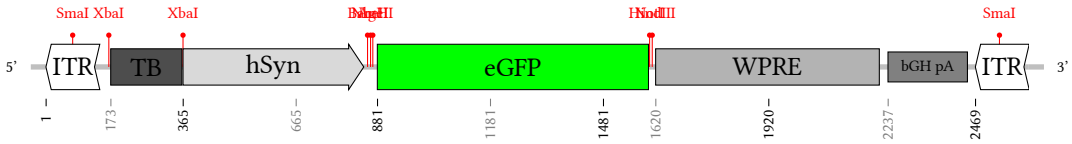


Adeno-associated virus (AAV) vector plasmid provided by Sebastian Kügler. This plasmid was used as a backbone by first removing the GFP insert when cloning sensors and synucleins. Transcription of the insert is driven by the human synapsin promoter (hSyn). The insert is followed by a woodchuck hepatitis virus (WHP) posttranscriptional regulatory element (WPRE) to enhance expression. The promoter and WPRE sequences are flanked by inverted terminal repeat (ITR)s. The ITR can have promoter like activity and a transcription blocker is placed between the ITR and the hSyn to supress this.

### AAV6-3TB-EWB


AAV vector used throughout this thesis as a control for toxicity of AAV vector transduction. The promotor is replaced by a transcription blocker (TB) sequence in triplicate, preventing transcription of the GFP.

### AAV6-s-ATeam1.03-WB

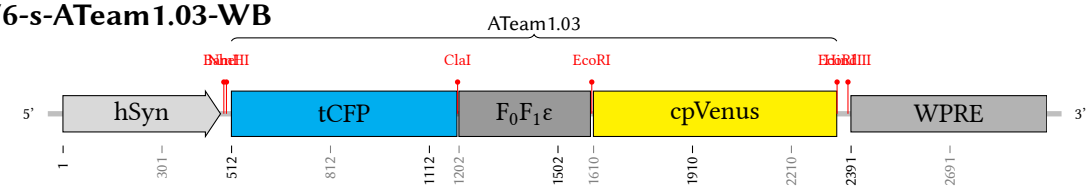


AAV vector coding for the expression of ATeam1.03. ATeam1.03 is a FRET based GES with the ε-subunit of $F_0F_1$-ATP synthase placed between CFP and cpVenus. This sensor is sensitive to changes in ATP levels between 1 and 10 mM and has a reported $K_d$ of 3.3 mM (Imamura et al., 2009). The sensor was provided by Hiromi Imamura and Hiroyuki Noji.

### AAV6-s-D3cpV-WB

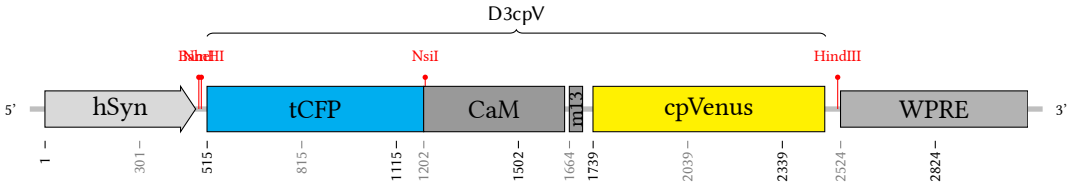


AAV vector coding for the cytosolic expression of D3cpV. The binding sites of the calmodulin (CaM) and m13 domains have been mutated for decreased endogenous binding (Palmer et al., 2006).

### AAV6-s-4mtD3cpV-WB

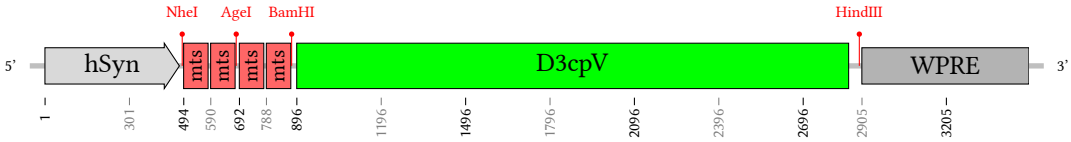


AAV6-s-D3cpV-WB modified for mitochondrial expression. Four copies of the mitochondrial targeting sequence (MTS) from cytochrome *c* oxidase (COX) subunit VIII was placed N-terminally of the sensor.

### AAV6-s-GCaMP3.5-WB

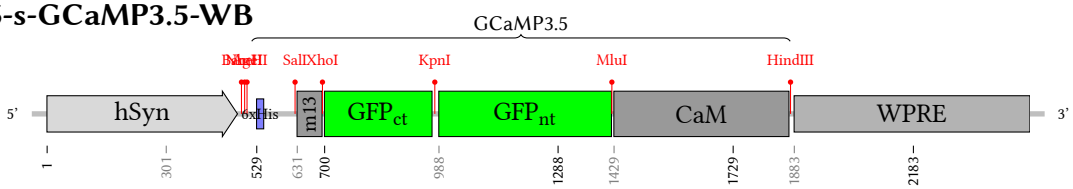


AAV vector coding for the expression of GCaMP35. GCaMP35 is a GECI based on a circularly permuted eGFP flanked by CaM and m13 peptide domains. GCaMP35 is GCaMP3 without CaM-N60D mutation (Nagai et al., 2001; Akerboom et al., 2013).

### AAV6-s-RCaMP1e-WB

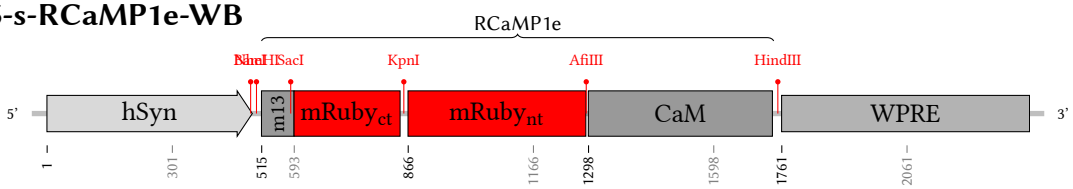


AAV vector coding for the expression of RCaMP1e. RCaMP1e is a GECI based on a circularly permuted mRuby flanked by CaM and m13 peptide domains (Akerboom et al., 2013). RCaMP1e was provided by Loren Looger.

### AAV6-s-mtRCaMP1e-WB

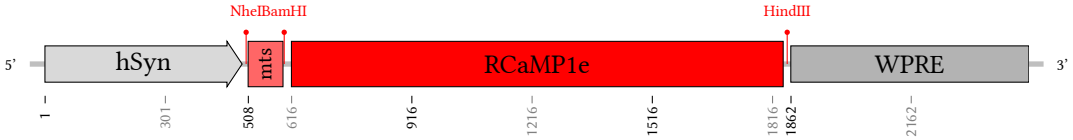


AAV6-s-RCaMP1e-WB modified for mitochondrial expression. A single copy of the MTS from COX subunit VIII was placed N-terminally of the sensor.

### AAV6-s-aSynWT-WB

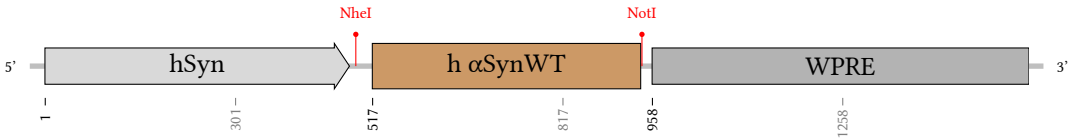


AAV vector coding for the expression of human wild type α-Synuclein.

### AAV6-s-aSynWT-SEIS-WB

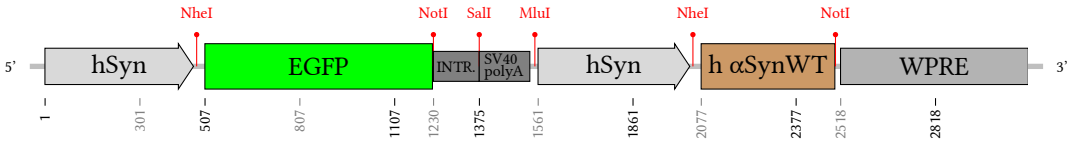


Bicistronic variant of AAV6-s-aSynWT-WB with GFP coexpressed as a reporter label for transduction.

### AAV6-s-bSynWT-WB

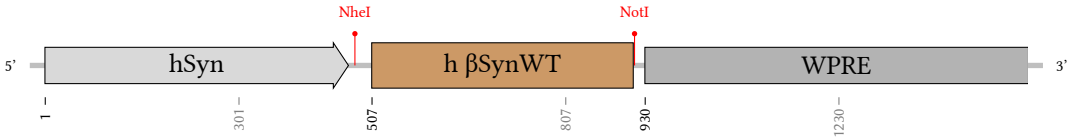


AAV vector coding for the expression of human wild type β-Synuclein.

### AAV6-s-bSynWT-SEIS-WB

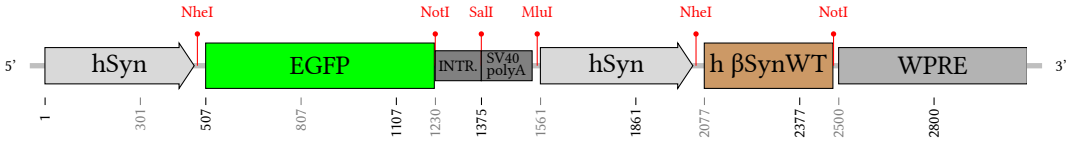


Bicistronic variant of AAV6-s-bSynWT-WB with GFP coexpressed as a reporter label for transduction.

### AAV6-s-gSynWT-WB

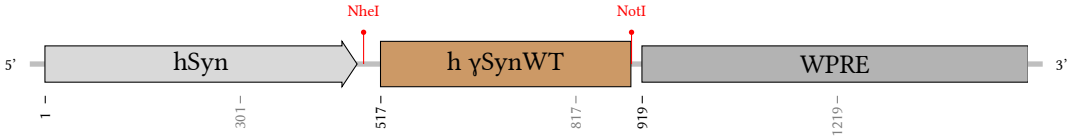


AAV vector coding for the expression of human wild type γ-Synuclein.

**AAV6-s-gSynWT-SEIS-WB**

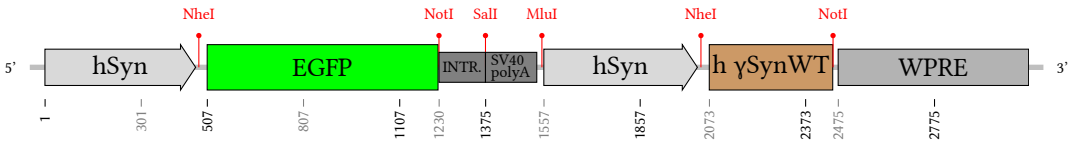


Bicistronic variant of AAV6-s-gSynWT-WB with GFP coexpressed as a reporter label for transduction.

## 2.5 Cloning of sensors into AAV-plasmids

The first step done when cloning a new sensor was to do virtual cloning using SECentral (Scientific & Educational Software, NC, US). This consisted of the loading of a vector map for the sensor to be cloned and a vector map for the backbone to clone in to. Then finding proper cloning sites by searching the multiple cloning site (MCS) for sites that uniquely opened the backbone and cut on both sides of the sensor. In most cases no such sites were found and the strategy then turned to adding new cloning sites using polymerase chain reaction (PCR). For this purpose two sets of primers were designed in SECentral. The first set served as templates for the insertion of new restriction sites through overhangs. The second set was designed as sequencing primers of ~8 bp that bound ~200 bp upstream of the insert and the same downstream (reverse direction). Since PCR is error prone, these sequencing primers were used for sequencing of the cloned plasmid to ensure integrity of the original sequence. When design of restriction sites were necessary, the design was made in such a way as to ensure that the Kozak consensus sequence, CCACC(ATG)(Kozak, 1986), was present between the restriction site and the cDNA start codon of the insert. As a reference, most procedures were done according to those described in "Molecular Cloning: A Laboratory Manual" (Sambrook and Russell, 2001). All restriction nucleases used were from New England Biolabs.

### 2.5.1 PCR amplification

PCR amplification of cDNA sequences of interest was carried out on a PTC-150 MiniCycler thermocycler. Initially an optimization PCR was carried out with different (0, 1.5 and 3 mM) magnesium chloride ($MgCl_2$) concentrations and different annealing temperatures (between 60 and 72 ℃ in order to establish optimal conditions. While most sensors have similar size and are composed of mostly fluorescent proteins which are very similar in structure, it was quickly noticed that this step for most cloning could be skipped. If nothing special was required 3 mM $MgCl_2$ and an annealing temperature of 72 ℃ was used. 50 µL PCR reaction mix then contained:

1. 27 µL millipore $H_2O$
2. 10 µL reaction buffer (Phusion HF 5x)
3. 1 µL backbone template (5 ng µL$^{-1}$)
4. 5 µL forward primer (4 pmol µL$^{-1}$)
5. 5 µL reverse primer (4 pmol µL$^{-1}$)
6. 1.5 µL dNTP mix (dATP, dCTP, dGTP, dTTP 10 pmol µL$^{-1}$)
7. 0.5 µL Phusion polymerase (2 U µL$^{-1}$)

The thermocycler was programmed according to the following:

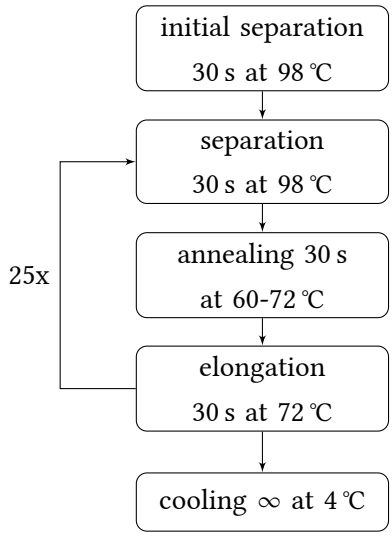

Meaning that separation, annealing and elongation was done for the given time at the given temperature and that it was repeated 25 times. The last step meant that the PCR reaction was cooled to 4 ℃ after finishing and could thus be run over night if needed.

After amplification the reaction was analyzed for the correct size with agarose gel electrophoresis (see section 2.5.3).

### 2.5.2 Restriction of DNA

Restriction of DNA was done according to the enzyme manufacturers (New England Biolabs) intructions. Enzymes and DNA were mixed in the correct buffer and incubated in water bath at the recommended temperature for 60 min. Restriction was done in a total volume of 50 µL with 5 µg plasmid backbone or ~1 µg PCR reaction, 5 µL buffer and 1.5 U restriction enzyme per µg DNA. In the case that the temperature and activity in the same buffer was at least 75% enzymes for both restriction sites were both added to the reaction. If the temperatures did not match, incubation with the enzyme with lower optimal temperature was done first, the second enzyme then added and the temperature raised to the new optimal. If the buffers had to be switched the reaction was first restricted with one enzyme, purified using a PCR purification kit (Qiagen) and then prepared again with the second enzyme in the new buffer and incubated again.

### 2.5.3 Agarose gel electrophoresis

Agarose gel electrophoresis was used to analyze the fragments from DNA restriction digests for purity, quantity and size. The gel was prepared by weighing the proper amount of agarose, dissolving it in 1x TBE buffer by heating in a microwave oven. When completely dissolved, the bottle was held under cold flowing water for about one minute to reduce the time taken for polymerization. 1 µL ethidium bromide per 50 mL solution was then added, mixed and poured into a gel tray. A lane comb was inserted and the gel left to polymerize for ~30 min at room temperature. The amount of agarose was chosen based on the size of the fragment of interest. For fragments smaller than ~500 bp a 2% gel was used. For fragments between ~500 bp and ~1000 bp 1.5% and for fragments larger than ~1000 bp 1%. The gel tray was put in the gel chamber and 1x TBE was added to cover the gel. Samples were mixed with DNA loading buffer (6x) and TE to a final volume appropriate for the wells of the gel and pipetted in the wells. The gel chamber was closed and connected to a power supply which was set

to deliver direct current of 80 V and left to run until sufficient separation of the fragments of interest had occurred. The DNA bands in the gel was then visualized under UV-illumination on a Gel Documentation 2000 UV-transilluminator with a camera connected to a computer running Quantity One (BioRad) software.

### 2.5.4 DNA production, extraction and purification

In cases were the DNA from a agarose gel electrophoresis was to be further used, the band was cut out under low-intensity UV illumination and purified using a QIAquick Gel Extraction Kit according to the manufacturers instructions. For mini preps, extraction of DNA from lysed bacteria was done using a QIAquick Mini Prep Kit according to the manufacturers instruction. The DNA was eluted in 36 µL 10 mM Tris-buffer of which 6 µL could be used to determine the concentration. The purity of the sample after extraction with either of these two kits was high enough that no further purification such as precipitation was necessary for sequencing, ligation or transformation of bacteria.

To obtain plasmid DNA in milligram quantities, a mega-prep was done using a Macherey-Nagel NucleoBond PC2000 kit on two liters of bacterial culture cultivated over night from a 1 mL mini-prep aliquot. The procedure was the same as the one given in the manufacturers manual with the exception that the column was used twice. After the first run through and elution the column was washed with the right buffer and the second half of the batch was loaded. The plasmid DNA extraction procedure consists of the following steps:

1. pelleting of bacteria by centrifugation
2. resuspension in resuspension buffer supplemented with 100 $\mu g\,ml^{-1}$ Rnase A to degrade
3. alkaline lysis of bacterial cells (1% SDS, 10 mM EDTA, 200 mM NaOH)
4. precipitation of SDS, proteins and protein associated DNA and removal by centrifugation (2.8 M KAc, pH 5.1) supernatant contains plasmid DNA
5. binding to a pre-equilibrated anion-exchange resin column
6. washing of the column to remove chromosomal DNA and proteins (100 mM Tris-HCL, 15% ethanol, 1.15 M KCl, pH 6.3)
7. elution (100 mM Tris-HCL, 15% ethanol, 1 M KCl, pH 8.5)

After elution, plasmid DNA from large scale production was concentrated and desalted first by isopropanol precipitation and subsequently again by ethanol precipitation. Finally the pellet from ethanol precipitation was resuspended in 1x TE buffer over night.

### 2.5.5 DNA concentration determination

The concentration of DNA was determined by measuring the optical density on a spectrometer at 260 nm. A ratio of the optical density measured at 260 and 280 nm of more than 2 was taken as indicative of low protein contamination of the DNA sample. In cases were the DNA-concentration was to low to be recorded on the spectrometer, the concentration was assessed on a agarose gel. In this case, a λHindIII digest was used as reference. Bands in the sample of similar size to those in the standard was compared to the intensity of the bands in the standard. Those that most closely matched in intensity was assumed to have the concentration of the corresponding band in the standard.

### 2.5.6 Ligation and transformation of bacteria

The restricted backbone and insert was ligated and transformed into bacteria for growing and selecting of clones. First the concentration of restricted backbone and insert was assessed as described in section 2.5.5. Then a total amount of between ~150-250 ng backbone and insert was mixed in a 1:3 molar ratio together with T4 ligation buffer and 2000 U T4 DNA ligase with sterile water added to a final volume of 20 µL. The ligation reaction was left to react at room temperature for 20 min. To control for religation events of the backbone due to insufficient separation or purification from gel extraction, a second ligation was set simultaneously with the first were the insert DNA was not added. After ligation, the reactions were put on ice before being used to transform bacteria.

For transformation, electroporation cuvettes were pre-cooled on ice. 70 µg electrocompetent bacteria suspension was thawed on ice. DH5α E.coli cells (ElectroMAX) was used when pre-cloning of received vectors had to be done. Otherwise, since all cloning was done in order to create pAAV vectors, electroporation-competent cells, “stop unwanted rearrangement events” (SURE) E.coli cells were used in order to reduce the number of clones with corruption of ITR sequences in the plasmid genome. 4 µL ligation reaction was transferred to the vessel containing the E.coli, mixed carefully and left for 1 min on ice. The full volume of bacteria/ligation mix was then transferred to the electroporation cuvette. The outside of the

cuvette was quickly wiped with a paper napkin to remove ice and moisture. The cuvette was then placed in the electroporator (Bio-Rad Gene Pulser II) and flashed with 1.8 kV potential, 200 Ω resistance and 25 µF capacitance. Immediately after flashing, 800 µL $SOC^{++}$ medium was added to the cuvette, carefully mixed and transferred to a 1.5 mL eppendorf tube. The procedure was repeated for all ligation reactions after which the tubes with the flashed bacteria suspension were incubated at 37 ℃ with vigorous shaking for 45 min to let them recover and initiate expression of the antibiotics resistance protein encoded for by the plasmid before being exposed to antibiotics.

For plating, LB agar plates with the proper antibiotics (e.g. ampicillin 100 were pre-warmed to room temperature and 200 µL bacteria suspension plated with the help of a bent Pasteur pipette. For difficult ligations, the rest of the bacteria suspension was centrifuged shortly, 300 µL supernatant removed, the rest resuspended and plated on a second agar plate. The same was done with any control reactions. The plates were then incubated at 37 ℃ over-night for at least 15 hours or until colonies were easily seen by the naked eye.

### 2.5.7 Picking of clones and verification of plasmid

The number of clones on LB agar plates from control ligation were compared with the proper ligation. In most cases the ratio of proper to control was $> 100$ and about 8 colonies were picked and cultivated in 4 mL LB media over night. From this, 2 mL was used with a QIAquick Mini Prep Kit (QIAGEN) (see section 2.5.4) to prepare DNA for checking plasmid integrity and sequencing of PCR insert fragment. 100 ng from this preparation was restricted with SmaI restriction nuclease (NEB) and analyzed using agarose gel electrophoresis (see section 2.5.3) to verify the integrity of the ITRs of the AAV plasmid. A virtual restriction was done to infer the correct size of the bands from SmaI restriction and the bands on the gel was compared to these. Corrupted ITRs were evident as the wrong band from that expected due to SmaI not restricting in corrupted regions.

Since PCR amplification is an error prone process, the amplified fragment was sequenced in order to assure that it had the correct sequence. After mini-prep (section 2.5.4) and ITR integrity verification, a sample was sent for sequencing with the company SEQlab. The service at SEQlab used was "extended hotshot 800" which sequences ~800 bp in one stretch with high fidelity. SEQlab was supplied with 600 ng plasmid DNA and 20 pmol primer in 10 mM Tris-HCL. For PCR products that were longer than 800 bp a second sample with a primer for the

reverse direction was used. For really long inserts, were sequencing in the forward and reverse directions from the ends of the insert was not sufficient, additional sequencing primers were designed either from the vector map or if not at hand, from a previous sequencing step done from the ends of the insert.

## 2.6 Primary cell culture

Primary neuronal cortex culture was prepared from E18 rat embryos according to Varon and Raiborn Jr. (1969) and Yavin and Menkes (1973). All surgical procedures were performed on ice. In brief, cortex tissue pieces were collected in ice-cold $Ca^{2+}$/$Mg^{2+}$-free (CMF) medium and centrifuged at 800 rpm for 4 min at 4 ℃. The medium was removed and the pellet incubated in 750 µL 0.25% trypsin for 15 min at 37 ℃. Trypsin activity was then blocked by addition of 700 µL ice-cold FCS (inactivated) supplemented with 25 µL DNAse to dissolve DNA-aggregates released from damaged cells. The pellet was then mechanically dissociated by gentle up-down pipetting trough a Pasteur pipette with fire-polished opening. After centrifugation at 800 rpm for 4 min, the pellet was resuspended in warm HCN culture medium. Cells were seeded in poly-L-ornithine/laminin coated 24-well culture plates at a density of 250 000 cells/well. Cultures were maintained at 37 ℃ in 5% $CO_2$ and 95% humidity in HCN medium.

Cells were initially fed every third day by removing 250 µL and re-adding 300 µL fresh, equilibrated HCN media. Upon comparison of culture that was fed at said interval with culture where the media was not replenished, no difference in cell size, cell number or dendrite network density could be could be detected. Because of this finding, no replenishing of the media was conducted for any of the experiments with this cell culture listed in the results.

## 2.7 Adeno-associated virus vectors

Recombinant AAV vectors were prepared according to standard protocols (Kugler et al., 2007). Serotype 6 vectors were propagated in HEK293 cells, purified by iodixanol step gradient ultracentrifugation and heparin affinity fast protein liquid chromatography (FPLC), followed by extensive dialysis against phosphate buffered saline (PBS). Genome copies were determined by quantitative real time PCR and purity > 99% by SDS gel electrophoresis and silver staining. All prepared AAV vectors are listed in section 2.4.

## 2.8 Western blots

Western blots for the determination of relative levels of protein expression were done according to Towbin et al. (1979) and Burnette (1981).

Quantification of integrated gray levels in order to determine approximate overexpression levels and relative levels of expression increase between different multiplicity of infection (MOI) were done as follows. Images of the blots were taken on the day of the respective AB incubation with an exposure time of 10 s on a transluminator from Bio-Rad. Images were exported as raw data in 16-bit TIFF format from the Quantity One software from Bio-Rad and loaded into the Fiji distribution of ImageJ. The gel analysis tools of Fiji were used to quantify the integrated density of the gray level from individual bands in the lanes of the blots. The data from Fiji for each blot was saved to a single tab separated .dat file and was further analyzed within R. To calculate the estimate of overexpression of a protein compared to the endogenous expression, the integrated gray level value of the endogenous band was subtracted from the band with overexpression. This was then divided by the value of the endogenous band to give the overexpression factor.

## 2.9 Imaging

Imaging protocols for the different GESs are described in their respective sections in the results chapter. The protocol for the determination of changes in mitochondrial membrane potential is described in the text in section 3.2.9. The methods for determination of mitochondrial fragmentation and movement speed are likewise described in section 3.2.3 and section 3.2.4 respectively.

### 2.9.1 Microscope setup

Life-cell fluorescence imaging was done on a Zeiss Examiner microscope stage equipped with a Colibri LED light source with LED modules of 360, 455, 505, 590 nm wavelength. The microscope stage was adapted to accommodate two MRm (Zeiss) CCD cameras for simultaneous dual wavelength recordings. Emission light was directed to a second dichroic filter cube that directed light to respective camera. For imaging of cell culture on coverslips 20 or 63x magnification objectives were used depending on the structure of interest. With sensors

expressed in the cytosol, images were captured using a 20x objective whereas for sensors expressed in mitochondria a 63x objective was used. Except for overview snapshots imaging was usually done using 2x2 binning of the cameras which gave a full frame resolution of 692x512 pixels. For the 20x objective and from the camera manufacturer (Zeiss) stated pixel pitch of 6.45 µm this gave a distance between pixels in the recorded image of 0.645 µm. For the 63x objective the distance was 0.205 µm. Acquisition was controlled using Axiovision software from Zeiss.

### 2.9.2 Perfusion

For temperature controlled administration of bathing media and application of drugs a gravity fed VC-8T perfusion system from Warner Instruments was used. This system included eight polytetrafluoroethylene (PTFE) valves for switching between solutions. Application was done as follows, two large 200 mL reservoirs for bathing media and six 20 mL reservoirs were placed at a level that produced a flow of 4 ml $min^{-1}$. Perfusion was started and switching controlled using a custom built valve controller, see section 2.9.4. Tubes from the valves were attached to inputs of a SHM-8 in-line heater connected to a TC-344B heating controller (both from Warner Instruments). The output was connected by a short tube (~2 cm) to BNC connector inputs of the imaging chamber. Two imaging chambers were used, RC-25 allowed complete fixation of a 12 or 13 mm coverslip and was used for most experiments. For experiments with field stimulation, a RC-26GLP chamber that was adapted to accommodate platinum electrodes was used instead. This chamber had a glass bottom and the coverslip was put within and kept in place using only capillary forces. Both chambers were from Warner Instruments. These two chambers were mounted on the microscope stage in their respective heating platforms (PH-3, PH-1). The heating platforms were connected to the TC-344B heating controller.

Both channels of the TC-344B heating controller were set to hold the temperature at 37 ℃ which with perfusion at a rate of 4 ml $min^{-1}$ resulted in a stable temperature in the chambers of 34 ℃. All solutions were pre-heated to room temperature before being put in the perfusion reservoirs.

Perfusion lines that were not used during an experiment were filled with sterile filtered $H_2O$ during experiments. After experiments were finished for the day, all perfusion lines were flushed with sterile filtered $H_2O$, excavated and blown dry. All tubing used was PE-160 from Warner Instruments.

### 2.9.3 Field stimulation

For field stimulation two platinum electrodes were placed in a RC-26GLP imaging chamber parallel to each other with a separation of 15 mm. The electrodes were shaped in such a way that a 1 cm long stretch of each electrode was submerged in the bathing solution to the level of the coverslip on the bottom of the imaging chamber. A SIU-102 stimulus isolation unit (Warner Instruments) was used to supply voltage clamped at $10\,\mathrm{V\,cm^{-1}}$ electrode separation. The stimulus isolation unit was triggered using a custom built function generator (section 2.9.4). The stimulus isolation unit was set to output bipolar current meaning that a 500 µs pulse width trigger from the function generator translated to 1000 µs over the electrodes but with the sign reversed after 500 µs.

### 2.9.4 Perfusion valve controller interface and function generator

For computer controlled operation of the perfusion valves a valve controller interface was constructed using an Arduino Duemilanove[1] single-board microcontroller. The Arduino allows interaction with a computer over a serial-over-usb interface and has 14 digital 5 V outputs. Eight of these outputs were directly connected to the inputs of the VC-8T valve controller. When the three-position switch of a valve on the valve controller is set in its lower position the valve can be opened by setting the BNC input to high at 5 V. This allowed individual control of all eight valves of the perfusion system. A computer program was written in Python(et al., 2013) for timed control of the perfusion valves through this valve controller interface. This program includes a simple graphical user interface where individual valves can be opened or closed, a cleaning program started or loading of a program from file that when started opens or closes valves at specific time points. An example of the contents of a file containing such a program is given below:

```
FCCP application
1::120
6:180:600
```

Here the first line,

```
FCCP application
```

[1] `http://www.arduino.cc`

simply states the name of the program and is ignored by the interface software. The remaining lines contains instructions for the interface on what valve to open and for how long.

```
1::120
```

instructs the interface to open valve 1 for 120 seconds.

```
6:180:600
```

is similar but opens valve 6 for 180 seconds then closes the valve and opens valve 6's corresponding wash valve for $600 - 180 = 420$ seconds.

The definition of wash valves and a description of what solution and concentration is currently in what reservoir is defined in a separate valves definition file. Here follows an example of the contents of such a file:

```
1:aCSF-H:::
6:FCCP:2:120:1
```

The first line defines valve 1 with a bathing/wash media with fields separated with ':'. 1 is the valve number, aCSF-H the name of the solution in the reservoir connected to valve 1 and the three last fields are empty. The next line defines valve 6. Here the first two fields are the same, with the difference that the name field can contain multiple names separated by ';'. The third (2) field however designates the concentration in micro liter of the drug or other addition that this solution contains, again multiple concentrations can be given separated by ';'. The fourth field (120) is the default time in seconds to open this valve. And the last field (1) is the valve definition that corresponds to the solution in which this drug was dissolved/added. This example then states that the reservoir connected to the first valve contains HEPES buffered artificial cerebrospinal fluid (aCSF-H). The reservoir connected to the sixth valve contains FCCP with a concentration of 2 µM in aCSF-H that should be applied for 120 seconds if nothing else is stated.

The second function that this interface has was that of a function generator for a SIU-102 stimulus isolation unit (Warner Instruments) used for field stimulation. A second Arduino was programmed to output a square wave with configurable pulse width, frequency and duration. The software for the valve controller interface was adapted to accept a new line in the program definition for applications:

```
9:1;10;500:180
```

meaning to trigger field stimulation ("valve" 9) for 1 second at 10 Hz with a pulse width of 500 µs. For field stimulation the bath solution defined for the "valve" was never turned of and in this example continued for 179 seconds after field stimulation would stop. A valve definition for "valve" 9 would then look like this:

```
9:FieldStimulator::1;10;500:1
```

where 9 is the "valve" that must be activated/triggered from the program file. `FieldStimulator` is the name of this definition. No concentration since it is not defined for field stimulation. Then the default parameters (length;frequency;pulse width) and finally the bathing solution (valve) that should be opened during the field stimulation. If field stimulation was to be applied with different bathing solutions a second or third (or fourth and so on) definition could be used with successively higher valve numbers and the right bathing media valve at the end.

### 2.9.5 Typical imaging experiment

A typical imaging experiment was conducted in the following way. A plate containing coverslips with cultured neurons was taken out from an incubator located next to the microscope. A coverslip was removed from one of the wells of the plate and either fixed to the bottom using a clamp or put on the floor of the imaging chamber depending on the chamber (section 2.9.2). 500 µL of pre-heated bathing media was then carefully pipetted to the imaging chamber and perfusion with bathing media started. A region of the coverslip slightly off center was located using the oculars of the microscope in brightfield or fluorescence light and when the desired spot with cells were found the microscope was switched to camera mode. Focus was readjusted while cells were observed with the cameras on the computer screen and an overview snapshot was taken at 1x1 binning. An experiment was then started in the fast acquisition mode of the Axiovision software and recorded for the desired time. Axiovision was configured to set one of the transistor–transistor logic (TTL) output ports of the Examiner microscope to high upon starting an experiment. This output port was connected to the valve controller interface (section 2.9.4) which was programmed to start its loaded application program upon this trigger.

## 2.10 Data analysis

### 2.10.1 Acquisition and preprocessing

Time-lapse data was acquired using Axiovision (Zeiss) software. After imaging the image stacks were transfered to a workstation using portable hard drives and the `.zvi` files converted to `.tiff` + metadata using LOCI tools (Linkert et al., 2010). These files were semi-automatically preprocessed in ImageJ to correct for misalignment in dual channel images and movement due to instability of the coverslip. Custom macros/plugins and the TurboReg package was used for this purpose.

The image stacks were then again loaded into ImageJ and appropriate region of interests (ROIs) were created using either the ellipse or freehand tools. These ROIs were saved for later use. The average intensities were measured from these regions in all frames of the stack. The background intensity was estimated for each frame as the average of the lower (in brightness) 5% of all pixels. A custom macro was written for this purpose which excluded pixels with an initial value of 0 from the calculation. Usually, the measurement of manually created ROIs and calculation of background was done using a script for all image stacks of an experiment.

### 2.10.2 Evaluation

Next, the `.csv` files were read into `data.frame` structures in R(R Development Core Team, 2011) for further analysis. For $\Delta F/F_0$, $F_0$ was taken as the mean average of at least 10 data points preceding any stimulation that fell within the inter-quartile range of values. The calculation was then done for any time point $t$ as:

$$\frac{(F_t - BG_t) - (F_0 - BG_0)}{F_0 - BG_0}$$

The FRET-ratio $R$ was calculated as:

$$R = \frac{(Ac_t - AcBg_t)}{(Do_t - DoBg_t)}$$

where $Ac_t$ is the integrated "acceptor" emission at time point $t$, $AcBg_t$ the background, $Do_t$ the "donor" emission and $DoBg_t$ its background.

The dynamic range of ratiometric sensors are given as:

$$R_{max}/R_{min}$$

where $R_{max}$ and $R_{min}$ are the maximum and minimum FRET ratios as taken from *in vitro* values from the literature or determined *in cell* where possible.

### 2.10.3 Statistics

Results from any statistical analysis presented in this thesis was made using R (R Development Core Team, 2011) with additional packages. t-tests were carried out using base R. Analysis of variance (ANOVA) and linear regression was carried out using the CAR (Fox and Weisberg, 2011) and nlme (Pinheiro et al., 2013) packages. Post-hoc tests were done with either base R or the multcomp (Hothorn et al., 2008) package. Where necessary or appropriate, pre-tests were carried out. Normality was tested for with the Shapiro-Wilks test using the `shapiro.test` R function. Homogeneity of variance was tested for with Levene's test using the `leveneTest` function of the CAR package. Data is reported as mean±standard deviation (SD) unless stated otherwise in the text. A p-value $< 0.05$ was considered as significant difference from the mean.

# 3 Results

The results section of this thesis is divided into two parts. The first part deals with the creation of mitochondrially targeted genetically encoded sensors (GESs) as well as characterization of both targeted and cytosolic variants. The characterization of the ATP sensor ATeam1.03 has been given extra space and includes results from measurements using that sensor. The second part covers experiments in primary cortical cell culture that is overexpressing α-Synuclein (αS), β-Synuclein (βS) or γ-Synuclein (γS). These experiments focus on the impact of the synucleins on the mitochondria relative to each other and uses GESs for physiological measurements.

Throughout this chapter, each major section ends with a box like this, containing a short summary of the results that were presented.

## 3.1 Targeting and characterization of genetically encoded sensors

To study neuronal physiology in living cells, a significant number of adeno-associated virus (AAV) vector constructs were created that coded for the expression of different fluorescent GESs. Schematic representations with descriptions of the different vector constructs are given in section 2.4. Because the properties of such sensors are sensitive to their environment it is important to characterize them in every new system were they shall be used. This means characterization for each new cell/tissue type but also for every compartment where the sensor might be targeted for expression. The most important factor is to ensure that the dynamic range of the sensor is large enough to reliably report on the changes that are of interest. For these reasons, characterization of the sensors used was considered an important part of this thesis and is described in the following sections.

### 3.1.1 Construct design

The constructs created for expression of GESs were based off of AAV6-s-SEWB, a AAV vector plasmid provided by Sebastian Kügler. This plasmid drives the expression of the target protein using human synapsin promoter (hSyn) for neuron specific expression. See Kügler et al. (2003) for the properties of the hSyn promoter in viral vector constructs. A GES gene was introduced by subcloning from the original plasmid using sites present in the multiple cloning site (MCS) flanking the green fluorescent protein (GFP) gene of AAV6-s-SEWB. This procedure is described in section 2.5. In the case of GESs targeted to the cytosol, the sequence of the sensor followed the promoter in frame after the MCS and the Kozak consensus sequence.

### 3.1.2 Targeting to mitochondria

Previously, free $Ca^{2+}$ in mitochondria has been assessed in live cell imaging using rhodamine based calcium indicators that accumulate in mitochondria with intact membrane potential. The drawback of these are increased unspecific signal when the mitochondria loses their membrane potential, difficulties with overloading and most importantly for the purposes of this thesis, the lack of cell type specificity. To test the suitability of different genetically encoded calcium indicator (GECI) as mitochondrial calcium sensors and to examine calcium homeostasis and activity in neurodegenerative diseases, these sensors were targeted to the mitochondria.

#### Mitochondrial targeting sequence

Targeting to the mitochondria was accomplished by attaching a mitochondrial targeting sequence (MTS) through molecular cloning N-terminally to the sensor proteins. The MTS chosen was from subunit VIII of cytochrome *c* oxidase (COX) due to its already proven efficiency in targeting GFP to the mitochondrial matrix (Rizzuto et al., 1995). Upon integration into the mitochondrial matrix the MTS peptide is cleaved of by the mitochondrial processing peptidase leaving only the cargo protein with a few extra residues on the N-terminal side (Mukhopadhyay et al., 2002).

Single fluorescent protein (FP) based GESs such as GCaMP35 or RCaMP1e contain on only one FP plus a binding domain. This gives them a molecular weight (MW) that is slightly lower

than twice that of GFP (~27 kDa). When these sensors were targeted to the mitochondria using the MTS of subunit VIII from COX they showed very specific targeting. An example of this can be seen in figure 3.1d. Förster resonance energy transfer (FRET) based sensors have an additional FP which gives them a MW of at least twice but often close to three times that of GFP depending on the size of the binding domain of the sensor. Since the MW of the complete subunit VIII is only ~8 kDa, including the MTS (Van Kuilenburg et al., 1988), FRET based sensors are very large proteins in comparison. For these, only one copy of the MTS proved unable to target the protein to the mitochondria with high specificity. This corresponds with what has been shown previously by others for some GECI (Filippin et al., 2005). To avoid time-consuming cloning of repeated structures a 4xMTS sequence was designed and ordered from GeneArt. A schematic of the 4xMTS is given in figure 3.1a. This sequence was designed with a restriction site after the first two MTSs such that they could be removed leaving only a 2xMTS sequence. With 4xMTS there was no visible leakage of targeted sensor from the mitochondria to the cytosol (figure 3.1c) for any of the FRET based sensors.

### Functional characterization of the specificity of mitochondrial targeting

To further assess the specificity of targeting to the mitochondria the GECI mtRCaMP1e was expressed in neuronal cell culture and a train of 10 action potentials (APs) at 10 Hz (pulse width 1 ms) was applied. Traces of the change in fluorescence intensity resulting from influx of $Ca^{2+}$ was compared between different regions (with and without mitochondria) and those from RCaMP1e expressed in the cytosol and is shown in figure 3.2b. The shape of traces from regions with no visible structure had the same general shape (amplitude and slope of the rising and falling part of the trace) as those from mitochondria whereas the shape of the response from cytosolic RCaMP1e was completely different (larger amplitude, faster rising as well as falling parts of the trace). This implied that the response seen from regions without structure is out of focus light from sensor proteins located in mitochondria rather than from sensor proteins that have leaked from the mitochondria to the cytosol.

Also, the average intensity levels of region of interests (ROIs) covering mitochondria, surrounding cytoplasmic region or image background was quantified from images of neurons that coexpressed mtRCaMP1e with cytosolic GCaMP35. The average intensity of a ROI covering a part of a neurite without mitochondrial structure from the mtRCaMP1e channel showed no significant difference in value to a region outside the neurite. This is shown in figure 3.2c,d.

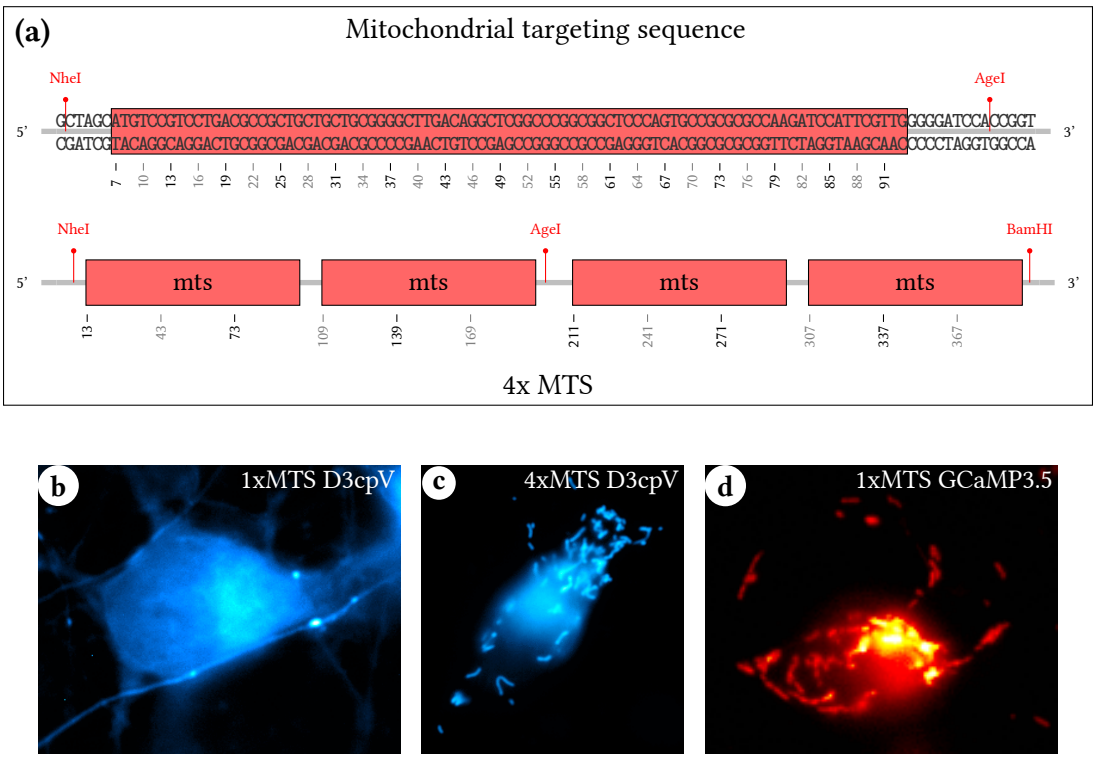


**Figure 3.1: Mitochondrial targeting sequence**
Schematic of the MTS and images of GES targeted to mitochondria of neurons in neuronal primary cell culture. **(a)** Schematic of the MTS (top). The 4x repeated MTS construct necessary for targeting bulky GES (bottom). **(b)** The calcium sensor D3cpV (~73 kDa) with only one copy of the MTS added, showing unspecific targeting and leakage to the cytosol. **(c)** D3cpV with a 4x repeated MTS. **(d)** GCaMP35 (~49 kDa) targeted to the mitochondria with only one copy of the MTS.

### Adapting multiplicity of infection for expression in the mitochondria

It is known that GFP can exhibit cytotoxic effects due to generation of reactive oxygen species (ROS), a phenomena called phototoxicity (HS Liu et al., 1999; Greenbaum et al., 2000; Dixit and Cyr, 2003). Another source of toxicity of FPs is a tendency for aggregation and due to higher propensity for aggregation of red FPs, they can be more toxic than GFP (RL Strack et al., 2008). Additionally, since the total volume of mitochondria within a neuron can be assumed to be significantly smaller than the volume of the cytosol, expression of a protein within the mitochondria at the same expression levels as for the cytosol can produce levels of protein expression that will overload the mitochondria. Therefor the protocol used for expression of mitochondrially targeted proteins must be adapted from that used for cytosolic expression. To test what expression levels were appropriate for mitochondrially targeted GESs, primary cortical neurons were transduced with different multiplicity of infection (MOI)

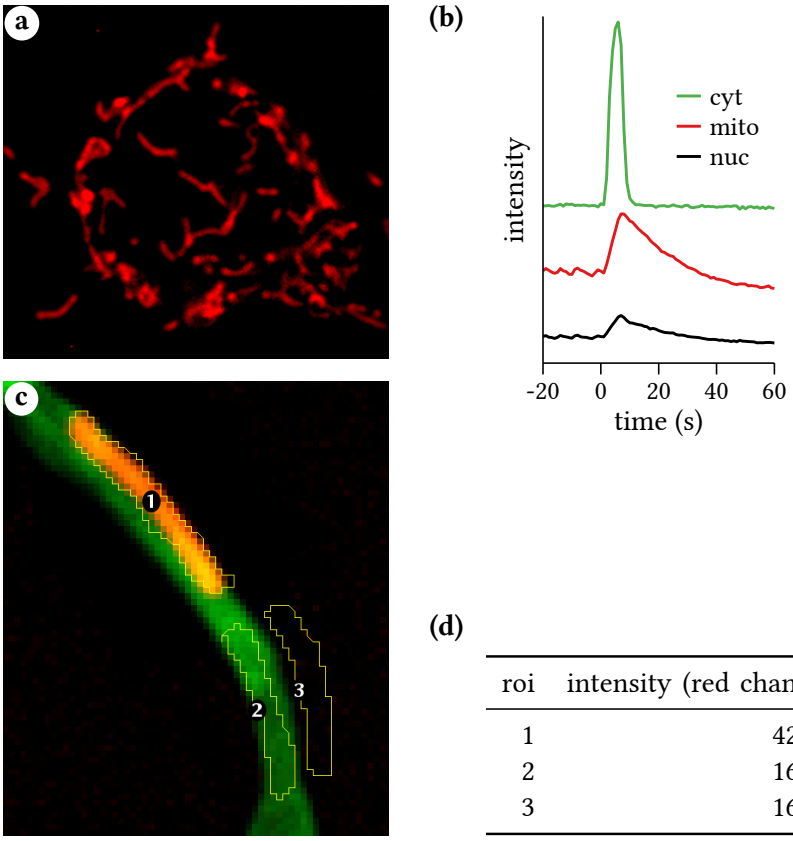


(d)

| roi | intensity (red chan.) |
|---|---|
| 1 | 424 |
| 2 | 169 |
| 3 | 168 |

**Figure 3.2: Specificity of mitochondrial targeting**
Mitochondrial targeting was assessed in terms of its specificity. **(a)** Image showing targeting of RCaMP1e to the mitochondria. Mitochondria are clearly seen without visible fluorescence from cytosolic regions, indicating highly specific targeting. **(b)** *cyt*: an example trace from another recording with the same stimuli where RCaMP1e was present in the cytosol showing the shape of the cytosolic response for comparison. *mito*: time-lapse trace from (a) with a ROI drawn over visible mitochondria. *nuc*: as *mito* but with the ROI drawn over the dark region created by the nucleus where there are no visible mitochondria. The *nuc* and *mito* traces have the same general shape and there is no visible *cyt* component in the *nuc* trace. This indicates that the fluorescence measured from the *nuc* ROI comes from out of focus light from mitochondria and not from cytosolic sensor due to leakage from the mitochondria. **(c)** ROIs in an image showing mitochondria in neuronal neurite:

1) mitochondria in neurite.
2) ROI shaped as in 1 but from a region without mitochondria.
3) region outside of neurite (background).

**(d)** Average intensity measured from the *red channel* of the ROIs in (c). There is a clear higher average intensity in ROI but no differences between ROI 2 and 3 indicating again that there is no leakage of sensor from the mitochondria to the surrounding cytosol.

and the mitochondrial morphology was assessed qualitatively at 6 and 12 days post transduction (DPT).

Figure 3.3 shows that when RCaMP1e is expressed in the mitochondria using AAV with the same MOI as used for cytosolic expression (~2400), changes in mitochondrial morphology occurs. This was true in both young and old cultures (figure 3.3c,f). Virus concentrations were subsequently reduced and with MOI 600 there were consistently no visible changes after 6 DPT and only moderate changes in a fraction of cells at 12 DPT. This MOI level was tested for all sensors that were expressed in mitochondria with the same results. Because of this all further experiments with mitochondrially targeted sensors used a MOI for AAV vector transduction of 600.

- Targeting to the mitochondria of single FP GESs was efficient with a single copy of the MTS from subunit VIII of COX
- FRET based GESs required repeats of the MTS and a 4x repeat was sufficient for efficient targeting
- expression of GESs within mitochondria initially caused morphological changes which was overcome by reducing the expression level

### 3.1.3 Genetically encoded calcium sensors

There is no lack of choice when it comes to GECI, numerous groups have produced sensors of different types that covers a range of $K_d$ values and exhibits different kinetics (Miyawaki et al., 1997; Palmer et al., 2006; Akerboom et al., 2012). Recently, GECIs based on other FPs than GFP has become available including red variants with spectra that can be optically separated from sensors based on GFP, enabling simultaneous imaging of different GECI without the need for spectral unmixing or other post processing of the signal (Zhao et al., 2011; Akerboom et al., 2013). When these were targeted to different cell types or compartments of cells, we previously showed that they can be used to examine interactions of calcium dynamics between these cells or compartments during the same experiment (Akerboom et al., 2013).

During the work for this thesis several GECIs were used to assess calcium dynamics in neurons and this section contains a description of how these sensors were used and the characteristics that were observed while using them.

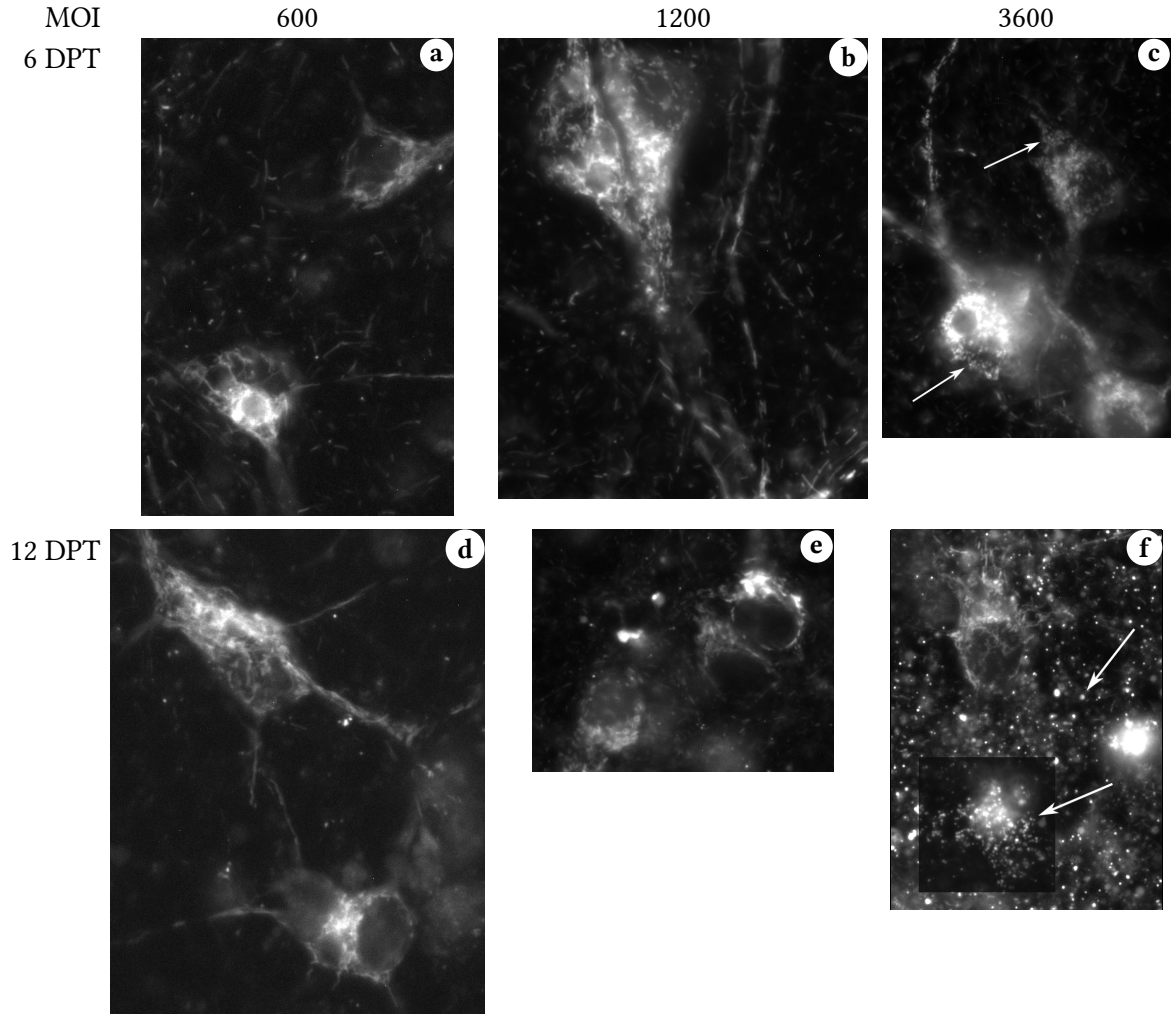


**Figure 3.3: Toxicity of RCaMP1e expressed in mitochondria**
Cortical primary neuronal cell culture transduced with a AAV vector coding for mitochondrially targeted RCaMP1e at different MOI. **(a)** MOI 600, 6 DPT. Mitochondria in soma had elongated shape. Very few mitochondria in neurites had rounded appearance. **(b)** MOI 1200, 6 DPT. Most soma still had elongated mitochondria but some had a fragmented shape. Mitochondria in neurites still had a elongated appearance **(c)** MOI 3600, 6 DPT. Many more soma had fragmented mitochondria. A higher number of mitochondria in neurites were rounded. Arrows point to clusters of fragmented mitochondria in soma. **(d)** MOI 600, 12 DPT. Mitochondria in soma were still mostly elongated. Many mitochondria in neurites were rounded. **(e)** MOI 1200, 12 DPT. More soma than in both (c) and (d) had fragmented mitochondria. Many mitochondria in neurites were rounded. **(f)** MOI 3600, 12 DPT. Most but not all soma had mitochondria with fragmented shape. The neuron in the top of the image shows normal elongated mitochondria. The mitochondrial network in the soma of the neuron below is completely fragmented. Most mitochondria in neurites were rounded. Top arrow points to a fragmented/swollen mitochondria in the neurites. Bottom arrow points to fragmented/swollen mitochondria within soma.

### 3.1.4 FRET based GECI D3cpV

As described in section 1.4, the calmodulin and calmodulin binding peptide that are used in most GECIs can bind to endogenous calmodulin and calmodulin peptide, especially in parts of the cell where these are present in high concentrations such as close to the plasma membrane. This can lead to perturbation of the sensor that introduces inaccuracies or artifacts in the measurements. To solve this problem, Palmer et al. (2006) produced a set of GECIs with a reengineered binding interface between the calmodulin and calmodulin binding peptide. One of these sensors was D3cpV which had its binding domain inserted between a CFP and circularly permuted Venus FP which also increased its dynamic range.

#### Maximum range of D3cpV

To understand what kind of stimuli of a neuron that produces a response of the sensor that lies within the sensors dynamic range, the sensor was expressed in the cytosol of primary cortical cell culture from rat embryos using the AAV vector AAV6-s-D3cpV-WB. Different stimuli were then applied using either the perfusion system described in section 2.9.2 for drug delivery or field stimulation (FS) with the system described in section 2.9.3.

Ionomycin is a ionophore that raises intracellular calcium levels and equilibrates the intracellular concentration with that of the extracellular media (A Takahashi et al., 1999). If calcium is removed from the bathing solution, $Ca^{2+}$ will leak out of cells that have been treated with ionomycin. This allows estimation of the sensor response to the zero $Ca^{2+}$ level. When calcium is readministered, the cell is flooded with $Ca^{2+}$ and the sensor is saturated, showing the maximum response that the sensor will produce. This gives values for $R_{min}$ and $R_{max}$ that can be used to calculate the dynamic range, $R_{max}/R_{min}$ of the GECI.

Figure 3.4 shows the response of the sensor to:

1. depolarization of primary neurons with 64 mM $K^+$ (first part of trace)
2. treatment with 10 µM ionomycin (second part of trace, low ratio values)
3. treatment with ionomycin together with 10 mM $Ca^{2+}$ (second part of trace, sudden increase to high ratio values)

The average maximum and minimum FRET ratios (FRET/CFP) measured during this experiment were 18.2 and 4.6 respectively. This gives an effective dynamic range of ~4 fold increase

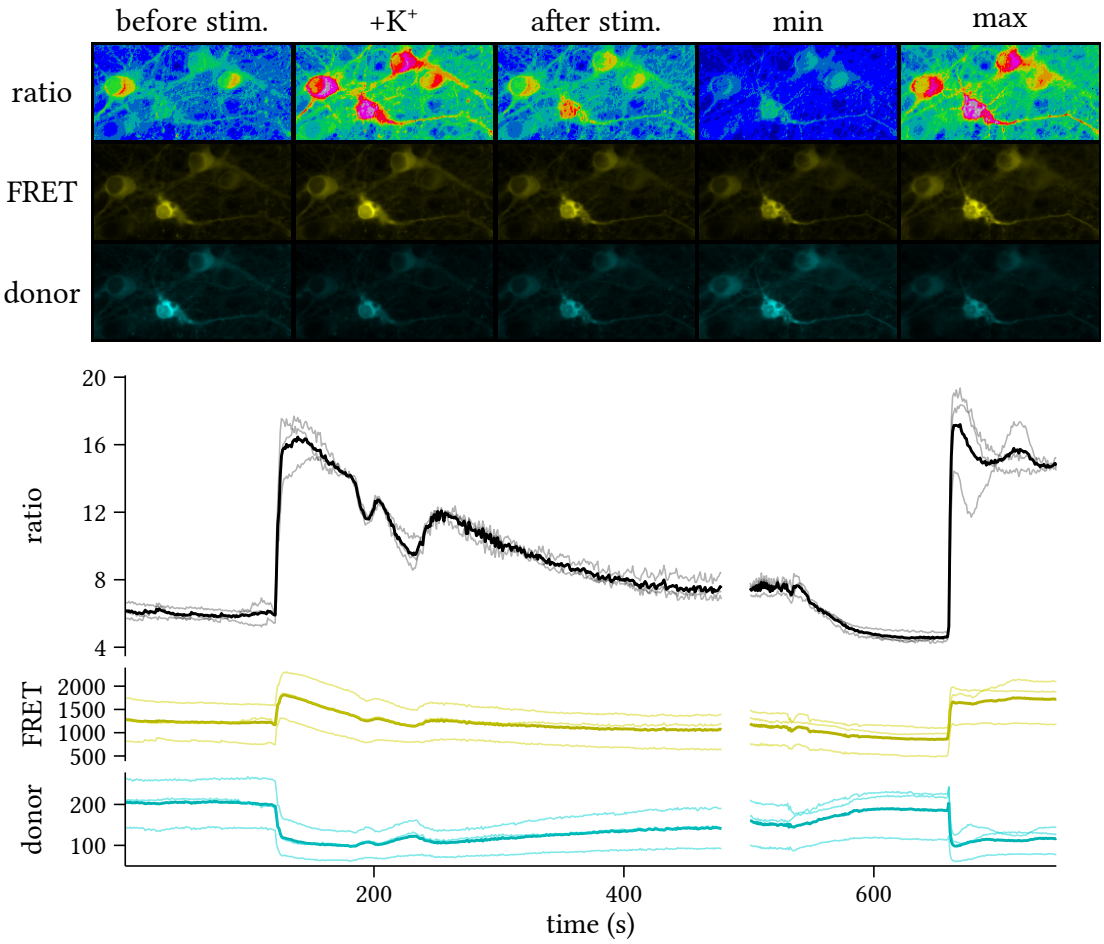


**Figure 3.4: Response to high potassium depolarization and saturation of the D3cpV calcium sensor**

Primary cortical cell culture transduced with a AAV vector coding for cytosolic expression of the D3cpV calcium sensor with a MOI of 1200. The neurons were imaged at 14 DPT with 1 frame per second. **(a)** Overview of a subset of cells from one imaged coverslip. **(b)** Traces from a larger set of cells from the same coverslip. Before stimulation the cells exhibit an initial baseline ratio representative of the free-$Ca^{2+}$ level of the resting neuron with a mean and standard deviation (SD) of $5.68 \pm 0.382$. After 2 min, 64 µM $K^+$ is applied for 60 s to estimate the maximum $Ca^{2+}$ uptake from depolarization of the cells. The mean and SD of the peak sensor signal during high potassium depolarization was $16.6 \pm 1.21$. After the high potassium stimulus, 10 µM ionomycin in $0Ca^{2+}$-media is applied to wash out the intracellular $Ca^{2+}$. This eventually reduces the signal of the sensor to the minimum which had a mean and SD of $4.6 \pm 0.319$. During continued application of ionomycin, 10 mM $Ca^{2+}$ is added which produces a rapid saturation of the sensor. This gives a max value for the sensor range which was measured to have a mean and SD of $18.2 \pm 0.871$. n = 30.

in FRET ratio, comparable to published data for D3cpV by Palmer et al. (2006). These values were used as a reference in order to ensure that a stimuli produced a response that was within the dynamic range of the sensor. To do this, the FRET ratio from the sensor readout was normalized between these two values and the response was expressed as percentage of the dynamic range.

### Response of D3cpV to FS

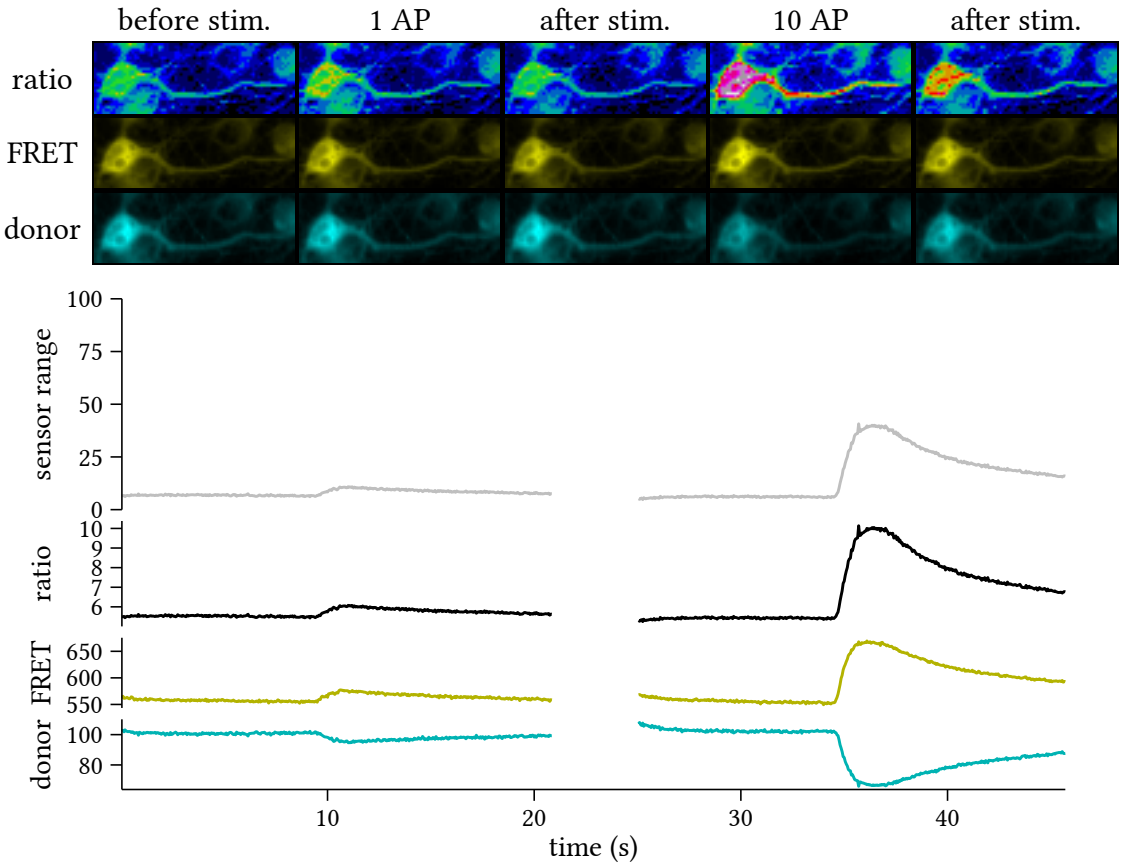


**Figure 3.5: Response of D3cpV to field stimulation**
Primary cortical cell culture transduced with a AAV vector coding for cytosolic expression of the D3cpV calcium sensor with a MOI of 1200. The neurons were imaged at 6 DPT with 20 frames per second. **(a)** Overview of the FRET ratio, FRET and CFP emision from one one cell of a coverslip. **(b)** Example trace showing response to 1 AP (left trace) and 10 AP FS at 10 Hz. No individual peaks can be seen with the 10 Hz stimuli.

The condition of prolonged complete depolarization of the plasma membrane by reversal of the ion concentrations for $Na^+$ and $K^+$ does not occur under physiological conditions. Because of this, high potassium depolarization can not be regarded as a physiological stimuli. A

better stimuli for examining the properties of calcium handling in neurons is field stimulation (FS). FS allows generating stimuli with defined properties such as pulse-width, frequency and exact duration. The result of applying an electrical field over the neurons is to depolarize the plasma membrane for a defined duration, simulating the triggering of an action potential.

There was a visible response of the sensor to stimuli as low as one AP (1 ms pulse-width). This response had a very slow rate of decay meaning that any subsequent stimulation added to the initial response leading to accumulation of sensor signal and blurring of the individual APs. This can be seen in figure 3.5 were a overview and trace from applying 1 or a train of 10 APs with 10 Hz is shown. No individual peaks can be distinguished even though the frame rate of the acquisition was 20 frames per second (FPS). Applying longer trains further increased the peak of the response but the increase was successively smaller. Going from 10 to 30 to 50 AP resulted in average peak responses of 44.67, 50.66 and 54.88 percent sensor range respectively.

### Response of D3cpV targeted to the mitochondria

Using a 4x repeat of the MTS, it was possible to efficiently target D3cpV to the mitochondria (figure 3.1c). The AAV vector created for targeting of D3cpV to the mitochondria was called AAV6-s-4mtD3cpV-WB. It was not possible to use ionomycin to acquire the total range of the sensor when targeted to the mitochondria, possibly due to low penetration of ionomycin to the mitochondria in the neuronal cell cultures used. Figure 3.6 shows the response of the mitochondrially targeted variant of D3cpV (4mtD3cpV) to high potassium depolarizing stimuli. In terms of maximum response, this stimuli had similar characteristic to the response of the cytosolic sensor. From this it was concluded that any response lower than the maximum seen with high potassium depolarization was within the sensor range.

- A ~4-fold dynamic range for D3cpV was measured *in cell*
- The response to high potassium depolarization was close to saturation of the sensor
- FS at 10 Hz produced only ~50% saturation of the sensor
- A response to single AP stimuli was visible but peaks in trains of 10 Hz were not distinguishable
- D3cpV showed efficient targeting to the mitochondria with a 4x repeat of the MTS
- It was not possible to use ionomycin to acquire $R_{max}$ within the mitochondria
- Potassium depolarization produced a response in the mitochondria corresponding to ~75% saturation of the cytosolic variant

Using FS at 10 Hz as a stimuli, it is possible to use *D3cpV* both in the cytosol and the mitochondria for sensitive measurement of relative differences in calcium influx.

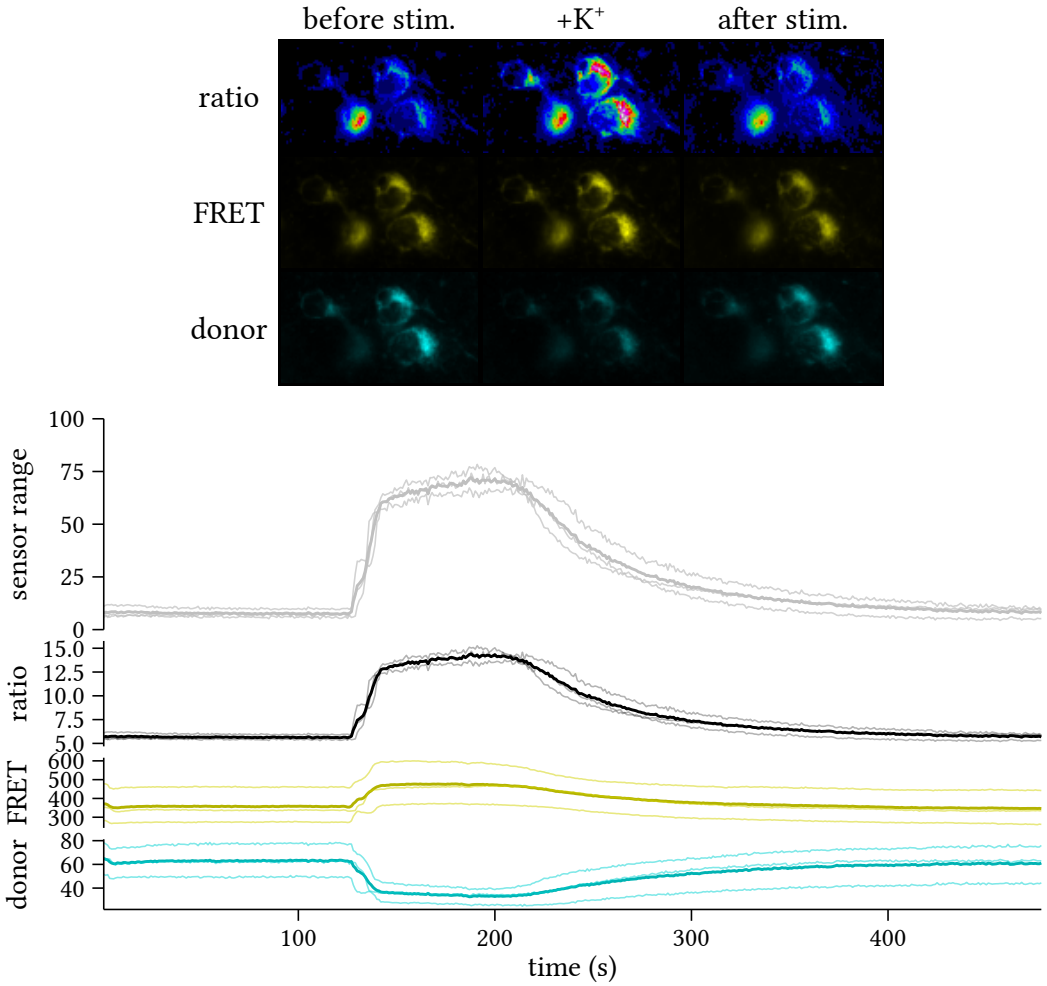


**Figure 3.6: Response of D3cpV expressed in mitochondria to high potassium depolarization** Primary cortical cell culture transduced with a AAV vector coding for mitochondrial expression of the D3cpV (4mtD3cpV) calcium sensor with a MOI of 600. The neurons were imaged at 14 DPT with 1 frame per second. **(a)** Overview of a subset of cells from one imaged coverslip. 64 µM $K^+$ was applied for 60 s which caused the increase in FRET-ratio seen in the trace in (b). The baseline ratio before application had a mean and SD of 5.56 $\pm$ 0.286. During depolarization with high potassium, the maximum ratio measured had a mean and SD of 14.5 $\pm$ 0.695. After washing with aCSF-H, the FRET-ratio returned to the initial baseline within four minutes. The mean and sd of the final baseline was 5.68 $\pm$ 0.4. n = 34.

### 3.1.5 RCaMP1e: a red GECI

The use of GECIs has previously been limited by the lack of sensors with spectral characteristics other than in the green range. This was due to GECI all being based on one form or other of GFP. In 2011, Zhao et al. (2011) published a paper on the creation of the first GECI based on a red FP called R-GECO1. In 2013, we co-authored a paper describing a new red GECI called RCaMP1e, based on a circularly permuted mRuby FP (Akerboom et al., 2013). We found that compared to R-GECO1, RCaMP1e exhibited reduced photobleaching and no photoswitching, issues that complicates the usage of R-GECO1. Having access to a red GECI enables measurement of free-$Ca^{2+}$ together with many common green fluorophores and FPs used for labeling cells. Also, since most sensors are based on GFP in one form or another, red GECI can be used with these for dual readouts. Two examples of this are given in section 3.1.7 and figure 3.14. Further examples as well as spectra for one and two-photon excitation for RCaMP1e can be found in Akerboom et al. (2013).

Expression of RCaMP1e in primary cortical cell culture using AAV vectors with MOI of 3600 led to fluorescence under 590 nm excitation in approximately four days. This fluorescence could not be seen by eye and was only barely detectable with a Zeiss MRm charge-coupled device (CCD) camera at sub-second exposure times. The fluorescence increased upon further expression and at 7 DPT the fluorescence intensity was enough to be seen by eye and usable for $Ca^{2+}$-imaging experiments (sub-second exposure times). The intensity remained very weak compared to that emitted by D3cpV or GCaMP35. RCaMP1e exhibited very little photobleaching with this excitation and was usable for long term measurements. The sensor was not excluded from the nucleus as with D3cpV and GCaMP35, as seen by the lack of distinguishable nucleus in figure 3.7a.

#### Dynamic range of RCaMP1e

As for D3cpV (section 3.1.4), proper usage of RCaMP1e requires knowing the dynamic range of the sensor in the system were it is to be used. To test this, the cytosolic variant was expressed in neuronal primary cell culture using AAV and ionomycin was applied together with 10 mM $Ca^{2+}$, leading to equilibration of the 10 mM extracellular calcium concentration with the inside of the cell. This led to rapid saturation of the sensor which can be seen in figure 3.7c. The sensor signal was normalized by converting to $\Delta F/F_0$ and the maximum intensity increase over baseline measured was $351 \pm 19.6\%$. This was taken as the maximum

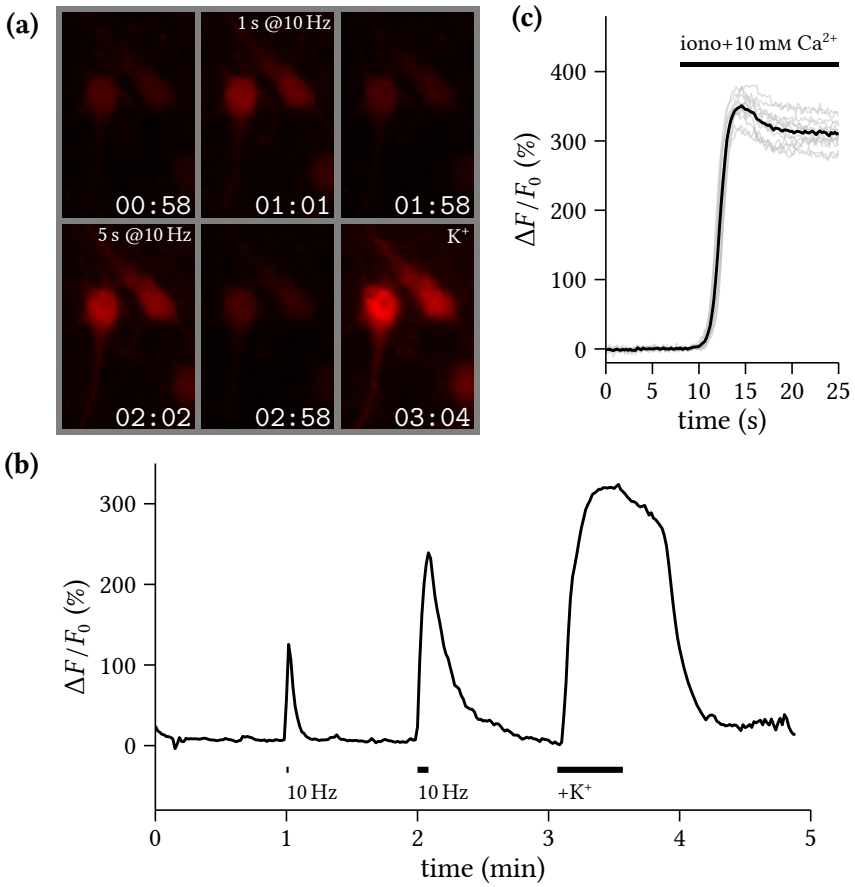


**Figure 3.7: Response of RCaMP1e to ionomycin+$Ca^{2+}$, high potassium and field stimulation** Primary cortical cell culture transduced with a AAV vector coding for cytosolic expression of the RCaMP1e red calcium sensor with a MOI of 1200. **(a)** Overview of a subset of cells from one imaged coverslip. FS applied for 1 s with 10 Hz at 1 min. FS applied again for 5 s with 10 Hz at 2 min. Neurons depolarized with high potassium at 3 min. The neurons recover between stimuli. **(b)** Trace from recording in (a) with one frame per second. Peak responses: $FS_{1s}$ = 113 ± 13.1, $FS_{5s}$ = 236 ± 16.8, KCl = 321 ± 25.3. n = 42. **(c)** Trace of response from RCaMP1e to treatment with 5 µM ionomycin and 10 mM $Ca^{2+}$. Max response: 351 ± 19.6. n = 12. Values are mean±standard deviation.

response of the sensor and was used as a upper limit of sensor range for further experiments.

### Response of RCaMP1e to FS

As described in section 3.1.4 for D3cpV, FS was used as a physiological stimuli leading to accumulation of $Ca^{2+}$ in the cytoplasm. In figure 3.7a,b, the typical response of RCaMP1e in the cytoplasm to 10 and 50 AP at 10 Hz is shown. Also shown is the response to depolarization

with 64 mM $K^+$ for 30 s. The peak influx after high potassium depolarization was 323 ± 25.3, close to the maximum of about 351 meaning the sensor is close to saturation with this type of stimuli. FS at 10 Hz on the other hand produced responses both with 10 and 50 AP that were in the middle of the sensor range (113 ± 13.1 and 236 ± 16.8 respectively).

### Response of RCaMP1e targeted to the mitochondria

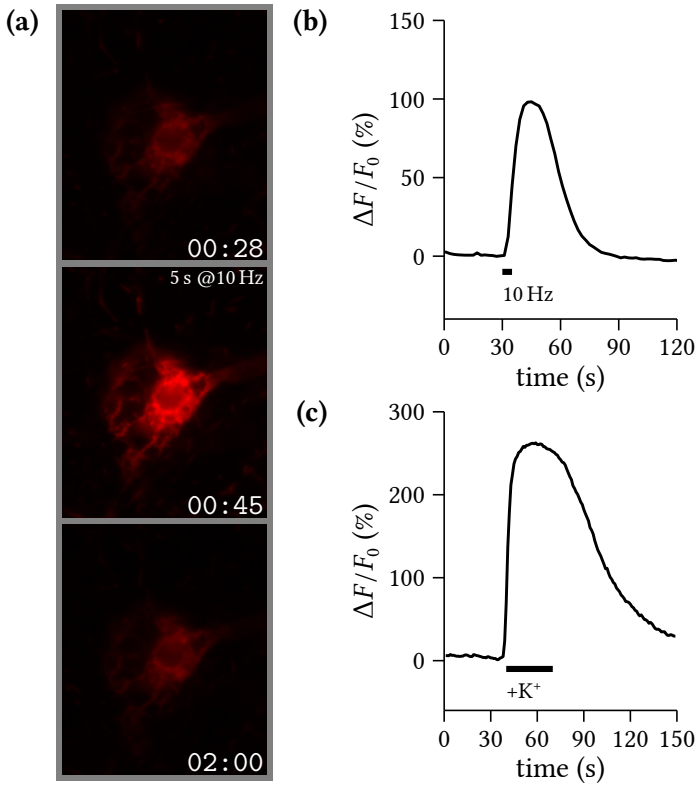


**Figure 3.8: Response of mtRCaMP1e to field stimulation and high potassium depolarization** Primary cortical cell culture transduced with a AAV vector coding for mitochondrial expression of the RCaMP1e red calcium sensor with a MOI of 600. **(a)** Images of a typical cell. Cell at rest (top image). FS applied again for 5 s with 10 Hz (middle image). Recovery of the cell one and a half minute after application of stimuli. **(b)** Trace from recording in (a) with one frame per second. Peak response: $FS_{5s}$ = 94.2 ± 18.9. n = 19. **(c)** Typical trace from a neuron expressing mtRCaMP1e that has been depolarized with 64 mM $K^+$ for 30 s. Peak response: $K^+$ = 263 ± 21.7. n = 16. Values are mean±standard deviation.

RCaMP1e was targeted to the mitochondria using a single copy of the MTS (mtRCaMP1e). The targeting was specific as expected for a circularly permuted single FP sensor. The fluorescence intensity was higher when expressed in the mitochondria compared to the cytosol

and imaging could be done with lower excitation light intensities. Both FS and high potassium stimuli was tested with this variant of the sensor and typical traces are presented in figure 3.8. Upon a stimuli of 50 AP, calcium was accumulated in the mitochondria and the fluorescence intensity of the sensor increased. The intensity readout was normalized by converting to $\Delta F/F_0$ and the peak increase was measured to be approximately $94.2 \pm 18.9$. The peak fluorescence intensity increase upon 30 s depolarization with 64 mM $K^+$ was higher at $263 \pm 21.7$.

This shows that also for the mitochondrially targeted variant of RCaMP1e, a stimulus of 50 AP at 10 Hz was enough to evoke a robust response but did not saturate the sensor. The high potassium response on the other hand was lower than in the cytosol but since the absolute range of RCaMP1e in the mitochondria is unknown, the response from high potassium depolarization was regarded as at least close to saturating.

- The baseline fluorescence of RCaMP1e is weak, especially in the cytosol
- The max $\Delta F/F_0$ measured for RCaMP1e in the cytosol was ~351%
- The response to high potassium depolarization reached a $\Delta F/F_0$ of ~321% which was close to saturation
- FS at 10 Hz never saturated the sensor
- Targeting to the mitochondria was efficient using only a single copy of the MTS
- The response of RCaMP1e in the mitochondria to FS was far below saturation

Using FS at 10 Hz as a stimuli, it is possible to use *RCaMP1e* both in the cytosol and the mitochondria for sensitive measurement of relative differences in calcium influx.

### 3.1.6 Genetically encoded ATP sensor

Measuring ATP levels in cells has previously been a difficult process involving biochemical methods on cell/tissue lysates or through measuring the consumption of ATP by luciferase bio-luminescence (Fukuda et al., 1983; Ainscow et al., 2002; Mironov, 2007). Recently, a FRET based sensor called ATeam1.03 that can report on changes in intracellular ATP was created by Imamura et al. (2009). At the time of writing this thesis there had only been a few publications were the usage of this sensor was described and none of those covered the calibration in neurons. For this reason a slightly longer description of the findings with this sensor will follow. The best scenario for a sensor would be to be able to accurately measure absolute levels of whatever the sensor is responsive to. To accomplish this the sensor needs to respond linearly in the range of ligand concentrations that one hopes to measure. The ATeam1.03 sensor is engineered to show differences in ATP concentrations between $1 \times 10^{-4}$ and $1 \times 10^{-2}$ mM and can be used to monitor the dynamics of ATP changes with rates up

to 0.1 $s^{-1}$. This makes it suitable for measurements of cytosolic ATP concentrations that according to the literature lie within this concentration range (Veech et al., 1979; Fukuda et al., 1983; Ainscow et al., 2002; Mironov, 2007).

### In cell calibration of ATeam1.03

In order to determine absolute intracellular ATP concentrations using a sensor such as ATeam1.03, the intracellular response of the sensor to different known ATP concentrations must be determined. This requires access of extracellular ATP to the cytosol of the cell. A chemical such as β-escin which perforates the plasma membrane can be used for this purpose. Application of β-escin creates pores in the plasma membrane through which intracellular ATP will leak out as we have previously shown (Mollajew et al., 2013). After flushing out the ATP from the cell, the zero level or min response of the sensor can be determined. Next, through perfusion one can add different known ATP concentrations to the extracellular media that will then flood the cell through the pores created by β-escin. This was done for the primary cortical cell cultures used throughout this thesis.

The calibration experiment was conducted as follows. At first, β-escin was applied to perforate the cell. Different concentrations and application times for β-escin was tested before settling on 20 µM applied for 2 min. This was the lowest concentration and shortest time possible that ensured reproducible and complete depletion of ATP (as reported by sensor). Once perforated, the neurons stayed permeable until the nuclear membrane would disintegrate, visible by the appearance of sensor fluorescence in the previously dark and clearly distinguishable nuclear region. This meant that it was not necessary to continue β-escin application after 2 min. With the 20 µM concentration, at least 10 min would progress before the neurons changed morphology or the nuclear membrane became permeable. After reaching the minimal level, different ATP concentrations were applied. The published value for $K_d$ for the sensor is 3.3 mM (Imamura et al., 2009) and the ATP concentrations (1.1, 3.3 and 10 mM) applied during the calibration were chosen based upon this. Going from one concentration to three times higher, such as going from 1.1 mM to 3.3 mM took ~2 min before reaching a new stable baseline of the FRET ratio. Thus, 1.1 mM ATP was applied for 2 min, then 3.3 mM ATP and finally 10 mM which according to Imamura et al. (2009) should fully saturate the sensor.

A typical trace of the normalized ratio, FRET ratio, FRET and cyan fluorescent protein (CFP) readouts from the sensor is given in figure 3.9a. The FRET ratio which was calculated from

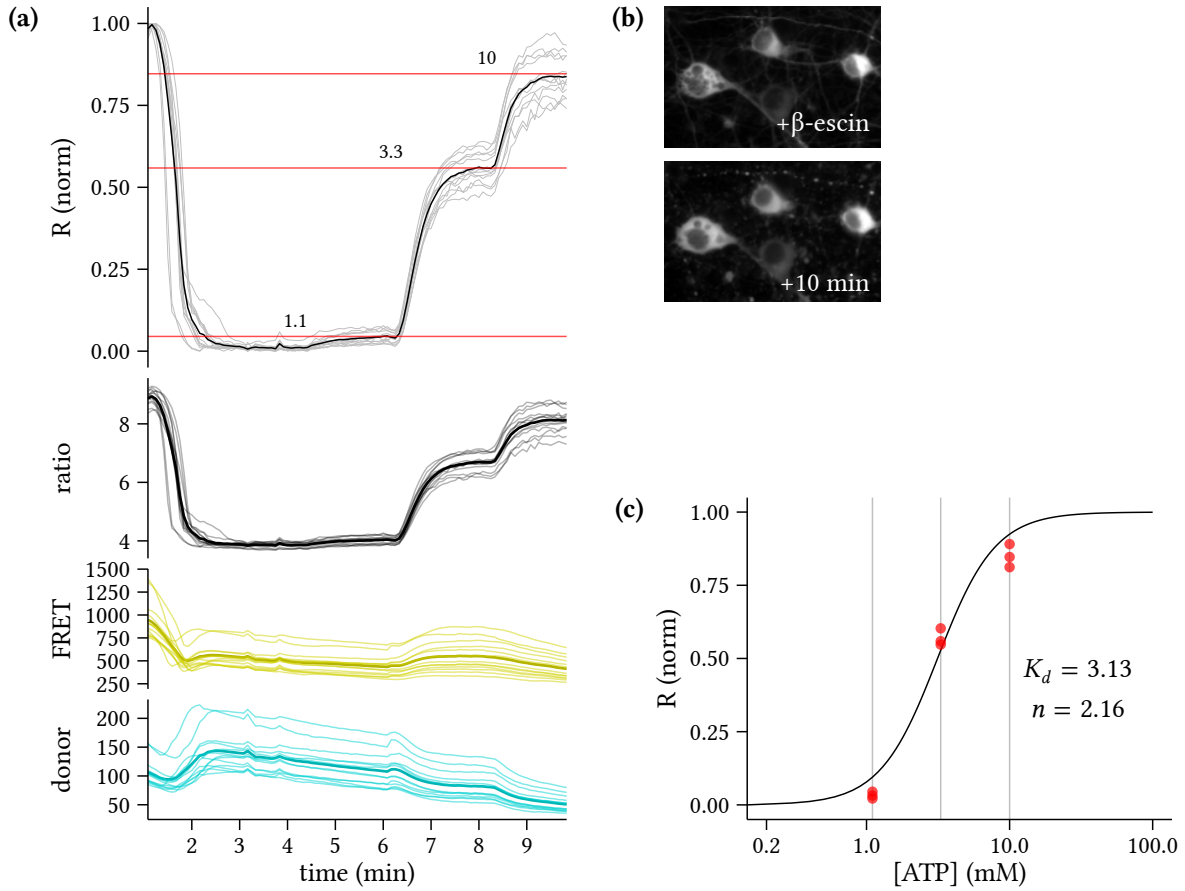


**Figure 3.9: Calibration of ATeam1.03 with the perforator β-escin**
Primary cortical cell culture transduced with a AAV vector coding for cytosolic expression of the ATeam1.03 ATP sensor with a MOI of 2400. The neurons were imaged at 7 DPT and a time-lapse captured with one frame per five seconds. **(a)** Traces of a typical calibration experiment. 20 µM β-escin is first applied for 2 min to perforate the plasma membrane. ATP is then rapidly flushed from the cells leading to a decrease of the FRET/CFP ratio ((a), second panel). ATP with three different concentrations are then applied in sequence flooding the cells with ATP leading to a stepwise increase in the FRET/CFP ratio. The max and min values measured from the sensor are used to normalize the ratio between 0 and 1 ((a), top panel). The maximum ratio is present before application of β-escin and with 10 mM ATP (max of sensor range) it does not recover to that level. This suggests that something happens to the sensor or the intracellular environment during the calibration, invalidating the results. n = 13. **(b)** Typical appearance of neurons at the moment of β-escin application and 10 min later. **(c)** Hill-plot of the applied ATP concentrations versus sensor ratio response from three replicates of the measurement in **(a)**. The function $r = \frac{[\mathrm{ATP}]^n}{\mathrm{K_d}^n + [\mathrm{ATP}]^n}$ was fit to the measured values using non-linear regression. The fitted values for the two parameters, $K_d$ and $n$ (hill-coefficient) were 3.13 and 2.16 respectively with residual standard error $\sigma = 0.0742$.

the background subtracted FRET (acceptor) channel intensity divided by the background subtracted CFP (donor) channel intensity was normalized between 0 and 1 using the maximum and minimum FRET ratio from the trace. As is evident from the figure, the FRET ratio present in the beginning of the experiment before application of β-escin was never reached upon reapplication of ATP. 10 mM ATP should saturate the sensor but to make sure, 100 mM ATP was tried as well but this did not increase the FRET ratio.

Figure 3.9c shows the FRET ratios at the steady-state for each ATP concentration from three different such experiments plotted with the applied ATP concentration on the x-axis and the measured FRET ratio on the y-axis. Using non-linear regression, the equation:

$$R_{\mathrm{N}} = \frac{[\mathrm{ATP}]^n}{\mathrm{K_d} + [\mathrm{ATP}]^n}$$

where $R_{\mathrm{N}}$ represents the normalized FRET ratio and [ATP] the ATP concentration, was fit to the measured min, max 1.1, 3.3 and 10 mM ratio values. This gave values for the parameters $\mathrm{K_d}$ and $n$ which represents the dissociation constant and hill-coefficient respectively. These were, $\mathrm{K_d} = 3.13$ mM and $n = 2.16$ which corresponded well with the already published values of $\mathrm{K_d} = 3.3$ mM and $n = 2.1$ for ATeam1.03 (Imamura et al., 2009).

Using this calibration curve to calculate ATP concentrations from the FRET ratio, one get cytosolic ATP concentrations in resting cells that range to above 10 mM which seems unlikely considering previously published values that range up to ~3 mM in neurons at rest (Fukuda et al., 1983; Ainscow et al., 2002; Mironov, 2007). As can be seen in the figure, the points for both 1.1 and 10 mM lie under the fitted line. Also, the distance between 1.1 and 3.3 mM and 3.3 and 10 mM is clearly not what it should be with a $\mathrm{K_d}$ of ~3.3 mM, where 3.3 mM would be right in the middle of the sensor range. Together with the observation that it was not possible to return to the FRET ratio observed before applying β-escin, this suggests that the calibration is not reliable. Since we are changing the intracellular environment, it is possible that this is changing the properties of the sensor, making the FRET ratio seen after perforation meaningless. Different $Ca^{2+}$ and $Mg^{2+}$ concentrations ranging between 0 and 10 mM and pH between 3 and 9 was tried but with similar results. Replacing β-escin with saponin or digitonin, two other perforators, also did not succeed in returning the FRET ratio to initial levels upon application of 10 mM or higher ATP concentrations. It might also have been the case that perforation/permeabilization leads to intracellular changes that alter the properties of the sensor only after some time. To test whether this was the case, β-escin and 10 mM ATP was applied together to intact cells, but also this did not raise the FRET ratio

above the initial baseline. Because of these inconsistencies, the calibration of ATeam1.03 in this way was abandoned.

### Calculating ATP concentration based only on minimum level

Carbonyl cyanide 4-(trifluoromethoxy)phenylhydrazone (FCCP) is a chemical decoupler of mitochondria that works by facilitating the rapid transport of protons across membranes (Benz and McLaughlin, 1983). This leads to a complete removal of the proton gradient over the mitochondrial inner membrane within seconds. One of the effects of this is the complete inhibition of oxidative phosphorylation and ATP production by the mitochondria. When 2 µM FCCP was administered to neurons expressing ATeam1.03, the cytosolic ATP concentration could be seen to deplete (see section 3.1.6). When a stimuli was applied together with FCCP that increased the need for ATP by the cell, this reduced the FRET ratio to the same low level as after 2 min of β-escin application. See figure 3.10 for the comparison of FCCP and β-escin application. This suggested that ATP was completely depleted and gave a simple, fast and effective way of measuring the zero level of ATP within the cell without the need for perforating agents.

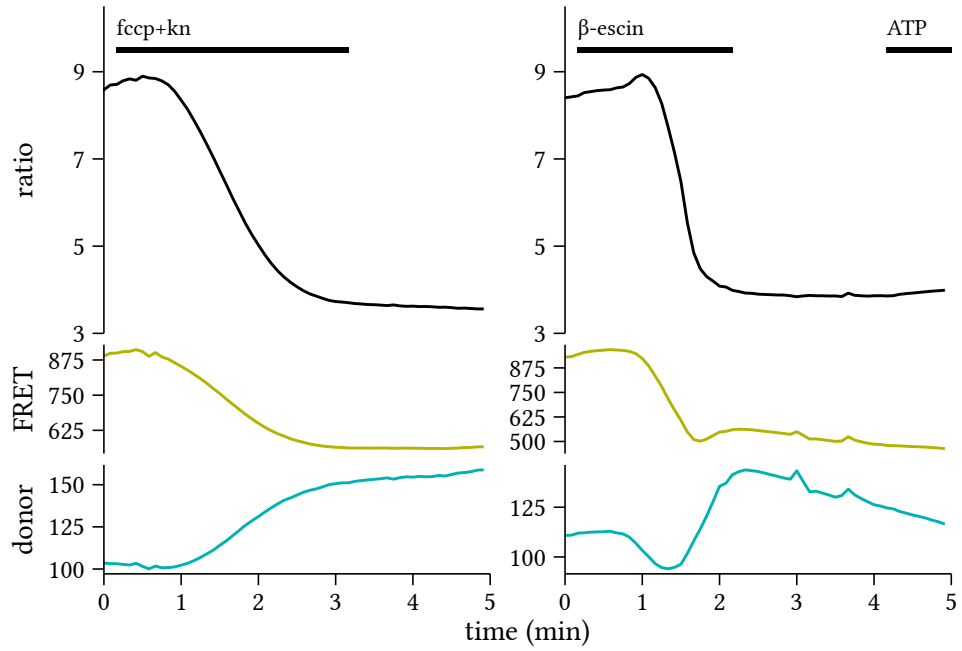


**Figure 3.10: FCCP application depletes cytosolic ATP to minimal levels**
Typical trace following the application of 2 µM FCCP together with 30 µM kainate to primary neurons expressing ATeam1.03 from AAV (left panel). Compared to the trace from β-escin application (right panel), FCCP depletes cytosolic ATP to the same levels.

ATP concentrations could then be calculated by using the min/zero level FRET ratio from FCCP depletion of ATP and values from the literature by rearranging the following equation:

$$R = R_{min} + \frac{(R_{max} - R_{min})[\mathrm{ATP}]^2}{\mathrm{K_d^2} + [\mathrm{ATP}]^2}$$

into:

$$[\mathrm{ATP}] = \mathrm{K_d}\sqrt{\frac{r-1}{R_{max}/R_{min} - r}}$$

where $\mathrm{K_d} = 3.3$ and $R_{max}/R_{min} = 2.3$ (Imamura et al., 2009) and $R/R_{min}$ has been substituted for $r$, representing the relative FRET ratio (change from min level). For simplicity, this assumes a hill-coefficient of 2 (2.1 according to Imamura et al. (2009)).

Figure 3.11a shows the FCCP trace from figure Figure 3.10 converted to ATP mM values using this equation. The resting ATP levels are once again outside the range reported in the literature for neurons and are close to the theoretical saturation of the sensor.

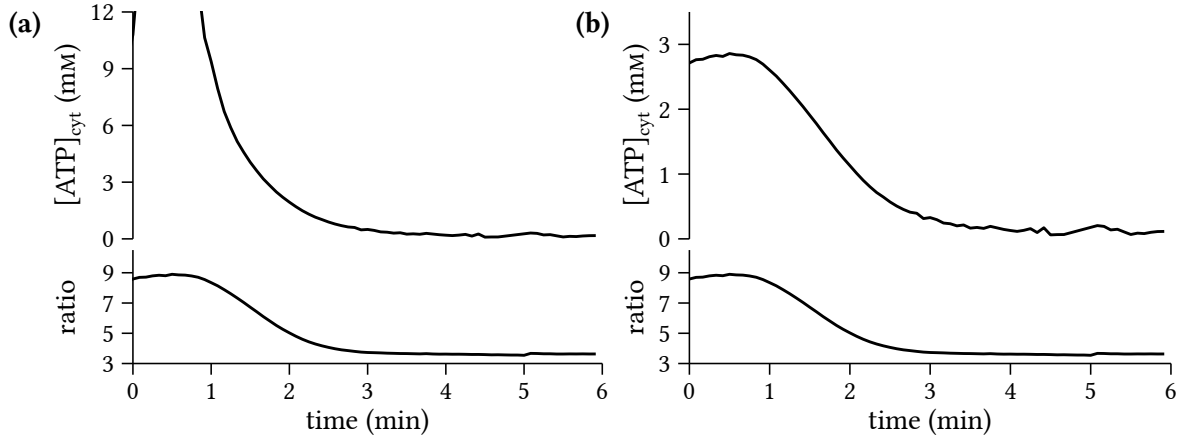


**Figure 3.11: Conversion of FRET ratio into ATP concentrations**
Part of the FRET ratio trace resulting from applying FCCP together with 30 µM kainate to primary cortical cell cultures expressing ATeam1.03 using a AAV vector. **(a)** The FRET ratio has been converted to ATP concentrations using 2.3 as a value for $R_{max}/R_{min}$. **(b)** The FRET ratio converted to ATP concentrations using 3.2 instead of 2.3 for $R_{max}/R_{min}$. This gives a range of ATP concentrations closer in line with values from the literature.

If an $R_{max}/R_{min}$ of 3.2 was used in the equation instead, the resting ATP concentrations came out as ~3 mM, see Figure 3.11a. It is perhaps possible that the neurons in the cultures used for this thesis have very high resting ATP levels, perhaps due to conditions of the growth media. To compare the ATP levels with another cell, hippocampal primary cell culture from mice pups kindly provided by Nicole Hartelt, were transduced with the AAV coding for ATeam1.03 but the same FRET ratio range was acquired with these cultures. More likely there is some-

thing else that changes the properties of the sensor from those published by Imamura et al. (2009) when expressed in neurons. Since relative levels were sufficient and determining absolute ATP levels was not within the scope of this thesis, no further attempts were made to find the root of these issues. For the rest of the experiments described below, an $R_{max}/R_{min}$ of 3.2 was used in calculations of ATP concentrations. The choice of 3.2 was made purely in order to have the calculated ATP concentration within a range that is known from previous measurements of ATP levels in neurons (Veech et al., 1979; Fukuda et al., 1983; Ainscow et al., 2002; Mironov, 2007).

### Rates of ATP decrease and regeneration after uncoupling of mitochondria

Even without having access to absolute ATP concentrations through the ATeam1.03 sensor, it can be useful in measuring relative levels that can be compared between cell types and different treatments of cells.

As was seen in figure 3.10, FCCP depleted cytosolic ATP when applied together with kainate. The same was true for FCCP alone, but with a slower rate of depletion. This was used to study the rate of consumption of ATP by neurons when there was no regeneration of available ATP by oxidative phosphorylation in the mitochondria. When the FCCP was washed out, the mitochondria was able to restore its membrane potential and resumed ATP production. This lead to complete recovery of the FRET ratio readout from the sensor, indicating that ATP production through oxidative phosphorylation was restored. The slopes of the falling and rising parts of the FRET ratio after first applying and then washing out of FCCP was used as measures for the rate of consumption and regeneration of ATP in neurons.

In figure 3.12 a typical experiment where the consumption and regeneration rates were quantified is shown. Neuronal cell cultures were transduced with a AAV coding for the expression of ATeam1.03 three days after preparation. Experiments were done seven days after transduction. An experiment was typically conducted as follows. Some frames were captured of the neurons at rest to establish the initial baseline FRET ratio. Then, 2 µM FCCP was applied for 3 min which resulted in slow reduction in ATP levels. The FCCP was then washed out which resulted in recovery of the FRET ratio.

FCCP was then reapplied to the same cells but this time together with a stimuli that requires consumption of ATP. In the figure, 10 µM kainate was used. This again resulted in depletion of ATP but this time with a higher rate. After again washing out the FCCP, the ATP recovered completely and with a higher rate than during the depletion.

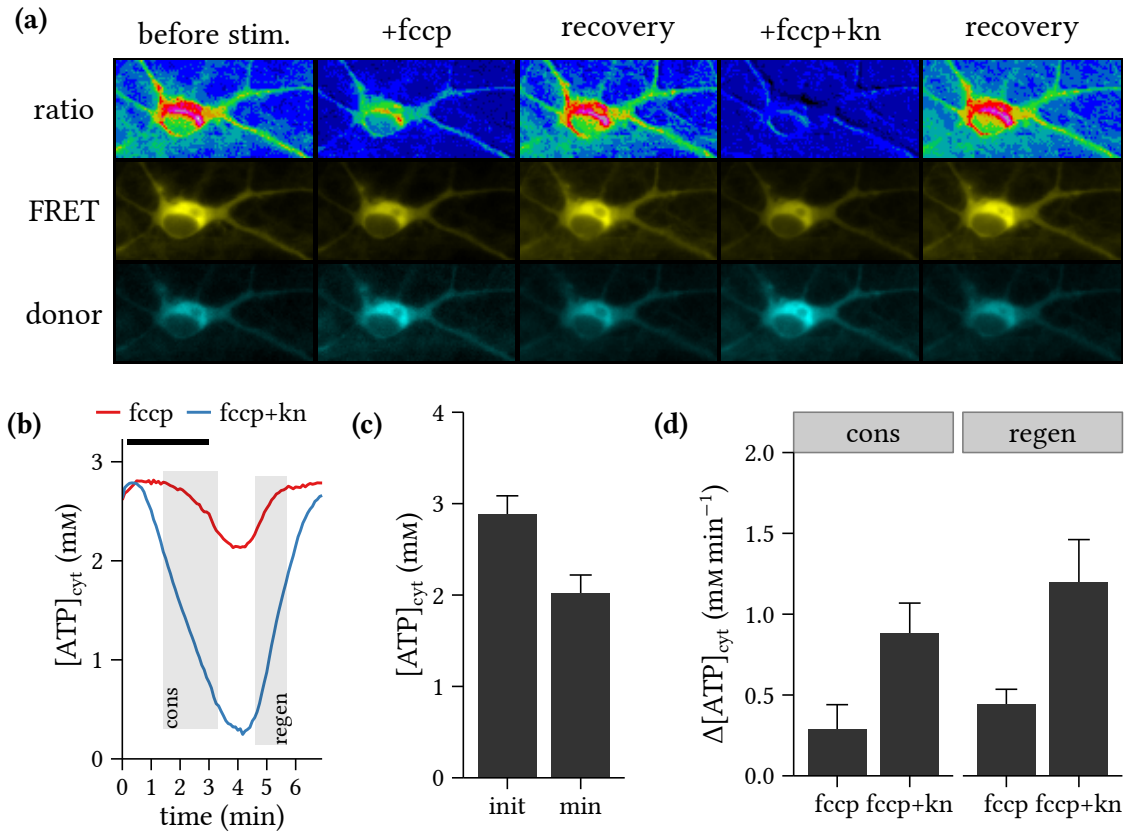


**Figure 3.12: Difference in rate of ATP consumption at rest and during activity**
Primary cortical cell culture transduced with a AAV vector coding for cytosolic expression of the ATeam1.03 ATP sensor with a MOI of 2400. The neurons were imaged at 7 DPT with one frame captured every five seconds. **(a)** Overview of the typical response of one neuron to stimulation and recovery of 2 µM FCCP and 2 µM FCCP+10 µM kainate applied in succession. (top) A lookup table (LUT) applied to the grayscale values of the ratio image to visualize the local and temporal differences in FRET ratio. FRET ratio calculated by dividing the FRET channel (middle row) with the CFP channel (bottom). (before stim. ) initial part of fccp trace similar to that in (b), (+fccp) lowest point of fccp trace, (recovery) initial part of fccp+kn trace, (+fccp+kn) lowest point of fccp+kn trace, (recovery, second) end of fccp+kn trace. **(b)** Typical traces of the average response from all cells of one coverslip treated as in (a). Shaded areas represent the parts of the traces used for determining the consumption and regeneration rates respectively. **(c)** Quantification of the initial and min measured ATP concentrations. $init = 2.91 \pm 0.242$ and $min = 2.02 \pm 0.201$. **(d)** Quantification of consumption and regeneration rates (slope of falling and rising parts of trace, shaded regions). $cons_{\text{fccp}} = 0.288 \pm 0.152$ , $prod_{\text{fccp}} = 0.445 \pm 0.0906$ , $cons_{\text{fccp+kn}} = 0.884 \pm 0.184$ and $prod_{\text{fccp+kn}} = 1.2 \pm 0.265$.

If FCCP was applied a third time, now again without kainate, ATP once more depleted slower than with FCCP and kainate together but significantly faster than the first time. This suggested that there was some residual effect from the first two applications that made the requirement for ATP higher than before any stimuli with kainate. This was true also if the order of the applications were reversed, with FCCP+stimuli applied before only FCCP. In any case, applying FCCP alone always resulted in slower rate of decrease than FCCP+stimuli. For all further experiments, the order of applications were FCCP alone then FCCP+stimuli.

When the consumption and regeneration rates from FCCP and FCCP + 10 µM kainate experiments were quantified (figure 3.10d), both consumption and regeneration rates were consistently higher when kainate was administered together with FCCP. Interestingly, the regeneration rate after washout of FCCP was consistently higher than the measured consumption rate. This shows that the neuron has a large potential to increase its ATP production in response to increased energy requirements. Please see section 3.1.6 for more results with different stimuli.

Kainate activates the kainate receptor, a ionotropic glutamate receptor channel (Huettner, 2003). This depolarizes the neuron leading to influx of sodium but also calcium (Lerma et al., 2001; Mollajew et al., 2013). Both sodium and calcium is then removed from the cytosol in ATP dependent processes. Sodium over the plasma membrane (PM) via the $Na^+/K^+$-ATPase (Howarth et al., 2012) and calcium over the PM via plasma membrane $Ca^{2+}$-ATPase (PMCA) or into endoplasmic reticulum (ER) via sarco/endoplasmic reticulum $Ca^{2+}$-ATPase (SERCA) (Nicholls, 1986). These are the same processes involved in recovering the resting membrane potential after synaptic firing and as such, kainate application is emulating the state that intense firing sets the neurons in. The difference between the rate of ATP consumption between kainate stimulated and non-stimulated cells can then be seen as a measure of the difference in ATP requirement by a neuron that is being activated and one which is at rest.

Applying only kainate, that is, without simultaneous application of FCCP, at up to 30 µM did not reduce ATP in cell cultures as measured by ATeam1.03. This makes sense considering that the regeneration rate was always higher than the consumption rate and suggests that increases in oxidative phosphorylation can immediately compensate for increased ATP requirements of the neuron.

### ATP consumption and regeneration with different stimuli

Figure 3.13 shows the results from experiments with different stimuli applied together with FCCP. These other stimuli are compared with 10 µM kainate (blue trace) or no stimuli (red trace).

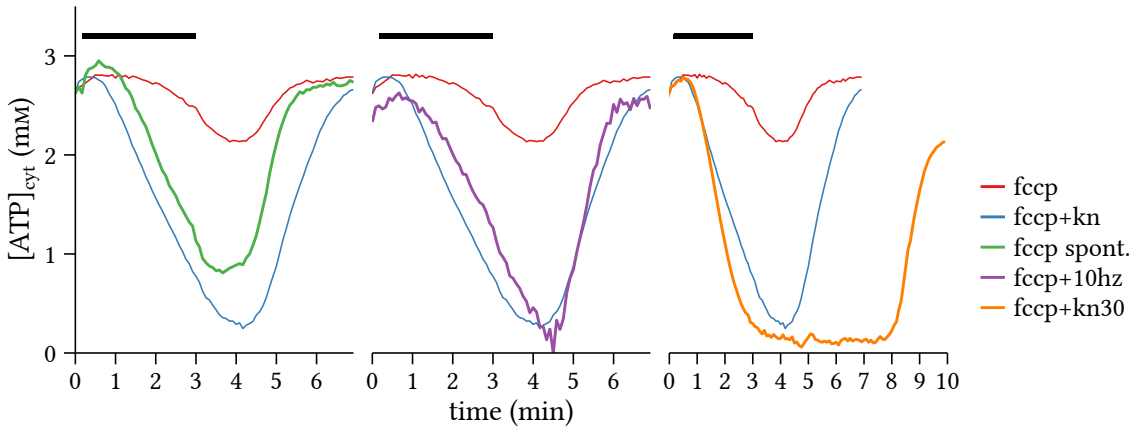


**Figure 3.13: Differences of rates in response to different stimuli**
Primary cortical cell culture transduced with a AAV vector coding for cytosolic expression of the ATeam1.03 ATP sensor with a MOI of 2400. Neurons imaged at 7 DPT with one frame captured every five seconds. Comparison of different treatments that together with decoupling of oxidative phosphorylation in the mitochondria with FCCP depletes cytosolic ATP. Treatments are compared to those of applying only FCCP (red) and FCCP+10 µM kainate (blue). **(green)** More pronounced/faster ATP consumption in subpopulation of cells treated with only FCCP. Increased regeneration rate after washout of FCCP with complete recovery at same time as cells with much smaller decrease. **(purple)** The rate of consumption and regeneration is similar in neurons stimulated with 10 Hz FS to that of 10 µM kainate. **(orange)** Increasing the concentration of kainate to 30 µM increases the rate of ATP consumption. The rate of ATP consumption is still lower than the rate of regeneration after washout of FCCP. Rate of regeneration is the same but the time to recovery is significantly delayed. Results based on observations of at least 10 neurons per stimuli type.

The first panel (green trace) shows what happened in a subset of neurons, where applying FCCP without kainate produced a much more pronounced depletion of ATP than expected for a resting neuron. The rate of consumption was also higher, similar to the rate seen when 10 µM kainate was applied. The rate of regeneration in this subset of cells was also increased and they recovered the original baseline faster than with 10 µM kainate. It is possible that these cells represent neurons that are for some reason spontaneously active, and therefor have a higher rate of consumption of ATP than the average cell.

The middle panel (purple) of the figure shows a typical trace where the stimuli was 10 Hz FS. The consumption and regeneration rates were both very similar to those with 10 µM kainate.

Complete recovery of cytosolic ATP also occurred at a similar time point.

The last panel (orange) shows what happened when the kainate concentration was increased from 10 to 30 µM. The consumption rate increased and there was a longer delay before recovery of the ATP began. The rate with which it eventually recovered was the same as for the other stimuli but there was no complete recovery. Instead the ATP level returned to a lower baseline level.

This shows that the ATeam1.03 sensor can report on differences in consumption and regeneration rates of ATP after decoupling and recoupling of oxidative phosphorylation and that the rates reported when applying stimuli such as 10 µM kainate or 10 Hz FS are comparable to rates that occur in cells that have no artificial stimuli applied. It also shows that the regeneration rate after depletion is related to the amount of depletion since there are differences in the rate of regeneration after small depletions (~0.5 mM) compared to larger ones (> 2 mM). But it also shows that when the depletion is larger, the ATP levels regenerate with the same high rate no matter what stimuli was used or how big the change from the initial ATP level was. This suggests that this is the maximum rate of ATP production that is available to the cell from oxidative phosphorylation. In all cases, this was still faster than the rate of consumption, meaning that none of these stimuli would be able to deplete ATP without the addition of FCCP in these primary neuronal cell cultures.

- ATeam1.03 is suitable for measurements of relative ATP levels within neurons
- *In cell* calibration of ATeam1.03 gave values for $K_d$ and hill-coefficient that corresponded with values from literature but it was not possible to recover the initial ratio baseline by application of ATP
- Decoupling of the mitochondria depleted ATP from neurons
- This allowed measuring the rate of consumption of ATP as well as the regeneration rate after washing out of FCCP
- Applying a stimuli such as kainate together with decoupling increased the rate of ATP consumption ~3-fold
- The rate of production of ATP through oxidative phosphorylation increased in response to the increased rate of depletion
- This regeneration rate was always higher than the consumption rate

### 3.1.7 Simultaneous use of two sensors

Since most GESs are based on GFP, they have spectral overlap that prevents using them together at the same time. Even sensors based on CFP or yellow fluorescent protein (YFP) have large enough overlap to make it difficult to use them together. Spectral imaging and

unmixing (Zimmermann et al., 2003) can help with this issue but due to the changes in spectra and intensity that is the basis for the readout of a sensor, this can become difficult. Preferable then, are GESs with spectra that can be completely separated from those of GFP already at the detection stage using optical filters.

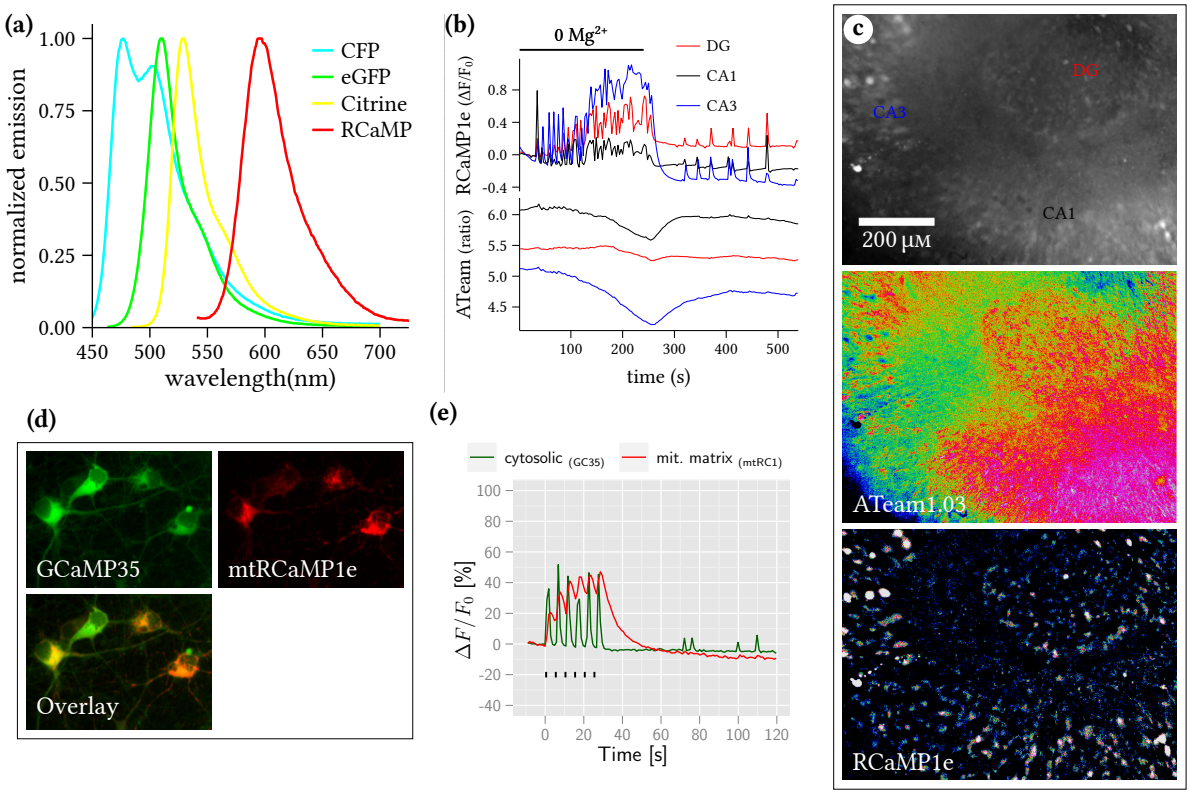


**Figure 3.14: Simultaneous use of two sensors**
**(a)** Emission spectra from CFP, GFP, Citrine (YFP variant) and RCaMP1e. A significant part of even the YFP peak does not overlap with that of RCaMP1e. Conversely, RCaMP1e can be isolated from YFP and the other GFP based peaks, albeit with some loss of signal. **(b,c)** Organotypic slice cultures of mice hippocampus transduced with two AAV vectors expressing RCaMP1e and ATeam1.03. (b) Removing $Mg^{2+}$ from the media induced epileptiform activity throughout the slice through activation of NMDA receptors as recorded with RCaMP1e. This was accompanied by localized ATP depletion, recorded from ATeam1.03. (c) Overview of the slice from (b). Top: brightfield. Middle: ATeam1.03 FRET/CFP ratio. Bottom: RCaMP1e $\Delta F/F_0$, background subtracted. The images are from before the removal of $Mg^{2+}$. **(d,e)** Primary cortical cell culture transduced with AAV vectors expressing GCaMP35 and mitochondrially targeted RCaMP1e. (d) Overview of four cells on a coverslip. Individual channels and overlay as labeled. (e) Trace of the response when FS was applied six times with 10 Hz and a duration of 1 s with 4 s pause. The $Ca^{2+}$ buffering of the mitochondria is illustrated by the saturation and prolonged decay of the mtRCaMP1e response (red) compared to the cytosolic GCaMP35 (green).

### GCaMP35 with RCaMP1e expressed in the mitochondria

RCaMP1e provides a GECI for such applications and in section 3.2.6 results are shown from experiments where RCaMP1e was used together with GFP labeling for identification of transduced cells. It was also possible to use RCaMP1e together with GCaMP35, another GECI which is based on GFP. Primary cortical cell culture was transduced with AAV vectors coding for the expression of GCaMP35 (AAV6-s-GCaMP3.5-WB) and mitochondrially targeted RCaMP1e. This produced separable emission such as in figure 3.14d. These cultures were electrically stimulated using FS at 10 Hz for 1 s multiple times with 4 s pause in between. The cytosolic free-$Ca^{2+}$ as reported on by GCaMP35 recovered between every stimuli but the mitochondrial free-$Ca^{2+}$ as reported by mtRCaMP1e did not. There was increasing saturation and prolongation of the decay of the mitochondrial free-$Ca^{2+}$ (figure 3.14e). This illustrates the calcium buffering capability of the mitochondria after accumulation of cytosolic free-$Ca^{2+}$.

### RCaMP1e together with ATeam1.03 in organotypic slice cultures

It was also possible to use RCaMP1e together with CFP/YFP FRET based sensors. As can be seen in figure 3.14a, the spectra of RCaMP1e and Citrine, a YFP variant, overlaps, but there are portions of both spectra that gives very little bleed through. Typical ATP responses measured by this sensor like those described in section 3.1.6, are slow in comparison to the fast changes in $Ca^{2+}$ recorded in firing neurons and thus operate on different timescales. This makes the results from experiments were RCaMP1e have been used with ATeam1.03 easily interpretable even if there is some bleed through present. For highly sensitive applications, where very small changes in ATP needs to be separated from large changes in $Ca^{2+}$ or vice-versa, proper controls should be done were each sensor is present by itself and the bleed through in each channel is recorded and subtracted.

Organotypic slice cultures of mice hippocampus were prepared and cultured on millipore membranes. The slices were transduced with AAV vectors coding for the expression of RCaMP1e and ATeam1.03 by putting a droplet (~2 µL) of virus mixture diluted in PBS directly on top of the slice. After about one week there was robust expression of both sensors as seen with the fluorescence microscope. In figure 3.14c an overview with labeled regions of a transduced hippocampal slice is shown.

The slices were imaged on an Zeiss Examiner microscope stage with Colibri LED illumination. A slice was cut out from a larger piece of millipore membrane and placed in the imaging chamber of the microscope. The slice was then superfused with aCSF-H. When $Mg^{2+}$ was removed from the superfusion solution, epileptiform activity appeared throughout the slice as seen from the changes in free-$Ca^{2+}$ reported by RCaMP1e. The activity was synchronized throughout the slice and it disappeared when $Mg^{2+}$ was readministered. If $Mg^{2+}$ was removed for extended times, more than 2 min, ATP was seen to start to deplete in regions of the slice. This depletion was most pronounced in the CA1 and CA3 regions with almost no detectable decrease of ATP present in the DG region as reported by ATeam1.03. After readministration of $Mg^{2+}$ the ATP recovered. An example trace of $Mg^{2+}$ removal is shown in figure 3.14b.

- Using the novel red GECI RCaMP1e it is possible to have dual readouts in one experiment using optical separation of signals
- RCaMP1e can be used together with GFP based sensors as well as FRET sensors using the typical CFP/YFP pair

## 3.2 Comparisons of overexpression of α-, β-, γ-Synuclein

As was laid out in section 1.1, Parkinson's disease (PD) is characterized by the appearance of Lewy bodies that consist in large part of the small soluble protein αS. This establishes a connection between αS and PD. Evidence that αS is relevant for the disease comes from the observation that several familial point mutations in SNCA (PARK1), the gene coding for αS causes early onset of PD. The mechanisms linking αS to PD are still not properly understood. αS has been shown to associate with isolated membranes and make membranes permeable to ions. Pore like structures have been observed in electron migrograph images of αS. A proposed method of action for the detrimental properties of αS would then be that it interferes with ion homeostasis.

αS has also been shown to accumulate in mitochondria where its uptake can be prevented by blocking import channel proteins. In isolated mitochondria exposed to αS, reduced activity of complex I of the electron transport chain (ETC) and an increase in the production of reactive oxygen species has been measured.

With the help of fluorescent GESs, tools that have been developed over the last couple of years, I wanted to study the effects of overexpression of αS in primary neuronal cell culture. Previous studies on the pathological function of αS has been done either using biochemical methods on cell lysates, in isolated systems such as mitochondria or in cell lines derived from tumors. This is to my knowledge the first time that a study that uses different GESs has been carried out to study the effects of αS directly in neurons.

During the work for this PhD-thesis our group discovered that βS, a protein closely related to αS encoded by the SNCB gene, has toxic effects similar to those of αS (Taschenberger et al., 2013). Previously, βS had been assumed to have a protective role in the pathogenesis of PD due to having been shown to reduce toxicity of αS when both proteins are present together. Because of this finding, I introduced βS and γS into this study of α-Synuclein. Several of the findings presented here are published in Taschenberger et al. (2013).

### 3.2.1 Expression of synucleins using AAV vectors

For neuron specific expression of αS, βS, or γS in neuronal cell cultures, two different types of AAV vector constructs were used. The first was the same hSyn controlled construct as used for the construction of GES as described in section 2.5 but with the sensor insert replaced with the gene coding for the corresponding human synuclein. These were:

- AAV6-s-aSynWT-WB coding for human wild type (WT) αS
- AAV6-s-bSynWT-WB coding for human WT βS
- AAV6-s-gSynWT-WB coding for human WT γS

For the experiments employing these constructs, a control vector called AAV6-3TB-EWB was used to assess the toxicity of the AAV vector itself. This vector had the promoter replaced with triplicate transcription blocker regions that prevented transcription of its insert (Maddalena, 2012).

The second type of construct was a bicistronic variant of the first. In it the hSyn was repeated after the synuclein and woodchuck hepatitis virus (WHP) posttranscriptional regulatory element (WPRE) and a second gene in the form of GFP was added after it. This ensured expression of both synuclein and GFP in cells that were transduced with this vector. These vector constructs were:

- AAV6-s-aSynWT-SEIS-WB coding for human WT αS and GFP
- AAV6-s-bSynWT-SEIS-WB coding for human WT βS and GFP
- AAV6-s-gSynWT-SEIS-WB coding for human WT γS and GFP

For experiments in which these vectors were used, the non expressing control vector was replaced with AAV6-s-SEWB, a construct encoding for the expression of GFP. This served as a control for both the toxicity of the AAV itself and for GFP.

All of these AAV vector constructs are listed in section 2.4. In the text, the complete name of the construct is not written out but they are instead referred to simply as the abbreviated name of the protein that they code the expression for, such as αS, βS, γS, or in the case of the bicistronic variants αS+GFP, βS+GFP or γS+GFP. Also, the word “vehicle” is used when referring to the control vector AAV6-3TB-EWB and GFP when referring to AAV6-s-SEWB.

When the bicistronic vector constructs were used for expression of both synuclein and GFP in the same neurons, the expression of GFP was lower than when neurons were expressing only GFP. This can be seen in figure 3.17b,q were the exposure time in images taken of GFP only expressing cells had to be kept at a third of that used for the bicistronic treatments in order to prevent overexposure. As well as in figure 3.15d where the integrated gray level of bands in a western blot were 1.5 to 2.5 times higher in lanes with lysates from GFP expressing neurons compared to those in lanes with lysates from αS+GFP expressing neurons. This suggested a roughly 1.5 to 3 times higher expression of GFP in these neurons. Since there was no WPRE

behind the GFP in these constructs and a three times enhancement of expression is consistent with previous reports for WPRE (Hlavaty et al., 2005), this was taken as the reason for this difference in GFP expression. See section 2.4 for a schematic representation of the vector constructs.

AAV vectors coding for the expression of human WT α-, β- and γS were used for this work.
- These are referred to as αS, βS or γS throughout the text and figures.
- For all experiments using these vectors a control plasmid was used, this is referred to as vehicle or in some cases ctrl.
- In some experiments, bi-cistronic variants that co-express GFP were used, they are referred to as αS+GFP, βS+GFP or γS+GFP.
- For those experiments, a vector coding for only GFP was used as control.

All vectors are listed in section 2.4.

### 3.2.2 Toxicity

First thing done was to establish if and at which concentration of virus, i.e. MOI, that αS overexpression becomes toxic to the neurons. This was accomplished by transducing neuronal cell culture at 3 days *in vitro* (DIV) with either αS+GFP or only GFP expressing AAV at different concentrations ranging from MOI 1200 to 25200. At 7 DPT images were taken at random positions excluding the center and edge regions of the cultures and they were scored for remaining cell numbers and cell body area. Figure 3.15a shows the decline in remaining neuronal cell bodies with increasing virus concentrations. At concentrations with MOI between 1200 and 3600, αS+GFP caused none or only a small reduction in cell numbers compared to cultures expressing only GFP at the same MOI. Increasing the MOI two-fold to 7200 reduced the number of remaining cell bodies per square millimeter to less than 100. With even higher MOIs the number of remaining neurons decreased further but with a much less rapid decline as before. There were never less than 50 neurons per square millimeter regardless of the MOI used.

To confirm that high MOI / high αS expression levels does not severely interfere with neuronal cell body morphology, figure 3.15b shows the cell body area of remaining cells given in $\mu m^2$ against MOI for the same cells as used in figure 3.15a. There was no significant difference in the cell body area with increasing MOI or between neurons expressing αS+GFP or only GFP.

To check what level of overexpression occurs within the neurons and how the increase in MOI relates to and increase in expression level, a western blot was conducted on cell lysates

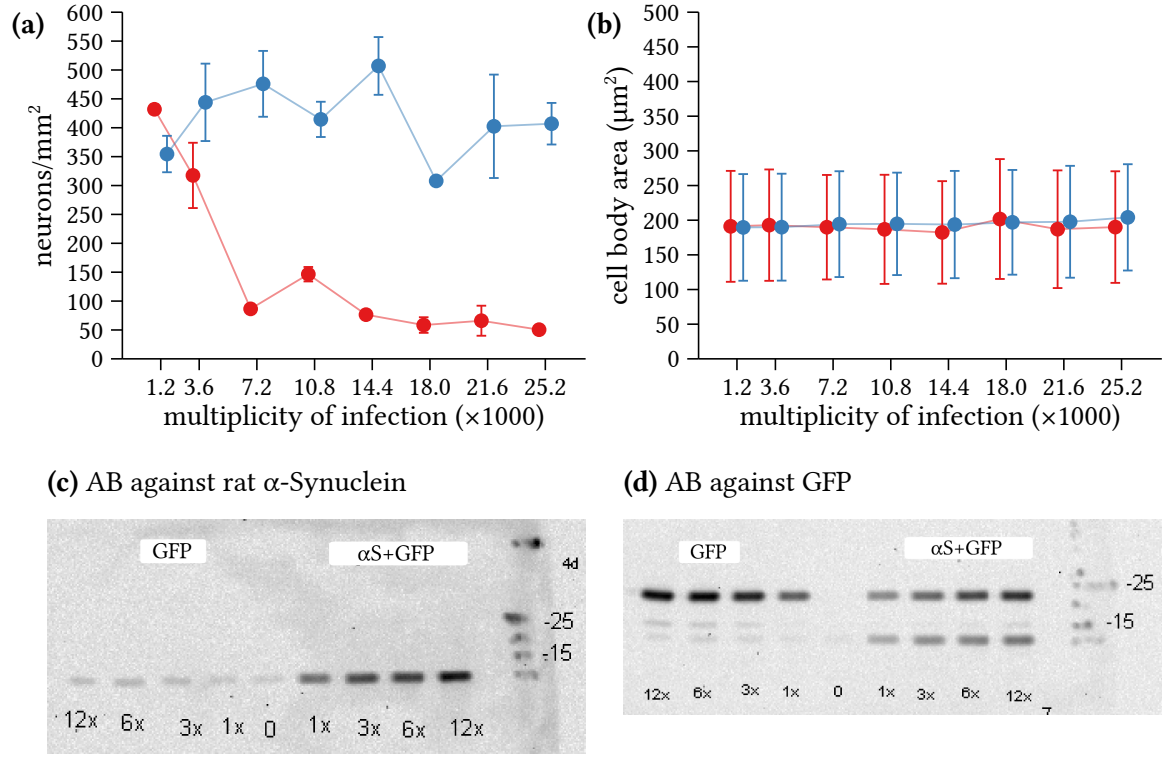


**Figure 3.15: Toxicity for different MOI of αSyn AAV vectors**
Primary neuronal cell culture transduced at 3 DIV with either αS+GFP (red line) or only GFP AAV vectors (blue line) with different MOI. **(a)** Remaining cell bodies per square millimeter at 7 DPT. Between a αS MOI from 3600 to 7200, the remaining neurons are reduced the most. At low MOI, less than 3600, there were no significant differences in the number of remaining cell bodies between αS+GFP and only GFP. With only GFP, cell numbers stay the same through all tested virus concentrations (multiple linear regression p-values: $moi = 0.7753$; $vector = 0.0028$; $interaction = 0.0013$, $R^2 = 0.89$). **(b)** Cell body area against MOI showed no significant changes in area with increasing MOI. (multiple linear regression p-values: $moi = 0.139$; $vector = 0.067$, $R^2 = 0.33$). The data in (a,b) are all from the same set of cells ($n = 2$ coverslips for each treatment, points and error bars are $mean \pm sd$ except in (a) where the range is *min* and *max*). **(c,d)** Western blot of lysates harvested and collected from primary neuronal culture at 4 DPT. The cultures had been transduced with either αS+GFP or GFP only expressing AAV at different MOI. 1x in the figure corresponds to MOI 1200. In (c), the blot has been incubated with an antibody against rat αS to label both endogenous and overexpressed αS. Calculations based on the integrated gray level of the bands gave values for overexpression of αS through the AAV vector at a factor 9-30 with increasing MOI. The relative increases in integrated gray levels between the different MOI bands were 1, 2.010, 2.286, 3.592. In (d), the same blot as in (c) is shown but after incubation with an antibody against GFP. The relative increases in integrated gray levels between the different MOI bands for GFP were 1.000, 1.812, 2.880, 3.870. The increase in expression with increasing MOI was thus the same for αS and GFP. The ratio between the integrated gray level between GFP from GFP only and αS+GFP lanes ranged between 1.5 to 2.5 suggesting a increase in GFP expression of this factor due to the WPRE. The analysis of a second blot done on cultures prepared and transduced on another occasion gave equivalent results.

from cultures that had been transduced with αS+GFP or GFP only expressing AAV vectors. A series of MOIs between 1200 and 14400 were examined. The neurons were harvested at 4 DPT. Figure 3.15c shows a western blot of the lysates where an antibody (AB) against rat αS has been used. This antibody is specific to both rat and human αS and this labels both the endogenous rat αS and the overexpressed WT human αS. The integrated gray level of the bands was quantified using ImageJ (section 2.8). The integrated gray level from the first five lanes corresponding to endogenous αS was averaged and subtracted from the integrated gray level of the last four lanes corresponding to the overexpressed αS. These four values were then divided by the average endogenous gray level to give an estimate of the level of overexpression of αS through AAV vectors at different MOI. The overexpression ranged from a factor of 9 to 30 times endogenous expression. The increase in expression between the different MOI was also calculated. The integrated gray level of each band from the last four of the blot was divided by that of the first of those four (1x in the figure). This resulted in values for the relative increase in expression of approximately 1, 2, 2.3 and 3.6. This corresponded very poorly with a direct relationship in increase of expression with increasing MOI. To check whether this was unique for αS, which might have suggested an increase in protein turnover for αS, the same calculation was done for GFP. This produced a similar series of increases, 1, 1.8, 2.9, 3.9, indicating that the difference was due to a saturation of virus uptake and/or vector copy number within the neurons.

With the observation that there is a strong dependence on MOI for the remaining cell numbers I decided to settle on two different MOI for further experiments. A low MOI that lay in the region that did not cause considerable reduction in cell numbers of the cultures i.e. led to non-toxic expression levels of αS and a high MOI that reduced cell numbers in all cultures i.e. led to toxic expression levels of αS.

According to figure 3.15a, the non-toxic region was located between MOI 1200 and 3600. Images of soma, neurites and mitochondria from neuronal cell cultures that were transduced with αS+GFP expressing AAV vectors at the level between these two, MOI 2400, showed no visible morphological differences of these compartments compared to cells expressing only endogenous levels of αS (see figure 3.16). MOI 2400 was therefore chosen as the MOI for non-toxic overexpression for further experiments.

Ideally, the high MOI would have been something that could reproducibly reduce cell numbers to the level seen between MOI 3600 and 7200 in figure 3.15a. It would then have been possible to know that the αS was affecting the cells strongly while still leaving most neurons remaining in the culture. It proved difficult however to ensure that the MOI used caused a

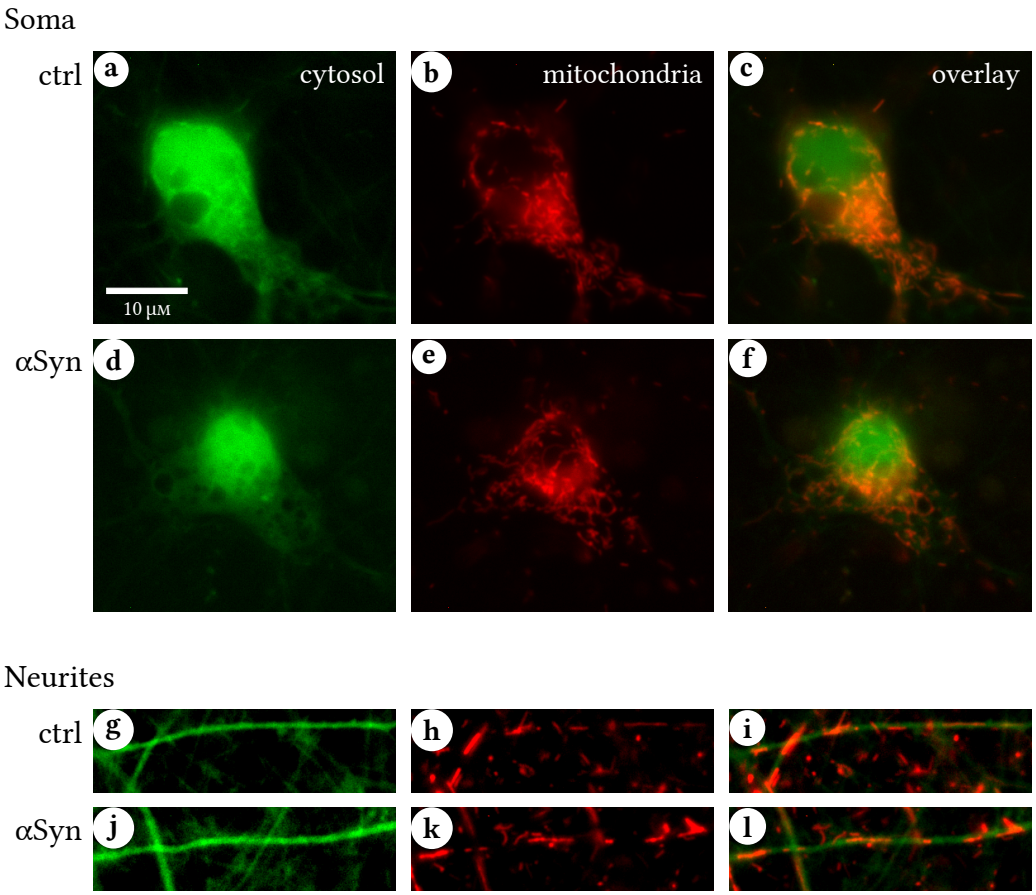


**Figure 3.16: Integrity of neuronal soma and neurites at non-toxic αSyn expression levels**
Primary cortical neurons transduced with AAV vector coding for GFP or GFP+αS with MOI 2400 and a second AAV coding for mitochondrially targeted RCaMP1e with MOI 600 at 3 DIV. Images were captured at 6 DPT. Scale is the same for all images. **(a-c)** Typical soma and mitochondria in the soma of neuron expressing only GFP. **(d-f)** Typical soma and mitochondria in the soma of neuron that express GFP and αS together. No apparent differences in mitochondrial shape were present. **(g-i)** Typical neurite and mitochondria within neurite of neuron expressing only GFP. **(j-l)** Typical neurote and mitochondria within neurite of neuron expressing GFP and αS together. Neurites are intact and mitochondria are elongated and comparable to those in GFP only expressing neurites.

similar reduction every time. This was most likely due to difficulties in ensuring the viability of the virus between experiments and differences in the number of seeded cells between culture preparations. Due to the strong dependence on MOI these small variations would cause great variability between experiments. For this reason the "high" MOI was chosen so that it reproducibly reduced the cell numbers to the high degree seen with the higher MOI in figure 3.15. The MOI finally chosen was 12000, a five times increase over the low MOI.

### Toxicity of synucleins compared

Since the control vector (vehicle) does not actually express any protein in the neurons, it is in most cases not a suitable control. The same goes for the GFP only expressing control vector since the GFP is expressed together with the synucleins in all the vector treatments and not only the control. A better control would be the expression of a protein of similar size to αS at similar levels. For this reason I added βS (14.2 kDa) and also γS (13.3 kDa) to my experiments, both of which have similar molecular weights to that of αS. βS has previously been described as being protective against αS toxicity (Hashimoto et al., 2001; Uversky et al., 2002; Hashimoto et al., 2004; Fan et al., 2006), and should therefor be the perfect control for αS toxicity and other effects due to its very close similarity in sequence to αS. γS has not been reported to play any detectable role in PD but might instead play a role in breast cancer (Ji et al., 1997).

An examination of αS toxicity to primary neurons in culture compared to that of βS and γS with the high MOI 12000 was now conducted in experiments made in cooperation with Dr. Grit Taschenberger. Neuronal cell cultures were transduced with AAV vectors coding for the expression of αS+GFP, βS+GFP, γS+GFP and only GFP. Images from random positions excluding the edges and center regions of the cultures were captured at 7, 10, 14, 18 and 21 DPT and the number of remaining cell bodies were counted. An overview of images of the cultures captured at these time points is given in figure 3.17a-t. Over time, the number of remaining neurons for αS and βS overexpressing cells decreased substantially. For γS and GFP only expressing cultures, the number of cells stayed constant however. There was also an increase in fluorescence intensity recorded between 7 and 10 DPT (all treatments) up until 21 DPT (γS and GFP only). This increase most likely reflects the increase in expression of GFP (and synucleins) from the vector since it was not removed from the growth media during the experiment.

The cell numbers remaining at the different time points were quantified and the result is shown in figure 3.17u. After 7 DPT there was only a moderate decrease in cell numbers and only with αS treated cells. After two weeks (14 DPT) the cell numbers for αS had decreased further to leave only about 100 cell bodies per square millimeter, very similar to that seen in the experiments with different MOI described above. Although βS did not cause any decrease in cell numbers at 7 DPT, at 14 DPT it too had caused significant reduction. This reduction increased somewhat at 18 and 21 DPT but seemed to level out, still leaving significantly more cells in culture than did αS.

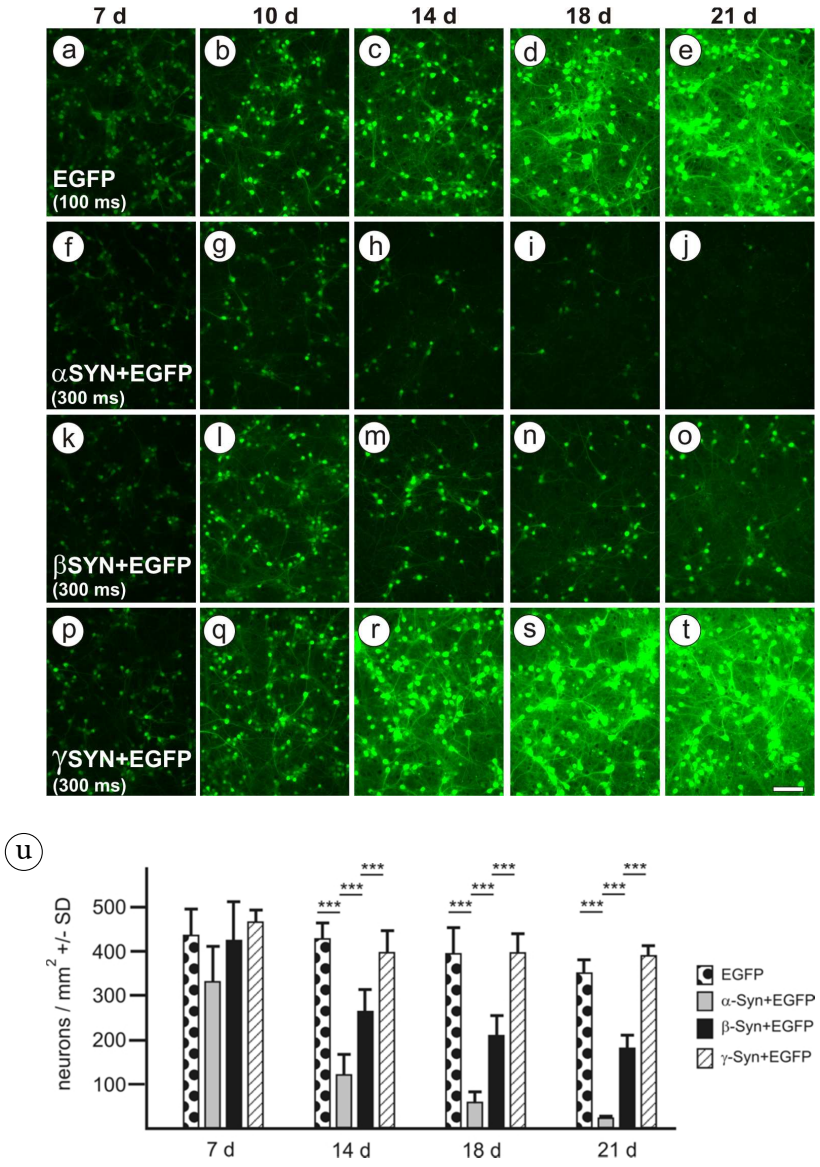


**Figure 3.17: Neurotoxicity of synucleins in cultured primary neurons**
**(a-t)** Primary cortical neurons were transduced at DIV 3 with the respective bi-cistronic AAV vectors co-expressing GFP with α-, β- or γS. GFP fluorescence was recorded with constant exposure time from living cultures at the indicated times after transduction (7 days: a, f, k, p; 10 days: b, g, l, q; 14 days: c, h, m, r; 18 days: d, i, n, s; 21 days: e, j, o, t). Neurons expressing only GFP are shown in (a-e), neurons expressing αS+GFP are shown in (f-j), neurons expressing βS+GFP are shown in (k-o), and neurons expressing γS+GFP are shown in (p-t). Fluorescence in GFP only expressing neurons was recorded with less exposure time due to the somewhat higher GFP levels expressed from this vector as compared to GFP levels expressed from the bi-cistronic vectors, which lack the enhancing WPRE sequence 3' to GFP. Scale bar = 100 µm. **(u)** GFP fluorescent neurons in living cultures were quantified at the indicated times after transduction. Dotted bars = GFP only expressing neurons, light grey bars = αS and GFP expressing neurons, black bars = βS and GFP expressing neurons, hatched bars = γS and GFP expressing neurons. Statistics performed by one way analysis of variance (ANOVA) / Tukey, *** $p < 0.001$; $n = 6$ independent transductions per condition.

It was surprising to see that βS but not γS exhibited toxic properties. To further study these effects I decided to include βS in further experiments. Since γS had similar properties to that of the previously used control, empty vector/vehicle/GFP, it was used in further experiments as an additional control.

- The level of overexpression of αS ranged from 9 to 30 fold depending on MOI as evident from western blot
- αS was found to be toxic to primary cortical neurons and this increased with both expression level and age of culture
- βS but not γS was also found to be toxic but less so than αS for the same MOI

### 3.2.3 Mitochondrial morphology

Mitochondrial morphology was assessed after observing that the appearance of mitochondria in the soma of neurons that were transduced with αS at toxic levels had a rounded appearance. Neuronal cell cultures were transduced at 3 DIV with AAV vectors expressing αS+GFP, βS+GFP, γS+GFP or only GFP. In addition, AAV6-s-mtRCaMP1e-WB was added with MOI 600 for visualization of mitochondria. At days 6 and 13 after transduction images were captured at random positions that excluded the edges and center regions of the coverslips at 63x magnification. Different sets of transduced neurons were imaged for the different time points and at least 30 neurons from 6 coverslips were imaged for each treatment. To analyze the data, the images had their filenames randomized using a computer script and were analyzed blind to the transduction. The mitochondria of soma were classified according to their appearance as either “tubular”, “partially fragmented” or “fully fragmented” (figure 3.18a-c). Only soma that had strong green fluorescence from GFP were classified. After analysis the correct filenames were recreated using the same script. The fraction of soma with fully fragmented appearance was quantified and is shown in figure 3.18d. At 6 days after transduction there was a statistically significant difference in the fraction of soma exhibiting a fully fragmented mitochondrial morphology for cultures expressing αS+GFP compared to the other treatments. At this stage there were no differences seen between βS+GFP, γS+GFP or only GFP expressing neurons. At 13 days a majority of αS expressing neurons now had the fully fragmented mitochondrial morphology (2.5 fold increase to ~80%). For βS it had increased 5 fold to ~50%. For both γS and GFP treated neurons there was a smaller approximately 2 fold increase (~20%). The differences between αS and βS to γS and GFP at each time point was statistically significant (see caption for figure 3.18d). Also, the difference in the fraction of soma with fully fragmented mitochondrial morphology between the two time points, 6 DPT and 13 DPT, was also statistically significant for all four treatments.

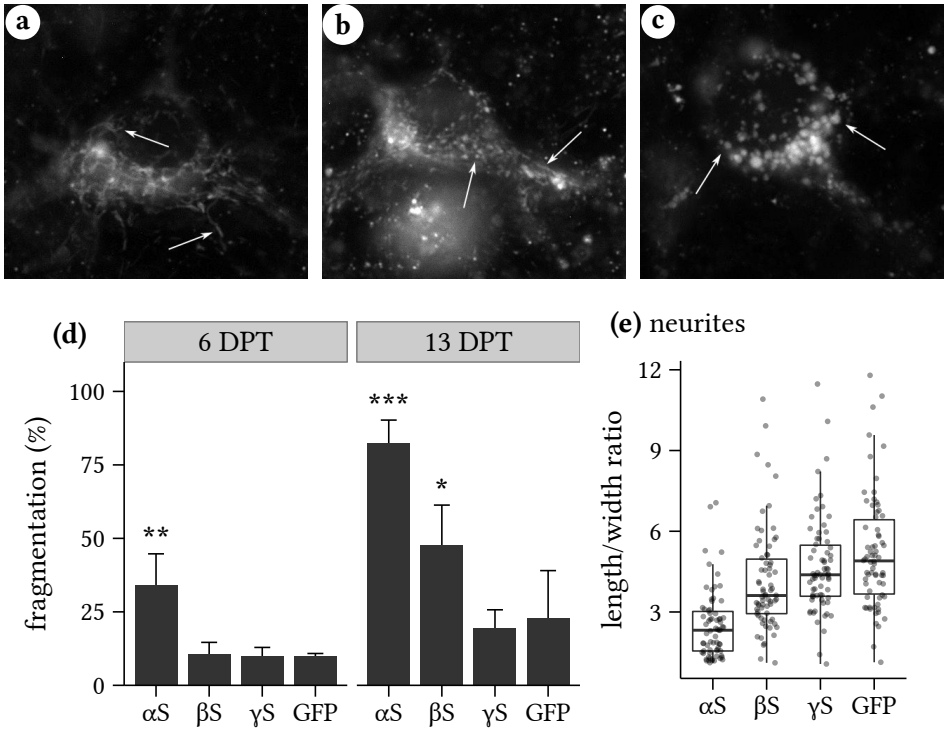


**Figure 3.18: α-Synuclein changes mitochondrial morphology**
Cultures of cortical neurons transduced with AAV vectors expressing αS+GFP, βS+GFP or γS+GFP with MOI 12000 were analysed for mitochondrial fragmentation (a-c). To visualise mitochondria, a AAV vector with MOI 600 expressing mtRCaMP1e was co-transduced together with the synucleins. **(a-c)** Mitochondrial morphology in soma classified as either "tubular" (a), "partially fragmented" (b) or "fully fragmented" (c). Mitochondrial fragmentation was calculated as the percentage of neurons per coverslip that contained a majority of fully fragmented mitochondria at 6 and 13 days post transduction.The difference in fragmentation was assessed with one-way ANOVA / Tukey, $*** p < 0.001$; $** p < 0.01$; $* p < 0.05$; n = 6 coverslips per treatment. Individual Student's t-tests for each treatment between the different time points (6 and 13 DPT) were significant for αS ($p < 0.001$), βS ($p = 0.0091$) and γS ($p = 0.047$). **(e)** The length/width ratio of mitochondria in neurites at 6 days post transduction. A Kruskal-Wallis test revealed a significant effect of treatment AAV on the mitochondrial length/width ratio ($p < 0.001$; n = 70 mitochondria from 5 coverslips per treatment). Post-hoc testing using Mann-Whitney tests with Bonferroni correction showed differences between αS-βS ($p < 0.001$), αS-γS ($p < 0.001$), αS-GFP ($p < 0.001$) and βS-GFP ($p = 0.004$).

In addition to the morphology of mitochondria in the soma, there was apparent rounding of mitochondria within neurites. This was quantified by calculating the ratio between the length and width of red mitochondria (mtRCaMP1e) located in neurites that were visible in the green (GFP) channel. In figure 3.18e this is shown for the early (6 DPT) time point. The situation in the neurites corresponded with that of the mitochondria in soma. There was a clear difference between αS and the other treatments in terms of the length/width ratio. For βS it seemed as if it had progressed slightly more towards fragmentation and this difference was statistically significant for βS compared with GFP only expressing neurons. γS and GFP were again similar.

- Mitochondrial morphology in neurons was classified as either tubular, partially fragmented or fully fragmented
- At 6 DPT, ~30% of αS overexpressing neurons had fully fragmented mitochondria in the soma
- For the other synucleins and GFP this figure was ~10%
- At 13 DPT, the number of neurons with fully fragmented mitochondria in the soma had increased to ~80% for αS
- For βS the frequency of fully fragmented mitochondria was now ~50%
- For γS and GFP it was higher as well but still less than ~25%
- The situation in the neurites was similar, with a stronger tendency for rounded mitochondria in αS

This shows that αS and βS both are able to influence mitochondrial morphology. The level and time of onset of increased fragmentation for βS matches that of the toxicity.

### 3.2.4 Mitochondrial motility

Impairment of mitochondria and/or impairment of the neurite network might lead to changes in mitochondrial motility. That this might happen became apparent while measuring mitochondrial morphology in the previous experiments. The average and max speed of movement in micrometers per minute was assessed by manually tracking moving mitochondria in neurites using the MTrackJ plugin for ImageJ on the same data as that used in section 3.2.3.

Quantification of this movement showed that after 6 days in culture, when changes in mitochondrial morphology had occurred in over 30% of neurons (see figure 3.18), there was actually an increase in the average movement speed of mitochondria from αS+GFP overexpressing cells but this difference was not statistically significant. After 13 days, when morphological changes were present in about 80% of αS overexpressing neurons, the average movement speed was significantly decreased and this difference was statistically significant.

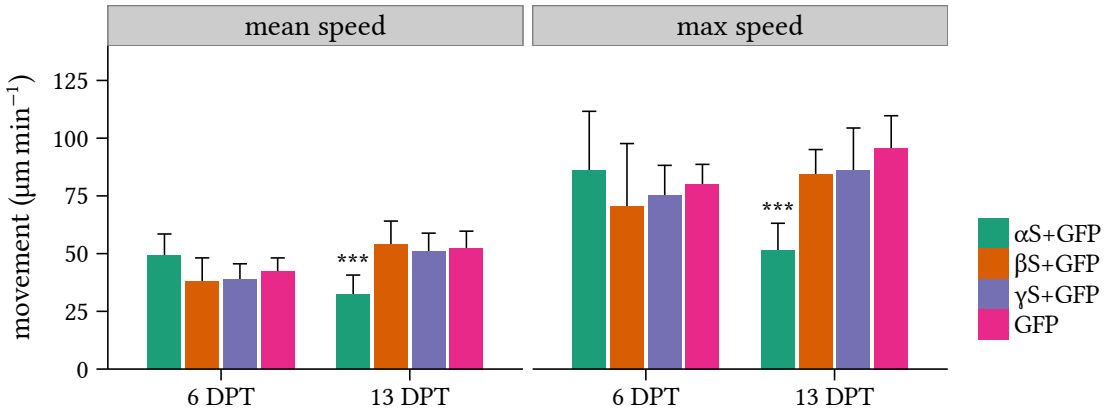


**Figure 3.19: Movement of mobile mitochondria in neurites**
The movement of individual mitochondria in neurites in cultures of cortical neurons transduced with AAV vectors expressing αS+GFP, βS+GFP or γS+GFP with MOI 12000 was analyzed for either mean or max speed. Mitochondria were made visible through co-transduction with mtRCaMP1e with MOI 600. Tracking was done using the MTrackJ plugin for ImageJ. The difference in either mean or max movement speed was assessed with one-way ANOVA / Tukey, *** $p < 0.001$; ** $p < 0.01$; * $p < 0.05$.

All the other treatments, βS+GFP, γS+GFP and only GFP, had similar average and max speed movement rates at both time points. The max speed correlated with the average speed for all treatments. See figure 3.19 for a graph of the data.

- The movement speed of mitochondria in neurites was unaffected or slightly increased for αS at 6 DPT
- The other treatments were all the same
- At 13 DPT, the mitochondrial movement speed was significantly reduced for mitochondria in neurites from αS overexpressing neurons
- βS and γS were the same as GFP and they were all slightly faster than at 6 DPT

### 3.2.5 Cytosolic and mitochondrial free-$Ca^{2+}$ handling at non-toxic expression levels

The common symptoms of PD such as tremors and rigidity, are due to degeneration of dopaminergic neurons in motor centers of the brain. If this is due to αS there should be some point in time before death of the neuron where αS affects the properties of the cell but the cell is still viable. This interference between αS and the normal functioning of the cell should be what finally leads to degeneration and cell death. Using overexpression of αS as a model for this early stage of αS pathology, I was interested in testing the response of neurons with moderately elevated levels of αS to stimulus that raise intracellular $Ca^{2+}$ levels.

The rationale was that if αS can produce ion permeable pores in living cells or in some other way interferes with the regulation of ion concentrations, this should be detectable in the way that neurons handle calcium. This change could then be measured using GECIs.

To assess the calcium handling of neurons overexpressing αS at moderate levels in primary cortical neuronal cell culture, either D3cpV with MOI 1200 or 4mtD3cpV with 600 was co-expressed together with αS or vehicle with 2400 using AAV vectors. Upon depolarization with 64 mM $K^+$ for 5 s the cells responded with uptake of $Ca^{2+}$ as expected. However, the FRET/CFP ratio showed levels close to saturation of the sensor with this stimulus and this data was not further analyzed. Instead, the classical organic calcium indicator dye Fura-2 which has a wider dynamic range than most GECI was used. This showed a small but significant difference in peak calcium levels upon high potassium depolarization as seen in figure 3.20c. Decay rates were unchanged however (not shown). This challenges previous findings by another group that were done on SH-SY5Y cells stably transfected with WT αS. Their findings showed large increases in the cytosolic peak calcium levels, up to two-fold increase in signal compared to control (Hettiarachchi et al., 2009). In my experiments this was significantly lower at only about 10% signal increase.

Since high potassium depolarization is a harsh stimulus that forcefully depolarizes cells without any intermittent relaxation and as such can not be regarded as physiological, I extended the measurements to use electrical stimulation in the form of field stimulation. This type of stimulus can be tuned to emulate the electrical depolarizations normally experienced by neurons that undergo APs firing.

Using FS as stimulus, neurons were stimulated for 3 s at 10 Hz. The peak signal and decay rates were quantified from traces of signals recorded from cytosol (D3cpV) and mitochondria (4mtD3cpV), see figure 3.20a,b. With FS there were no longer any difference in peak levels of accumulated cytosolic $Ca^{2+}$ between αS treated cells and control. The same was true for $Ca^{2+}$ accumulated/buffered in the mitochondria. When the decay rate was quantified by fitting a straight line to the linear part of the decay after logarithmic transformation it too was shown to exhibit no significant differences between αS overexpressing neurons and those transduced with only empty vector either in the cytosol or the mitochondria.

- Calcium handling in neurons expressing a non-toxic level of αS is unaffected in both the cytosol and mitochondria in response to physiological stimuli
- Resting levels as measured with the ratiometric GECI D3cpV were also unaffected
- With high potassium depolarization there was a slight ($< 10\%$) increase in $\Delta F/F_0$ for αS at non-toxic levels compared to control, suggesting a corresponding increase in uptake of calcium

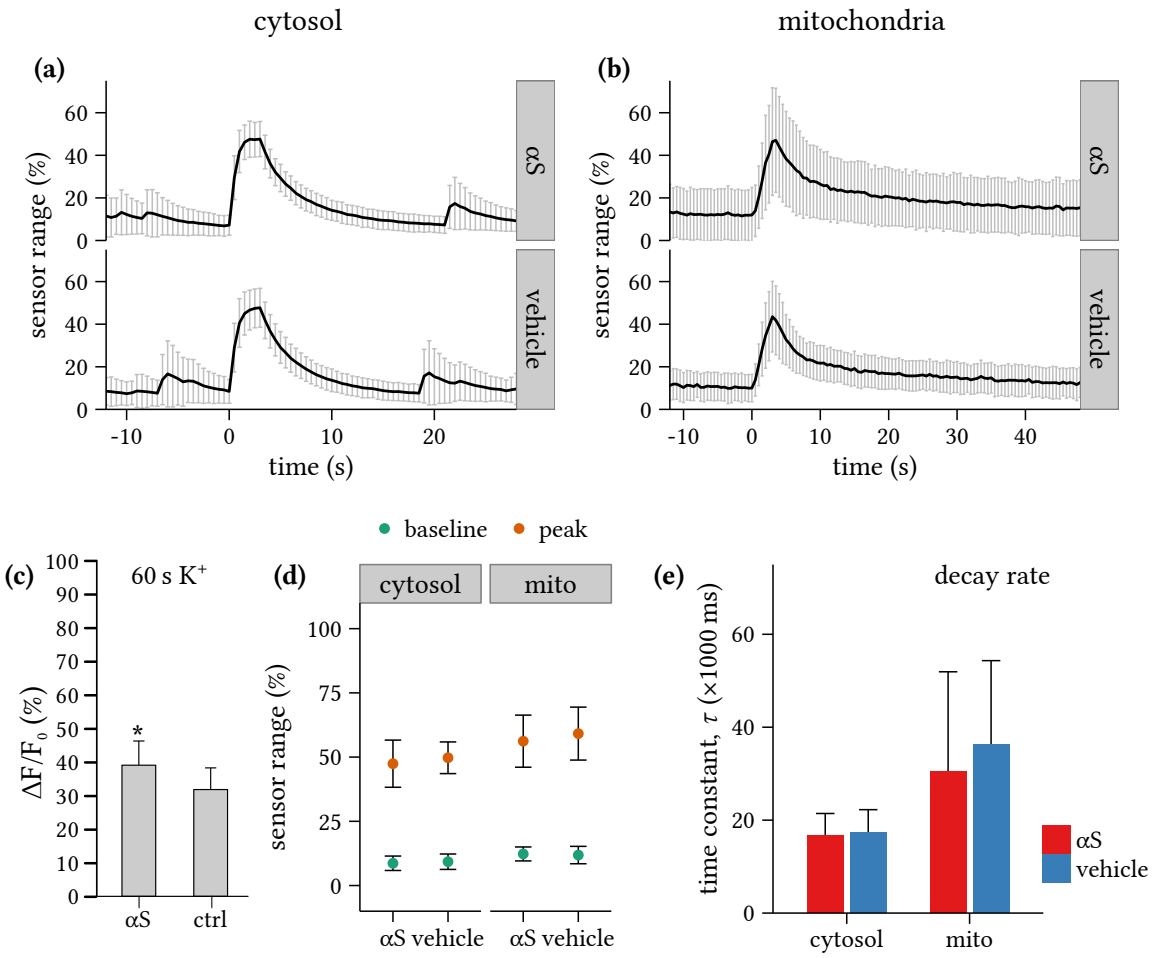


**Figure 3.20: Effects on cytosolic and mitochondrial $Ca^{2+}$ handling of non-toxic αSyn over-expression**

Assessment of $Ca^{2+}$ handling in neurons that over-express non-toxic levels of αS. Neuronal cell cultures were transduced with non-toxic (MOI 2400) concentrations of AAV vectors coding for the expression of αS or a non expressing control vector (vehicle/ctrl in the figure). The GECIs D3cpV (MOI 1200) or its mitochondrial variant 4mtD3cpV (MOI 600), also as AAV vectors, were used for co-transduction. **(a,b)** Shows typical traces measured from cytosol and mitchondria respectively. **(c)** Quantification of peak influx (max signal after stimuli) of neurons labelled with Fura-2 and having been depolarized with 64 mM $K^+$ for 5 s. These cells excibited a small but significant increase in peak signal indicating uptake of larger amounts of $Ca^{2+}$ than control. **(d)** Quantification of peak influx of neurons that express the GECI D3cpV either in the cytosol or the mitochondria. The cells were stimulated electrically using FS at 10 Hz for 3 s. This produced a non-saturating uptake of $Ca^{2+}$ in the cytosol and buffering in the mitochondria. Both baseline (before stimuli) and peak levels are indicated and they are both not significantly different between cells that express αS or only empty vector (vehicle). The baseline reading also confirms that initial $Ca^{2+}$ levels are not elevated which indicates that the reading in (c) is due to an increased peak uptake and not a change in initial levels. **(e)** Decay rates quantified from readings in (d). A straight line was fit to the linear stretch of the logarithmic transformation of the decaying part of the trace. Also for the decay rates there were no significant differences recorded between αS over-expressing neurons and those transduced with empty vector (vehicle).

### 3.2.6 Cytosolic and mitochondrial free-$Ca^{2+}$ handling at toxic expression levels

#### Measured in the cytosol

Calcium measurements were now repeated with the neuronal cell cultures transduced with AAV vectors expressing either αS+GFP, βS+GFP, γS+GFP or only GFP using the MOI (12000) that caused toxic overexpression of αS. The calcium sensor AAV6-s-RCaMP1e-WB was co-transduced with MOI 1200. Calcium handling was assessed at 6 and 13 DPT by applying FS at 10 Hz for 5 s. The change in fluorescence intensity of the RCaMP1e sensor was recorded and the $\Delta F/F_0$ was calculated. Peak influx was measured as the peak in signal from the traces of individual neurons. The decay rate after stimulation was measured from a linear region of the log transformed trace. Example traces and plots of the measured values are given in figure 3.21. No significant differences were seen between any of the treatments for either the peak influx or the decay rates as measured using one-way ANOVA. Also, no correlation between the decay rates and peak influx values were present (Pearson correlation). When DPT was added as an independent variable to the statistical model for peak influx to make a two-way ANOVA model, a significant difference in peak influx between 6 and 13 DPT was seen. This was interpreted as that the neurons that were measured at 13 DPT took up significantly more $Ca^{2+}$ than those measured at 6 DPT.

#### Measured in mitochondria

The experiment in section 3.2.6 was repeated but with AAV6-s-RCaMP1e-WB replaced with AAV6-s-mtRCaMP1e-WB with MOI of 600 for expression of the calcium sensor RCaMP1e in the mitochondria. As can be seen from the example traces and plots of the measured values given in figure 3.22, no significant differences between treatments were found also for the mitochondrial calcium handling at toxic expression levels. Also there was no correlation between peak and rate values (Pearson correlation) and in contrast to the values for the cytosol, there was no significant difference between 6 and 13 DPT when DPT was added to the statistical model.

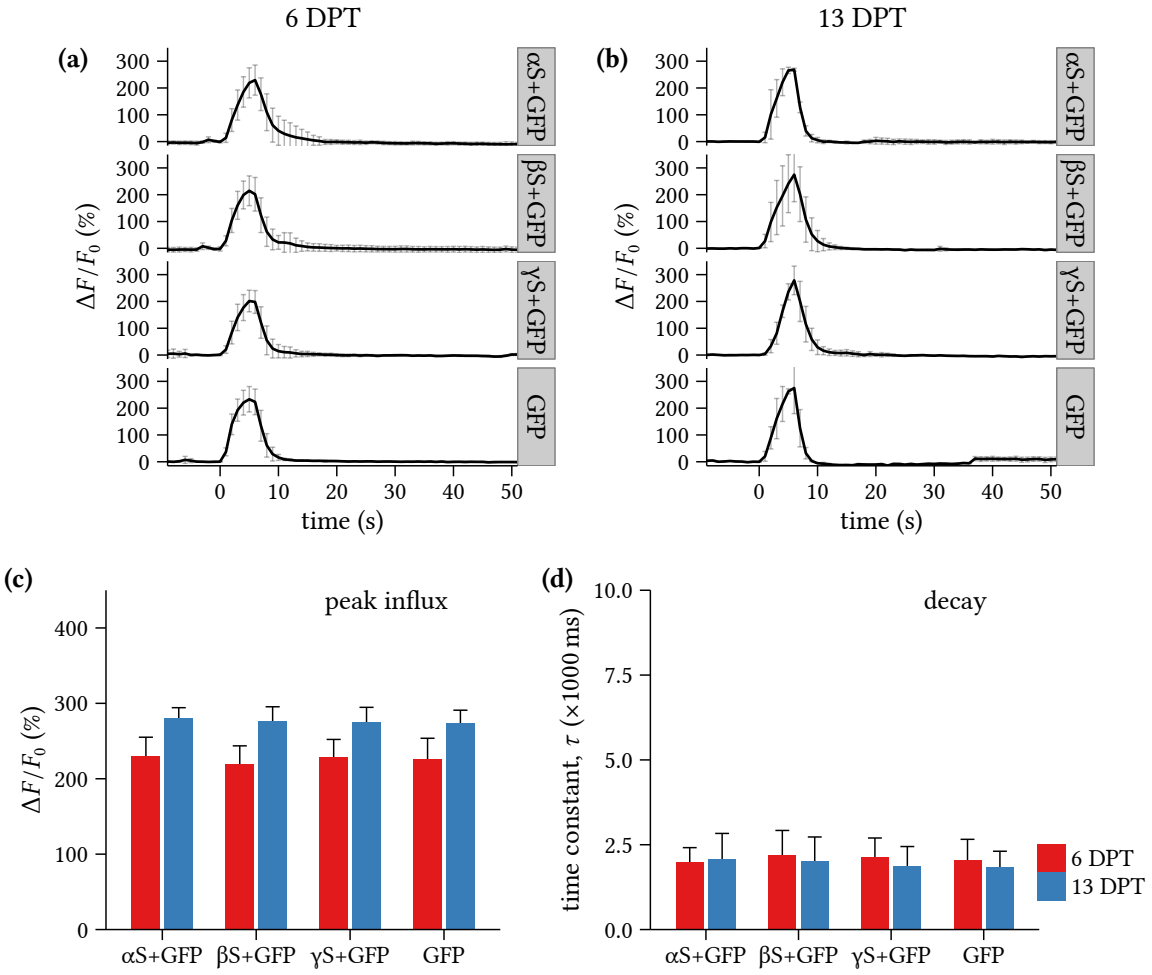


**Figure 3.21: Effects on cytosolic $Ca^{2+}$ handling of toxic αSyn over-expression**
Primary neuronal cell culture transduced with AAV vectors coding for the expression of αS+GFP, βS+GFP, γS+GFP or only GFP with MOI 12000. An AAV vector coding for the calcium sensor RCaMP1e was added together with the other vectors with MOI 1200. **(a,b)** Example traces of the calcium response from cytosol after field stimulation (5 s, 10 Hz) at 6 and 13 DPT. **(c)** Quantification of the peak response in (a) (red) and (b) (blue). One-way ANOVA showed no significant differences in mean responses between treatments, 6 DPT: p = 0.22, n = 34; 13 DPT: p = 0.8, n = 13. When DPT was added as an independent variable to the statistical model for peak influx, a significant difference in peak influx between 6 and 13 DPT was seen (two-way ANOVA $p_{dpt} < 0.001$; $p_{vec} = 0.19$ with no interaction $p_{int} = 0.81$). **(d)** Quantification of the decay time constant as in (c). Given as the absolute change in percent of $\Delta F/F_0$ over time. Again the one-way ANOVA showed no significant differences in the mean responses between treatments, 6 DPT: p = 0.43, n = 34; 13 DPT: p = 0.74, n = 13. No significant difference between 6 and 13 DPT (two-way ANOVA $p_{dpt} = 0.22$; $p_{vec} = 0.58$). Pearson correlation coefficient between decay and peak values: $r_6 = 0.064$; $r_{13} = -0.0053$.

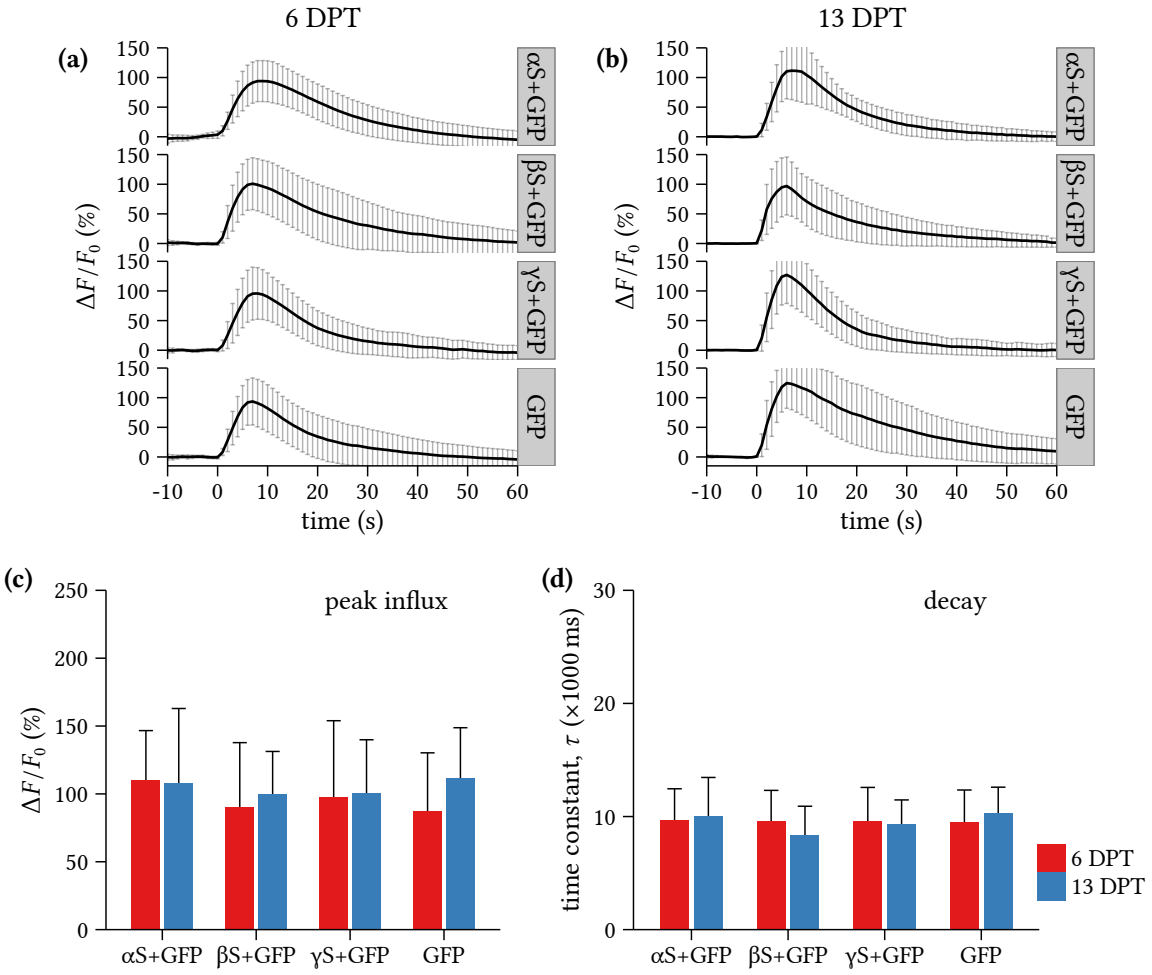


**Figure 3.22: Effects on mitochondrial $Ca^{2+}$ handling of toxic αSyn over-expression**
Primary neuronal cell culture transduced with AAV vectors coding for the expression of αS+GFP, βS+GFP, γS+GFP or only GFP with MOI 12000. An AAV vector coding for the calcium sensor mtR-CaMP1e was added together with the other vectors with MOI 600. **(a,b)** Example traces of the calcium response from mitochondria after field stimulation (5 s, 10 Hz) at 6 and 13 DPT. **(c)** Quantification of the peak response in (a) (red) and (b) (blue). One-way ANOVA showed no significant differences in mean responses between treatments, 6 DPT: p = 0.085, n = 42; 13 DPT: p = 0.82, n = 13. There was no significant difference between 6 and 13 DPT when DPT was added to the statistical model (two-way ANOVA $p_{dpt}$ = 0.14; $p_{vec}$ = 0.12). **(d)** Quantification of the decay time constant as in (c). Given as the absolute change in percent of $\Delta F/F_0$ over time. Again the one-way ANOVA showed no significant differences in the mean responses between treatments, 6 DPT: p = 0.99, n = 42; 13 DPT: p = 0.34, n = 13. No significant difference between 6 and 13 DPT (two-way ANOVA $p_{dpt}$ = 0.96; $p_{vec}$ = 0.92). Pearson correlation coefficient between decay and peak values: $r_6$ = 0.016; $r_{13}$ = 0.097.

- No differences in calcium handling in the cytosol or mitochondria in response to physiological stimuli was found for any of the synucleins
- An increase in peak cytosolic calcium was measured for neurons at 13 DPT compared to at 6 DPT

This shows that the mitochondria of neurons that overexpress αS and βS at toxic levels are able to handle the large influx of calcium in response to the depolarization occurring during AP firing

### 3.2.7 Morphological changes of mitochondria are not correlated with impaired $Ca^{2+}$ handling

A subset of the cells for the experiment in section 3.2.3 were also stimulated with FS and the response recorded. These cells were then used to quantify the mitochondrial calcium response of the neurons in relation to their morphological appearance. The idea was that even though the neurons could not be shown to have a changed mitochondrial calcium handling in the previous experiments, if the difference would be small and if the number of cells that were affected by the αS were also small, any effects might be hidden in the variance between the different mitochondrial morphological types. If one would differentiate between the morphological classifications and correlate this with the calcium response, one might be able to find differences that were previously hidden. The stimulation protocol was the same as the one used in section 3.2.6. Mitochondria in soma with all three types of morphology responded to the FS, but see below for a description of differences that were present. When quantified, there proved to yet again be no measurable difference in calcium handling between the treatments, or between the different morphological types. The data is presented in figure 3.23.

When analyzing the data for calcium measurements, cells were regarded as not responding if the max $\Delta F/F_0$ measured was not higher than that of the background (same as the contribution from out of focus light). In most cases this threshold was about 10%. In cultures that were measured 6 days after transduction, more then 95% of cells were responding. In the older cultures, those at 13 days after transduction, there was a reduction in the number of cells that responded to field stimulation for all treatments. It was more pronounced in αS and βS treated cultures. When the response rate of the cultures was correlated with the morphology of the mitochondria, αS had no responding cells with a “tubular” or “intermediate” morphology. For βS the distribution was more or less even with a similar number of cells responding for each of the three morphological classifications. For γS and only GFP expressing cells, there were for cells classified as having “fully fragmented” mitochondria a

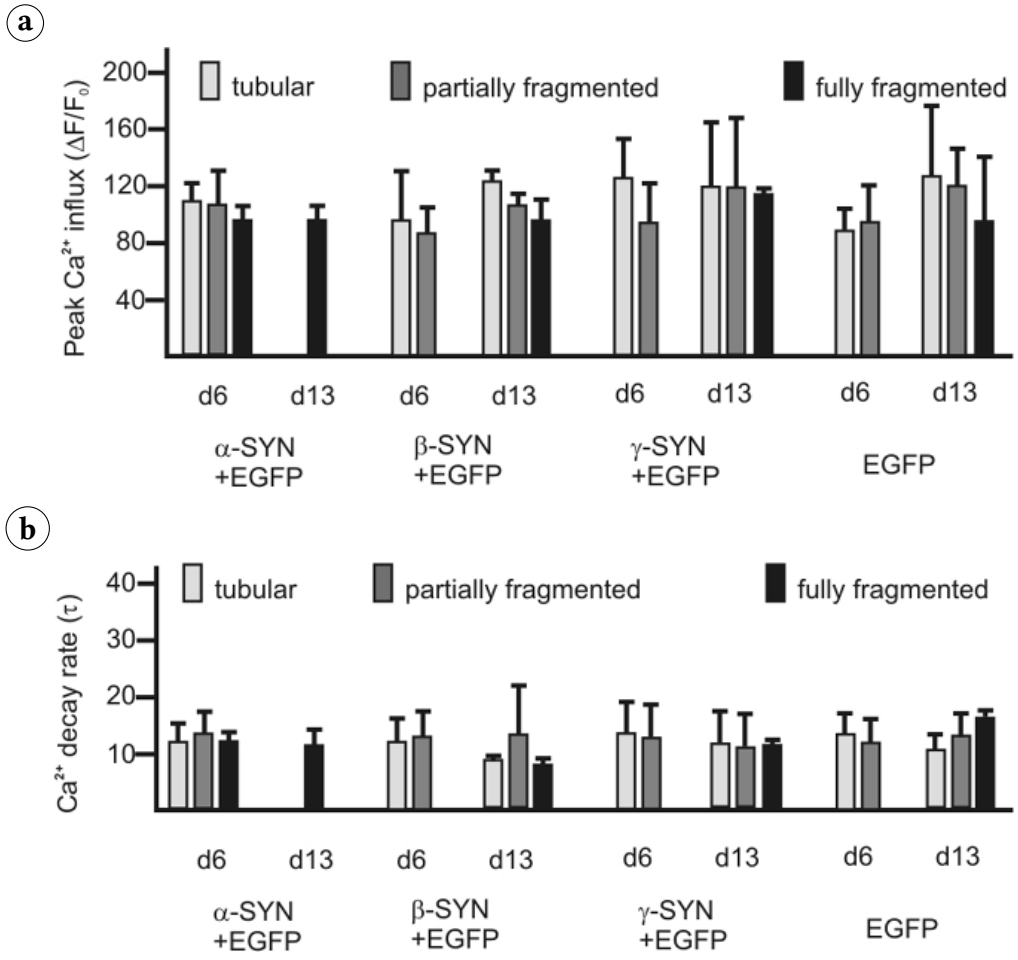


**Figure 3.23: Correlation between mitochondrial morphology and calcium handling**
Field stimulation of cultured neurons co-expressing either αS+GFP, βS+GFP, γS+GFP or GFP with a red fluorescent genetically encoded $Ca^{2+}$ sensor, RCaMP1e targeted to the mitochondria, was used to study $Ca^{2+}$ handling by quantifying the influx of $Ca^{2+}$ into mitochondria after action potentials and the time necessary to pump this $Ca^{2+}$ out of the mitochondria. Synucleins and GFP control was expressed using AAV vectors with MOI 12000. The calcium sensor was also expressed using a AAV vector but with MOI 600. Peak $Ca^{2+}$ influx (a) and decay time (b) after field stimulation were quantified at days 6 or 13 for cells containing either tubular (light grey bars), partially fragmented (dark grey bars) or fully fragmented (black bars) mitochondria. Two-way ANOVA was used to test for differences in peak calcium or decay time constants between treatments and morphological appearance (tubular, intermediate, fragmented). No differences could be detected. 6 DPT p-values: $peak_{vec} = 0.11$; $peak_{morph} = 0.65$; $tconst_{vec} = 0.2$; $tconst_{morph} = 0.42$. 13 DPT p-values: $peak_{vec} = 0.76$; $peak_{morph} = 0.8$; $tconst_{vec} = 0.61$; $tconst_{morph} = 0.9$.

similar fraction of responding cells as for αS and βS ( 25%) but for the two less severe classifications there were a lot more responding cells. For βS all three classifications had around 25% of responding cells. In figure 3.24 the percentage of responding cells for each treatment and morphological classification at 13 days after transduction is plotted.

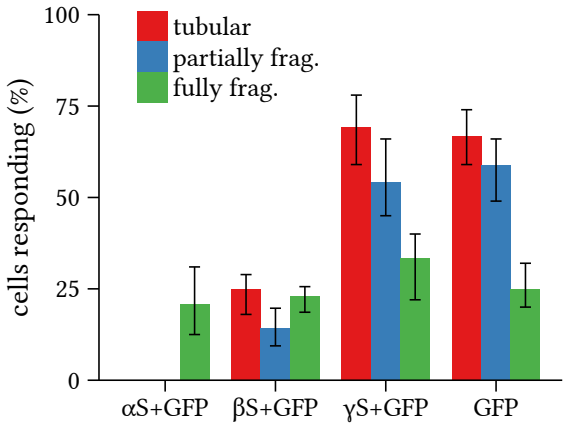


**Figure 3.24: Relative numbers of mitochondria responding to field stimulation**
Relative response frequences of mitochondria in cells expressing αS+GFP, βS+GFP, γS+GFP or only GFP from AAV vectors (MOI 12000). Co-transduction with the calcium sensor RCaMP1e targeted to the mitochondria. Stimulation for 5 s at 10 Hz with FS at 13 DPT. Plot shows mean±max/min; n = 3 coverslips. Differences in response was significant both for treatment and morphology (Fisher's exact test, $p < 0.001$ and $p = 0.0031$ respectively; n = 31 per treatment).

- No significant differences in calcium handling in the mitochondria for any of the synucleins were found when the response was correlated with mitochondrial morphology
- The number of responding neurons were drastically reduced for αS and βS however
- At 13 DPT ~25% of measured neurons overexpressing αS or βS were responding with calcium uptake
- For βS the type of morphology was irrelevant
- For γS and GFP, significantly more neurons with tubular or partially fragmented morphology were responding compared to fully fragmented

This shows that as long as a neuron can respond to depolarization the mitochondria is able to handle calcium without impairment

### 3.2.8 Measurements of mitochondrial ATP production and cytosolic turnover

An important function of mitochondria in neurons is the generation of ATP. As mentioned, in primary neurons from rat as well as in human postmortem tissue, αS has been shown to interact with the ETC by interfering with complex I (Devi et al., 2008; G Liu et al., 2009; Chinta

et al., 2010). To test whether the morphological changes and/or interaction with complex I has an effect on resting levels or the consumption and production of ATP within neurons a genetically encoded sensor for ATP was packaged as a AAV vector (AAV6-s-ATeam1.03-WB) and used to transduce neurons together with the synucleins. The sensor is called ATeam1.03, has a reported $K_d$ of ~3 mM and can report on cytosolic ATP levels in the range 1-10 mM (Imamura et al., 2009) which is within the range typically found in neurons (Veech et al., 1979; Fukuda et al., 1983; Ainscow et al., 2002; Mironov, 2007). A characterization of ATeam1.03 in the primary cortical cell culture used for the experiments in this thesis is given in section 3.1.6.

Three days old neuronal cell cultures were transduced with MOI 12000 with AAV vectors coding for the expression of αS, βS, γS and "vehicle" as control. The ATeam1.03 encoding vector AAV6-s-ATeam1.03-WB was added together with the others for co-transduction with MOI of 1200. After 6 or 13 days, measurements were conducted on the cultures as described in section 3.1.6. This produced data from which the baseline level, consumption rate without depolarizing stimuli, consumption rate during depolarizing stimuli, regeneration rate without depolarizing stimuli, regeneration rate after depolarizing stimuli and the minimum level at rest of cytosolic ATP could be assessed. Two types of stimuli were used to simulate activity in the neurons. Either FS at 10 Hz or stimulation of ionotropic glutamate receptors with the application of 10 µM kainate. Because the results with both types of stimuli were the same, only kainate were used for the later time point of 13 days and only these results are presented. A figure showing the traces from neurons stimulated with FCCP or FCCP+kainate is shown in figure 3.12b. The shaded regions show what parts of the trace corresponds to the consumption rate (cons) and regeneration rate (regen) respectively.

At 6 days after transduction the initial baseline levels (figure 3.25a, *init* panel) of cytosolic ATP were the same for all three of the synucleins but were lower than in those cultures that had been transduced with only "vehicle". At 13 days the level for the control was the same but βS and γS had increased to similar levels as that of control. The ATP level for αS had also increased compared to at 6 days but were still significantly lower than that of control and now also the other two synucleins. During FCCP application a new baseline was reached in cells that were not also stimulated (figure 3.25a, *min* panel). These values correlated with the initial baseline levels at both 6 DPT and 13 DPT. In table 3.1 the mean values ± standard deviation are presented.

When mitochondria were uncoupled through the application of FCCP the consumption rate of cytosolic ATP was slightly lower for αS than for the other treatments at 6 days after trans-

duction. At 13 days, the consumption rate of αS had increased to the same levels as for the other synucleins. The vehicle control had at 13 days, about 60% increase in its consumption rate of ATP. When kainate was applied together with the FCCP which depolarizes the plasma membrane, the consumption rate increased compared to at rest for all neurons. At 6 days, the increase was most pronounced for αS for which it was more than 4 fold. For the three other treatments the increase was approximately 2.5 fold. In the older cultures, at 13 days, the increase in consumption rate when kainate was applied was about 4 fold for all treatments except γS were it was instead approximately 3 fold. See table 3.1 for all the values.

While recovering after washing out the FCCP, the regeneration rate without kainate was approximately 0.5 mM $min^{-1}$ for all treatments and vehicle for both 6 and 13 days old cultures. The exception was vehicle at 13 days, here it was almost twice that of the other treatments. When kainate was applied, all regeneration rates at both time points were very similar at about 1.3 mM $min^{-1}$ and with the exception of vehicle the increase over the resting state was about 2.5 fold. See table 3.1 for the mean values. This shows that even though there exists slight differences in the rate of consumption of ATP in neurons overexpressing the different synucleins, the ability to produce ATP by oxidative phosphorylation as seen from the regeneration rate of ATP during the experiments is not impaired and is the same for all synucleins and control.

- Lower cytosolic resting levels were found for all three synucleins at 6 DPT
- At 13 DPT, neurons with βS and γS had increased their resting levels to those of control
- The consumption of ATP within the neurons either without or with kainate stimulation was similar for the synucleins with the exception of αS without kainate at 6 DPT where it was significantly lower
- The consumption rate for control was consistently higher
- Regeneration of ATP after washing out of FCCP was very similar for all treatments including control
- One exception was control without kainate at 13 DPT which had significantly higher regeneration rate

Regeneration of ATP following FCCP application was similar for all synucleins. Together with kainate which increased the regeneration, the rates were all very similar. This shows that the capacity for ATP production through oxidative phosphorylation in the mitochondria was not impaired by any of the synucleins.

### 3.2.9 Mitochondrial membrane potential

An important measure of mitochondrial viability is the mitochondrial inner membrane potential ($\Delta\Psi_m$). The $\Delta\Psi_m$ can be measured using positively charged, lipophilic fluorescent dyes

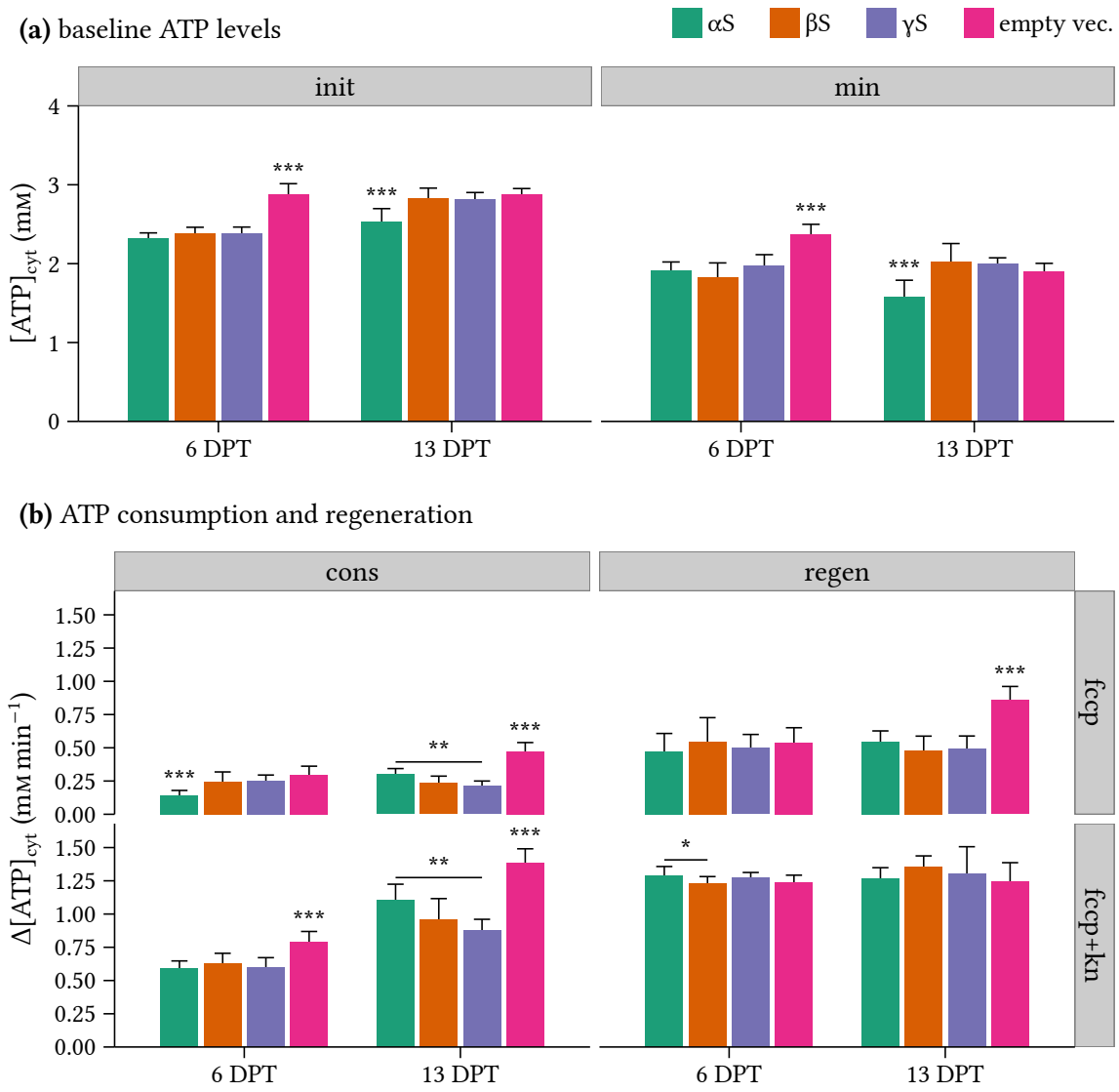


**Figure 3.25: Properties of ATP generation by oxidative phosphorylation**
Primary neuronal cell culture transduced with AAV vectors coding for the expression of αS, βS, γS or empty vector with MOI 12000 and co-transduced with the cytosolic ATP sensor ATeam1.03 with MOI 1200. Time-lapse recordings of the cultures were captured while applying 2 µM FCCP and either 0 µM or 10 µM kainate (kn). Measurements were done at 6 and 13 days after transduction. **(a)** Initial calibrated ATP concentration in the cytosol and the minimum measured ATP concentration in resting cells during FCCP application. **(b)** ATP consumption and regeneration rates during fccp or fccp+kn application. Statistically significant differences were calculated with one-way ANOVA / Tukey, *** $p < 0.001$; ** $p < 0.01$; * $p < 0.05$.

| *vector* | *age (days)* | *state* | *init* (mM) | *min* (mM) | *cons* (mM $min^{-1}$) | *regen* (mM $min^{-1}$) |
|---|---|---|---|---|---|---|
| αS | 6 | resting | $2.3 \pm 0.067$ | $1.9 \pm 0.11$ | $0.14 \pm 0.039$ | $0.47 \pm 0.13$ |
| βS | 6 | resting | $2.4 \pm 0.083$ | $1.8 \pm 0.18$ | $0.25 \pm 0.071$ | $0.55 \pm 0.18$ |
| γS | 6 | resting | $2.4 \pm 0.087$ | $2 \pm 0.14$ | $0.25 \pm 0.043$ | $0.5 \pm 0.1$ |
| vehicle | 6 | resting | $2.9 \pm 0.13$ | $2.4 \pm 0.13$ | $0.3 \pm 0.064$ | $0.54 \pm 0.11$ |
| αS | 13 | resting | $2.5 \pm 0.16$ | $1.6 \pm 0.22$ | $0.3 \pm 0.044$ | $0.55 \pm 0.078$ |
| βS | 13 | resting | $2.8 \pm 0.13$ | $2 \pm 0.23$ | $0.23 \pm 0.053$ | $0.48 \pm 0.11$ |
| γS | 13 | resting | $2.8 \pm 0.086$ | $2 \pm 0.074$ | $0.21 \pm 0.037$ | $0.49 \pm 0.097$ |
| vehicle | 13 | resting | $2.9 \pm 0.077$ | $1.9 \pm 0.11$ | $0.47 \pm 0.067$ | $0.86 \pm 0.1$ |
| αS | 6 | active | $2.3 \pm 0.069$ | | $0.59 \pm 0.053$ | $1.3 \pm 0.072$ |
| βS | 6 | active | $2.3 \pm 0.066$ | | $0.63 \pm 0.079$ | $1.2 \pm 0.051$ |
| γS | 6 | active | $2.3 \pm 0.059$ | | $0.6 \pm 0.071$ | $1.3 \pm 0.04$ |
| vehicle | 6 | active | $2.9 \pm 0.05$ | | $0.79 \pm 0.083$ | $1.2 \pm 0.053$ |
| αS | 13 | active | $2.4 \pm 0.18$ | | $1.1 \pm 0.12$ | $1.3 \pm 0.079$ |
| βS | 13 | active | $2.8 \pm 0.085$ | | $0.95 \pm 0.16$ | $1.4 \pm 0.086$ |
| γS | 13 | active | $2.9 \pm 0.1$ | | $0.88 \pm 0.082$ | $1.3 \pm 0.21$ |
| vehicle | 13 | active | $2.9 \pm 0.11$ | | $1.4 \pm 0.11$ | $1.2 \pm 0.14$ |

**Table 3.1: Synuclein cytosolic ATP mean values**
Table with mean values accompanying figure 3.25. Values are given as mean ± standard deviation. The *active min* values are used during calibration and are therefor all 0 and so are missing from the table.

that accumulate in negatively charged regions of both sides of the mitochondrial inner membrane (Scaduto and Grotyohann, 1999). When the membrane potential is disturbed the dye leaks out of the mitochondria and the ratio of mitochondrial to cytosolic fluorescence intensity is a relative estimate of the membrane potential. The initial $\Delta\Psi_m$ is estimated by decoupling the mitochondria which effectively nullifies the $\Delta\Psi_m$ and the difference in fluorescence ratio between before and after decoupling is taken as a measure for the $\Delta\Psi_m$. The $\Delta\Psi_m$ is established when the mitochondria pumps protons from the mitochondrial matrix to the intermembrane space during oxidative phosphorylation. An intact mitochondrial membrane potential is required for mitochondrial fusion and loss of the potential results in rapid fission of mitochondria (Legros et al., 2002). Also, during apoptosis the mitochondrial membrane potential is disturbed (Gottlieb et al., 2003). A loss of $\Delta\Psi_m$ in neurons overexpressing αS might therefor explain the change in morphology of mitochondria towards rounding and a fragmented appearance by lack of a functional physiological fusion machinery. It would also be an indication that the cells with this mitochondrial morphology are in a stage of apoptosis. To examine if this was the case, the relative $\Delta\Psi_m$ was measured.

Neuronal cell cultures were transduced with αS+GFP, βS+GFP, γS+GFP and only GFP ex-

pressing vectors with MOI of 12000. At either 6 or 13 days after transduction the cultures were labeled with 5 nM tetramethylrhodamine-methylester (TMRM) for 30 min and transferred to the imaging chamber of the microscope where they were continuously superfused with aCSF-H containing 2.5 nM TMRM. After recording the initial baseline fluorescence intensity, 2 µM FCCP was added to the aCSF-H superfusion media. This resulted in a rapid decline of fluorescence intensity of mitochondria and simultaneous increase in intensity of the surrounding areas. This is illustrated in figure 3.26a-c in which the trace depicts the change from baseline of the ratio of fluorescence in mitochondria divided by the increase in fluorescence of the surrounding cytosol. This change occurred with the same time course, amplitude and localization regardless of the vector treatment that the cell cultures had undergone. This showed that mitochondrial membrane potential is not impaired as a direct effect of αS overexpression nor from the mitochondrial fragmentation that accompanies it. It also suggests that these neurons are not in the process of apoptosis, at least not at a stage were loss of $\Delta\Psi_m$ and release of cytochrome *c* has occurred. That the $\Delta\Psi_m$ was intact for neurons that express the "toxic" levels of αS (MOI 12000) and this also at the late time point of 13 DPT indicates that the mitochondria are functional up until the neurons die and detach from the culture.

After washing out of the FCCP, mitochondria once again became clearly distinguishable from the cytosol indicating that TMRM reaccumulated in the mitochondria and that the mitochondria were able to restore their membrane potential. This occurred with all treatments with the same time course (not shown). The shape of mitochondria after recovery from FCCP was altered towards a more rounded appearance.

No impairment of mitochondrial membrane potential ($\Delta\Psi_m$) was found for any of the synucleins or GFP. This was expected considering that calcium handling and ATP production are dependent on the mitochondrial membrane potential.

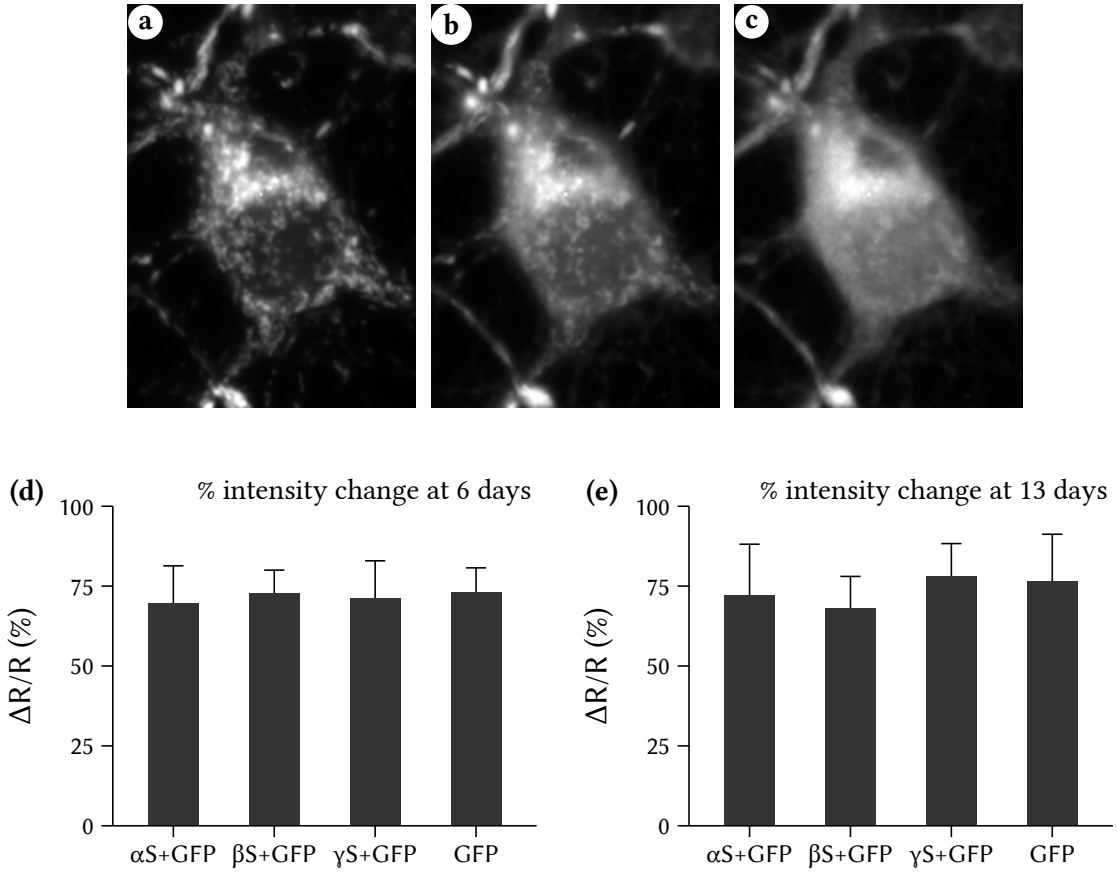


**Figure 3.26: Mitochondrial membrane potential in neurons expressing αSyn**
Neuronal cell culture transduced with αS+GFP, βS+GFP, γS+GFP or only GFP with MOI 12000 and labelled with 5 nM TMRM for 30 min. **(a-c)** The change in intensities of a neuronal cell body before (a), during (b) and after **(c)** applying 2 µM FCCP. **(d,e)** The relative change in mitochondrial membrane potential ($\Delta\Psi_m$) assessed from the change in ratio of intensity between mitochondria and surrounding cytosol before and after decoupling at 6 days (d) and 13 days (e) after transduction.

# 4 Discussion

This thesis has as its main objective the characterization of changes in mitochondrial function and morphology in neurons that are overexpressing α-Synuclein (αS) as a model for Parkinson's disease (PD) and is trying to compare this to changes caused by the other two synucleins, β-Synuclein (βS) and γ-Synuclein (γS). Genetically encoded sensors (GESs) are modern tools for the study of physiological systems and a number of novel sensors were employed in this study. In addition, the GESs were targeted to neurons and the mitochondria in order to specifically characterize and isolate the effects of αS to these locations. The following sections discuss the results described in the previous chapter and tries to show how the conclusion can be reached that even though αS affects mitochondrial morphology and dynamics of neurons in cell culture, it does not lead to loss of mitochondrial function. First however, is a discussion of the results pertaining to GESs, the difficulties and necessary controls that need to be carried out when using them as well as their general usefulness in the study of neurodegenerative disease.

## 4.1 Genetically encoded sensors

### 4.1.1 Targeting of genetically encoded sensors

Targeting of GESs can refer to the expression of the sensors in specific tissue regions or cell subtypes. This can be accomplished using different vector systems and/or promoters driving the expression. For this thesis all expression of sensors was done using adeno-associated virus (AAV) vectors and all constructs were using the human synapsin promoter (hSyn) to restrict expression to neurons (Kügler et al., 2003; Dodiya et al., 2010; Weinberg et al., 2013). Targeting can also refer to expression in specific subcellular compartments. Sensors can be coupled as fusion constructs to other proteins that gets transported and sequestered in specific regions or targeting sequences can be added. I used mitochondrial targeting sequences

(MTSs) to target sensors to mitochondria and this was successful. However, larger sensors, like the Förster resonance energy transfer (FRET) sensors based on cyan fluorescent protein (CFP) and yellow fluorescent protein (YFP), were not expressed without leakage to the cytosol when using only one copy of the MTS. Instead, a repeated sequence was necessary and with a 4x repeat of the MTS from cytochrome *c* oxidase (COX) subunit VIII, targeting was efficient as shown in section 3.1.2. The necessity for multiple copies of the MTS for efficient targeting has been demonstrated previously (Filippin et al., 2005; Palmer et al., 2006). Palmer et al. (2006) observed inefficient targeting and leakage to the cytosol in 20% of cells with 4x repeated MTS from COX subunit VIII. This was reduced to 1% with an 8 times repeat. This is different from my results in that I did not observe any cytosol staining when using a 4x repeat of the MTS. This could be due to differences in the cell types used, Palmer et al. (2006) were expressing in HeLa cells. More likely however, it is due to differences in the level of expression. Palmer et al. (2006) used FuGENE, a non-liposomal cationic lipid (Arnold et al., 2006) to transfect cultured HeLa cells and their constructs had been cloned into pcDNA3 plasmids that drive expression from the cytomegalovirus (CMV) promoter. Even though transfection efficiency is lower with non-viral vectors compared to AAV (Djurovic et al., 2004), actual protein expression in successfully transfected cells is higher. Additionally, the CMV promoter generally produces stronger expression than when expression is driven by hSyn (Kügler et al., 2003), the promoter used in the constructs described for this thesis. It is therefor likely that stronger expression levels in the HeLa cells were responsible for a higher rate of non-specific targeting i.e. leakage to the cytosol. Single fluorescent protein (FP) based GES were found to be targeted successfully with only one copy of the MTS. This suggests that the efficiency of targeting is based on the size of the protein.

### 4.1.2 Characterization of the genetically encoded sensors used

Published values for properties like $\Delta F/F_0$ and $K_d$ for a particular sensor are useful when choosing which variant to use. However, the actual properties often differ when the sensor is expressed in a system that is different from that which was used to obtain those values (Linse et al., 1991). Since the results from measurements using GESs were going to be used quantitatively and in order to compare properties between cells and preparations, it was deemed necessary to first characterize the sensors in the primary cortical cell culture preparations where they were to be used. For all sensors this meant finding proper expression levels, especially for targeted versions, that were not toxic or produced cells with apparent

changes in morphology due to expression of the sensor. Also, the practical max $\Delta F/F_0$ or complete dynamic range ($F_{max}/F_{min}$) was established *in cell* where possible.

### D3cpV and RCaMP1e

For genetically encoded calcium indicators (GECIs), the dynamic range is fairly small and the difference between the resting cytosolic free-$Ca^{2+}$ in neurons and the level of free-$Ca^{2+}$ after high potassium depolarization or another strong stimuli is large, between ~100 nM at rest and several µM after stimuli (Ross, 1989; Marambaud et al., 2009). This means that a GECI with a dynamic range of 10 will still get saturated upon calcium influx in a neuron that is stimulated if the sensor has a high enough affinity for $Ca^{2+}$. Thus, the sensor needs to be chosen based on its $K_d$, dynamic range and the type of stimuli that it shall be able to measure the response to. For this thesis, the interest lie with physiological stimuli of neurons and the stimuli used was trains of action potentials at 10 Hz.

For D3cpV and RCaMP1e the dynamic range was established by applying ionomycin which led to very high responses of the respective sensor signals. Ionomycin, a ionophore capable of acting as a mobile ion carrier to transport cations across solvent barriers (C Liu and Hermann, 1978; Erdahl et al., 1994), is commonly used for *in cell* determination of the dynamic range of both genetically encoded and organic calcium indicators. It facilitates the equilibration of the intracellular calcium concentration with that of the extracellular media (A Takahashi et al., 1999). If a sufficiently high extracellular calcium concentration is applied, it will saturate the sensor while ionomycin is present. To measure the response of a sensor to zero level of free $Ca^{2+}$ within a cell, ionomycin can be applied together with a chelator for calcium ions such ethylene glycol tetraacetic acid (EGTA). Calcium ions that leaks out from the cell, facilitated by ionomycin, will be sequestered by EGTA and eventually all calcium will have left the cell. The dynamic range acquired from ionomycin treatment was compared with the typical response to a physiological stimuli from field stimulation (FS) at 10 Hz. For both GECIs, the response from FS was within 75% of the sensor range measured with saturating stimuli with ionomycin and both sensors were thus usable for comparison experiments in the primary neuronal cell cultures used. Although not as important for this thesis, the dynamic range ($R_{max}/R_{min}$) measured from D3cpV of ~4 (section 3.1.4) corresponded with previously published values by Palmer et al. (2006). Likewise for RCaMP1e, for which only the maximum $\Delta F/F_0$ was measured (~3.5), corresponded with what has recently been reported for RCaMP1e by Akerboom et al. (2013).

When targeted to the mitochondria, the responses from either of D3cpV or RCaMP1e was unreliable when applying ionomycin. High potassium depolarization produced larger changes of the FRET ratio for 4mtD3cpV and the $\Delta F/F_0$ for mtRCaMP1e than did 10 mM $Ca^{2+}$ + ionomycin, suggesting that the $Ca^{2+}$ was not able to properly enter the mitochondria. When neurons were depolarized with high potassium, the response in the mitochondria was nevertheless higher than that caused by the FS stimuli used for later experiments. This showed that also in the mitochondria was a depolarizing stimuli using FS not enough to saturate the sensor and proved that it was feasible to use both D3cpV and RCaMP1e for mitochondrial measurements of calcium.

When the dissociation constant $K_d$, as well as the minimum and maximum response ($R_{min}$ and $R_{max}$) values are known, the measured ratio or response from ratiometric and single wavelength GECIs can be converted into approximate free-$Ca^{2+}$ concentrations according to the methods for single wavelength and ratiometric indicators put forth by Grynkiewicz et al. (1985). The $K_d$ values are taken from literature or determined *in vitro* using purified sensor protein. However, there are no guarantees that the values acquired correspond to actual intracellular calcium levels and there are problems associated with these conversions such as the sensitivity of indicators to photobleaching of the chromophore (Becker and Fay, 1987; Fowler and Tiger, 1997). Also, the binding properties of calmodulin (CaM), the binding protein domain used in both D3cpV and RCaMP1e, can be influenced by ionic strength and pH (Ogawa and Tanokura, 1984; Linse et al., 1991). Because of these issues and since a determination of absolute intracellular $Ca^{2+}$ levels was not deemed necessary, the data from experiments with GECIs is presented "raw", without conversion to calcium concentration.

### ATeam1.03

In addition to GECIs, ATeam1.03, a GES sensitive to changes in ATP levels was employed to study the effects of the synucleins on ATP consumption and regeneration from oxidative phosphorylation. Previously, measurements of ATP levels in neurons have established the resting ATP concentration to be between 1 and 3 mM. These values come from enzymatic measurements on whole brain lysates (Veech et al., 1979) or luciferase luminescence based assays on primary neuronal cell culture lysates (Fukuda et al., 1983) or from intact cells using genetically encoded luciferase (Ainscow et al., 2002; Mironov, 2007).

ATeam1.03 is a newly developed sensor created and characterized by Imamura et al. (2009). It relies on FRET between CFP (mseCFP) and YFP (cp173-mVenus) facilitated by binding

of ATP to the ε subunit of bacterial $F_0F_1$. When the work for this thesis started, the only publication mentioning the usage of this sensor was the original description. Therefor, a more in depth characterization of ATeam1.03 in the primary cortical cell cultures used here was deemed necessary. In section 3.1.6 an attempt was made to calibrate ATeam1.03 in cells of primary cortical cell culture according to a method described for other sensors (Dittmer et al., 2009). Cells were permeabilized with β-escin and superfused with media containing different extracellular ATP concentrations. The parameters from a fit of this calibration gave values for $K_d$ (3.13 mM) and Hill coefficient (2.16) that corresponded with the published values from *in vitro* characterization (3.3 mM and 2.1 respectively) (Imamura et al., 2009). However, the FRET ratio initially reported by the sensor, before permeabilization, was never recovered even with 10 or 100 mM ATP, which should saturate the sensor according to Imamura et al. (2009). Some possible reasons for this behavior was already mentioned in section 3.1.6. Another reason might be what Willemse et al. (2007) reports on regarding ATP and FRET. While creating a FRET based GES for ATP, they found that a sensor construct incorporating CFP and YFP with an protease cleavage linker, which should not interact with ATP, responded to changes in ATP concentrations *in vitro*. They show that this is likely to be related directly to FRET since it was not present in individual CFP or YFP units and it did not change the ratio measured from constructs were the two FPs where located far enough from each other to not allow FRET to occur. They also found that the effect most likely stems from interaction with $Mg^{2+}$ since variations in $Mg^{2+}$/ATP concentrations had dose dependent effects on the FRET ratios. This conclusion is not unreasonable considering the fluorescent properties and their modification by $Mg^{2+}$ of ATP (Amat et al., 2005). It has also been reported that ATP can quench the fluorescence of other fluorophores (C Li et al., 2005). That this does not occur with single FPs can be explained by considering the protected nature of the chromophore in FPs, due to the surrounding β-barrel. This also makes this unlikely to be an issue for single FP based sensors. This has consequences for all FRET based sensors however, and arguably, the issues for ATeam1.03 are of least concern since it is a sensor which has been characterized in regards to its behavior in the presence of ATP, something GESs usually have not. As for the other FRET based sensor used in this thesis, D3cpV, this is unlikely to affect the results. The results presented in this thesis shows that ATP levels in the cytosol of active neurons, i.e. stimulated with either kainate or FS, is hardly perturbed if the mitochondria is active and able to compensate with increased ATP production. This means that for measurements using D3cpV in the cytosol, no changes in ATP levels that might interfere with the FRET efficiency of the sensor was present. However, it is known that stimuli that causes uptake of $Ca^{2+}$ to the cytosol also increases oxidative phosphorylation, leading to transient increased ATP levels

in the mitochondria (Nakano et al., 2011). From the results in section 3.1.6 we can infer such an increase is happening as well since the production rate was higher after cells had been stimulated with kainate. Figure 3.12d shows this especially well. Nakano et al. (2011) targeted a modified version of ATeam1.03 to the mitochondria of HeLa cells and measured increases in ATP levels in response to elevated cytosolic $Ca^{2+}$ levels. They did not calibrate their sensor in the mitochondria but comparing their measured FRET ratio change within the mitochondria to their *in vitro* data for the sensor, the response in the mitochondria that they measured corresponded to an increase of approximately 20% or ~3.5 mM. The data by Willemse et al. (2007) shows that for a FRET construct incorporating a short Xa protease-sensitive cleavage linker, a change from 1 to 5 mM ATP produces a 24% decrease in FRET ratio. However, for a construct with a inosine monophosphate dehydrogenase type II (IMPDH2) domain linking the two FPs, the change was only ~4%. This estimation tells us that in the worst case scenario, a FRET sensor such as D3cpV will, when targeted to the mitochondria and responding to changes induced by a large increase of cytosolic $Ca^{2+}$, report with ~24% smaller ratio change due to interference from elevated ATP levels. For the results in this thesis this can be ignored since:

1. the response of D3cpV expressed in the mitochondria was within ~50% of the sensor range when using FS. Assuming that this is 24% less due to ATP interference, the actual sensor response would be ~74% which is still significantly below saturation.

2. the production rates of ATP from oxidative phosphorylation was the same between all synuclein treatments and control. This suggests that the ATP increase in the mitochondria is also the same and thus the interference from ATP was the same for all treatments and is not hiding differences in $Ca^{2+}$ accumulation in the mitochondria.

Interestingly, *in cell* calibration of ATeam1.03 has since been tried by another group (Ando et al., 2012) who did not report any inconsistencies. They used digitonin to permeabilize Huh-7 cells expressing ATeam1.03 in a fusion construct that targeted the sensor to hepatitis C virus (HCV) ribonucleic acid (RNA) replication sites. A ATP concentration of ~5 mM was reported at these sites with a cytosolic concentration of 1 mM.

### 4.1.3 Genetically encoded sensors for use in the study of neurodegenerative disease

As tools for studying the mechanisms behind neurodegenerative diseases, GESs can be very useful. It is fairly straight forward to construct sensors that respond to changes in the intracellular environment by combining FRET between FPs and binding domains from bacterial and other species. So far, most of the GESs that are available, respond either to changes in ligand concentrations, cleavage of peptide sequences or in some cases modifications such as phosphorylation (Tyas et al., 2000; Takao et al., 2005). For αS or any other disease involving the aggregation of proteins, a sensor that would report on the aggregation state or specific species of aggregation would be very useful.

Bimolecular fluorescence complementation (BiFC) provides a tool for studying dimerization of proteins and has been used to study αS (Outeiro et al., 2008) but it has some drawbacks. The main one being the very high affinity of the two green fluorescent protein (GFP) halves preventing dissociation and thus without proper controls (Morell et al., 2008) it is actually a measure of the association constant of the two halves of GFP rather than dimerization of fusion protein (Kerppola, 2006). A protein domain that would detect and change conformation in the presence of dimerized or oligomerized species of αS would be a great advantage over BiFC. New tools are becoming available that can recognize proteins, such as aptamers and nanobodies, and with clever engineering these have the potential to enable the construction of sensors for the detection of oligomerized species.

The clinical symptoms of PD are due to degeneration of dopaminergic neurons in the SNCA (PARK1). This is indication that these neurons are primarily affected in regards to the disease. Studying the effects of suspected mediators of the disease such as αS would therefore preferably be done in these neurons. However, the tools available for this are limited to immortalized cell lines such as the LUHMES cells (Lotharius et al., 2002) or primary cell cultures based on midbrain. Midbrain cultures have the drawback of, in the best case, having only about 10% dopaminergic neurons (Sawamoto et al., 2001). This then requires the subsequent fixing, labeling, identification and correlation of these neurons to those imaged during live cell imaging, a time consuming and tedious practice. Promoters such as hSyn can be used to drive expression of the sensor in only specific subtypes of cells. One idea would be to use a promoter that is more or less specific to dopaminergic neurons. Some progress has been made in this using the promoter from tyrosine hydroxylase (TH) (Matsushita et al., 2002; Oh et al., 2009). Another alternative for studying the possible effects of dopamine within neurons

other than naturally dopaminergic neurons is to use AAV vectors coding for the expression of two enzymes necessary for converting L-dopa into dopamine. DOPA decarboxylase (DDC) is the enzyme responsible for converting L-dopa to dopamine (Burkhard et al., 2001) and vesicular monoamine transporter (VMAT) utilizes the proton gradient of synaptic vesicles to load them with dopamine (Eiden et al., 2004). Then one would add L-dopa to the growth media before experiments to induce production of intracellular dopamine. This has been successfully tried by our group (Maddalena, 2012) but the necessity of using two viruses for dopamine production and loading plus two viruses for a sensor and αS made this strategy difficult. Nonetheless, Maddalena (2012) demonstrated that the presence of dopamine together with αS in primary cortical neurons did not reduce the viability of the neurons, nor did it promote aggregation of αS.

Characterization of the GECIs RCaMP1e and D3cpV both in the cytosol and targeted to the mitochondria showed that their dynamic range was adequate to allow comparative studies between neurons undergoing FS.
Even though *in cell* calibration of ATeam1.03 in the primary cortical cultures was inconclusive, and so determination of absolute ATP levels excluded, the usefulness of ATeam1.03 remains in its ability to report on relative levels and changes in ATP concentrations. ATP consumption during activity increases ~3-fold in neurons and this is answered with a similarly high increase in ATP production by the mitochondria.

## 4.2 Overexpression of synucleins in neurons

The major topic of the work done for this thesis concerned the effects of overexpression of synucleins in neurons in cell culture. The general toxicity was examined as well as the abilities of the neurons to handle raised intracellular $Ca^{2+}$ levels in response to depolarizing stimuli. Of special interest was the effects on mitochondrial morphology and in particular the ability of the mitochondria to carry out its major functions. The mitochondria was examined in multiple ways including its ability for calcium handling, ATP turnover, mitochondrial membrane potential ($\Delta\Psi_m$) and motility. What came out of this study was that αS has a profound negative effect on the survivability of neurons in cell culture and that this is strongly correlated with the amount of the AAV coding for αS being present. At low multiplicity of infection (MOI), the integrity of neurites, soma and mitochondria were still intact as compared with neurons expressing only GFP. That βS has a similar albeit smaller toxic effect as that of αS was new and surprising since it has previously been described as being protective (Hashimoto et al., 2001; Hashimoto et al., 2004) in neurons. The results also showed that

mitochondria in neurons that overexpress αS and to a lesser degree βS changes their appearance towards a rounded morphological phenotype. It could also be shown that for αS but not the other synucleins or GFP, the motility of mitochondria is reduced. These results led to the suspicion that overexpression of αS but also to some extent βS would produce some functional changes in mitochondria. However, none of the different modes of mitochondrial function that were examined showed any changes that could be attributed to the effects of αS.

### 4.2.1 Neuronal toxicity

As was laid out in section 1.1 and section 1.2, the main symptom in PD is the degeneration of dopaminergic neurons in the substantia nigra pars compacta (SNpc) of the midbrain. An important question is then whether αS itself has any properties that could cause such degeneration. This has been tested with different forms of αS, mutated and wild type (WT), in different model systems and the conclusion has been that αS does have toxic properties (Karpinar et al., 2009; Winner et al., 2011) suggesting a link to the disease. As for αS, the physiological function and possible pathological mechanisms behind βS are still unclear. Previously, βS has not been considered an actor in the etiology or progression of aggregopathies like PD. Instead, several studies have suggested an at least partially protective role for βS. These studies examined the interaction of βS with αS and showed that βS can prevent or reduce αS induced neurotoxicity in cell culture, transgenic (TG) animals and viral vector based models (Hashimoto et al., 2001; Hashimoto et al., 2004). Another view is emerging though since a contribution of βS and possibly also of γS to neurodegenerative processes have been documented. Both βS and γS have been detected at pre-synaptic and axonal sites associated with pathology in brains of sporadic PD and dementia with Lewy bodies (DLB) patients, but not in controls (Galvin et al., 1999). Also, a DLB linked mutation (P123H) in SNCB, the gene coding for βS, has been shown to produce axonal swellings, astrogliosis and memory deficits in TG mice (Fujita et al., 2010). Crossing these mice with αS TG mice led to an enhanced pathologic phenotype in showing neuronal cell loss and dopaminergic dysfunction. This further suggests an interplay between αS and βS function. For γS, the ability to cause neurodegeneration has been demonstrated by overexpression in mice (Ninkina et al., 2009). Those findings showed aggregation of γS and the appearance of various inclusions in neuronal cell bodies throughout the nervous system but interestingly more prominently in the spinal cord with loss of motor neurons.

The results on the toxicity of the synucleins presented here confirms that αS overexpression leads to neuronal cell loss in this system. A non-linear relationship between MOI and the number of remaining neurons in culture was found. This suggests that most neurons tolerate some overexpression of αS but above some level, αS abruptly becomes toxic. However, the relationship between the MOI used and the protein level expressed as seen by western blot (figure 3.15c,d) was not linear which suggests that protein expression is limited at high MOI. This could mean that the relationship between αS expression level and remaining number of neurons is more linear in reality.

The results also show that βS overexpression also leads to cell loss but that γS remains non-toxic compared to control. The toxicity of αS can be said to be higher than that of βS since the progression of cell loss is faster for αS and the total number of remaining cells is higher for βS than for αS using the same MOI. A view of βS as irrelevant or protective in neurodegenerative disease can not be accepted considering these findings. Instead further studies should be conducted on the role that βS plays and its possible interactions with αS in disease progression.

The toxicity of αS has been demonstrated before but this is the first time that βS has been shown to be toxic in neuronal cell cultures. Previously, a protective role for βS has been assumed, a view that this work challenges. Further studies are needed to find out what role βS plays in PD.

### 4.2.2 Mitochondrial morphology and dynamics

Since many of the proteins that has been found with mutations related to PD have direct or implied association with mitochondria, it lies close at hand to suspect involvement of these with mitochondrial fission/fusion. In fact, recently, parkin (PARK2) has been found to ubiquitylate mitofusins, targeting them for proteasomal degradation as a step in mitophagy (Youle and Narendra, 2011). It is thought that this inhibits re-fusion of damaged mitochondria thereby segregating them for mitophagy. In turn, P-TEN-induced putative kinase 1 (PINK1) is imported to mitochondria were it seems to normally be degraded and maintained at low levels. If a mitochondria becomes damaged, the levels of PINK1 rises within the mitochondria, which signals the recruitment of parkin (Youle and Narendra, 2011).

Mitochondrial fragmentation due to αS has been demonstrated by others while the work for this thesis was underway (Kamp et al., 2010; K Nakamura et al., 2011) and my findings in neuronal cell culture confirms their findings for both αS and βS. The finding that overexpression of βS also causes fragmentation is novel and again suggests a possible role for βS in

disease. In *in vitro* experiments, Kamp et al. (2010) found that αS directly prevented the fusion of small unilamellar vesicles in a concentration dependent fashion. They were also able to demonstrate mitochondrial fragmentation induced by overexpression of αS in *Caenorhabditis elegans* and the human derived cell line SH-SY5Y. Both their results and the results of K Nakamura et al. (2011) showed mitochondrial fragmentation in αS overexpressing cells to occur without the requirement of dynamin related protein 1 (Drp1), suggesting that fission is caused by αS directly also in cells. Kamp et al. (2010) also examined the expression of mitofusin 1 (Mfn1) and mitofusin 2 (Mfn2) together with αS and could show an increase in elongated mitochondria upon expression of the mitofusins that was partly restored to control levels by αS. They do not seem to have examined the possible role of αS in regulation of the mitofusins. The results presented in this thesis on mitochondrial fragmentation supports the findings by these two groups. The data shows αS to cause fragmentation in primary cortical cell culture and that the level of fragmentation increases with age of the cultures. βS has no effect on fragmentation in young cultures but causes fragmentation when the cultures age, suggesting a similar function but with reduced potential for βS compared to αS. Mitochondrial fragmentation was never seen when overexpressing γS, neither in young or old cultures where the fragmentation was always comparable to that of control. All three of the synucleins have lipid binding N-terminal regions and can associate with membranes (Ducas and Rhoades, 2012). The reason why αS and to a lesser extent βS and not γS causes fragmentation is not known.

I also examined the effects αS on average and maximum movement speed of mitochondria in primary cortical cell culture. In cells with decreased fission or fusion, the speed of mitochondrial movement is known to decrease (H Chen and Chan, 2009). The reason for the reduced motility in fusion deficient cells is unclear but these mitochondria have been shown to become stuck or move according to Brownian motion, without directionality (H Chen et al., 2003). Different movement speeds of mitochondria in neurons have been reported, but my results of 0.7-0.87 $\mu m\, s^{-1}$ (42-52 $\mu m\, min^{-1}$) average and 1.33-1.58 $\mu m\, s^{-1}$ (80-95 $\mu m\, min^{-1}$) maximum speed depending on age of culture matches that of others (De Vos et al., 2003; MacAskill and Kittler, 2010). Considering the relation between mitochondrial fragmentation/fission and movement (section 1.3) it is not surprising that a decrease in mitochondrial movement speed in neurons expressing αS was found as well. This was only present in old cultures even though fragmentation was present also in the younger cultures. This suggests that the fragmentation caused by αS precedes the impairment in movement. Since I found no fragmentation in γS overexpressing neurons, I did not expect to see impairment of movement either. βS however might have been expected to affect the movement of mitochondria since

it also causes fragmentation. That I did not see this for βS might have to do with the level of fragmentation and the age of the cultures. The level of fragmentation caused by βS did not equal that of αS even at 13 days post transduction (DPT). Thus a decrease in mitochondrial movement might only be detected when a majority of the mitochondria have become fragmented.

Mitochondrial fusion/fission is normally regulated by dynamins. A mechanism for αS in preventing fusion of mitochondria has been suggested. I found mitochondrial fragmentation in response to αS overexpression but without correlation with changes in calcium handling. This suggests that fragmentation by αS is unrelated to fission of mitochondria from elevated calcium levels. βS was also found to cause fragmentation of mitochondria, casting further doubt on a protective role for the protein.

### 4.2.3 Mitochondrial function

Numerous mechanisms of action for αS toxicity has been proposed, including generation of reactive oxygen species (ROS) through inhibition or interaction with complex I of the electron transport chain (ETC) and changes in ion handling through the association with ion channels or pore formation in membranes. It is not clear how increased ROS production in the mitochondria leads to apoptosis and cell death but mechanisms have been suggested that include the destruction of mtDNA (Ricci et al., 2008) or cytochrome *c* release due to oxidation of cardiolipin, an important component of the inner mitochondrial membrane (IMM) (Ott et al., 2007). ROS is a normal byproduct from the ETC and 1-2% of all oxygen consumed under physiological conditions is converted into radicals (Chance et al., 1979; Orrenius et al., 2007). An intuitive connection between ROS induced damage and the degeneration of dopaminergic neurons seen in PD exists in monoamine oxidase (MAO). MAO has been shown to produce $H_2O_2$ and can be the source of up to ~50-fold more ROS than oxidative phosphorylation (Hauptmann et al., 1996; Maurel et al., 2003). ATP depletion and ROS production through inhibition of complex I has been proposed as the mechanisms behind Rotenone and 1-methyl-4-phenyl-1,2,3,6-tetrahydropyridine (MPTP) induced parkinsonian symptoms (Ali et al., 1994; N Li et al., 2003). Mitochondrial fission has not been shown to occur from ROS production but starvation of cells caused fragmentation and mitophagy as well as moderately elevated ROS levels in at least one recent study (Frank et al., 2012). In *in vitro* experiments on mitochondria isolated from dopaminergic cells overexpressing αS and mitochondria from SNpc of PD patients demonstrated increased ROS production and complex I inhibition with increasing αS levels (Devi et al., 2008). They also show that αS in this system was taken up

by mitochondria through the outer mitochondrial membrane (OMM) transport outer membrane (TOM) complex in an energy dependent fashion. My results show no impairment in ATP production which suggests that mitochondrial fragmentation precedes any interference with the ETC caused by αS overexpression. This is further supported by the fact that I also did not observe any changes in mitochondrial membrane potential, something which has also been observed by others (Kamp et al., 2010; K Nakamura et al., 2011). Therefor I suggest that in contrast to the situation in isolated mitochondria, complex I inhibition is not the major cause of toxicity in primary cortical neurons.

Another suggested mechanism for αS toxicity is through interaction with membranes. Membrane binding, permeabilization and pore formation by αS have been demonstrated *in vitro* by several groups (Kim et al., 2009; Feng et al., 2010; Stöckl et al., 2013). This seems to occur preferentially by oligomeric (Kim et al., 2009) and monomeric (Zakharov et al., 2007) forms of αS but not larger structures such as fibrils. Lower membrane affinity has been reported for the A30P mutant of αS, most likely due to disruption of the α-helix due to the proline mutation (Jensen et al., 1998; Wislet-Gendebien et al., 2008). Conflicting reports exists regarding the ability of A30P to induce permeabilization and undergo pore formation in membranes (Zakharov et al., 2007; Camilleri et al., 2013). That membrane permeability in response to αS is not only occurring in artificial systems has been shown by Feng et al. (2010) who found increased membrane conductance in MN9 cells overexpressing αS. Another group reported no increase in membrane conductance for WT αS but increase for the A53T mutant in SH-SY5Y cells (Furukawa et al., 2006). This same group also found elevated basal and peak cytosolic $Ca^{2+}$ levels in response to high potassium depolarization for the A53T mutant. Another group, working with the same cell line, as well found increased peak levels of cytosolic $Ca^{2+}$ from high potassium stimuli (Hettiarachchi et al., 2009). They found the reverse behavior in that the A53T mutant took up lower amounts of $Ca^{2+}$ than WT αS. My own results showed a much smaller increase in peak levels of $Ca^{2+}$ upon high potassium depolarization for primary cortical neurons that overexpressed αS suggesting differences in the membrane conductance depending on cell type. When I used physiological stimuli such as FS of frequencies commonly present in neuronal systems, I did not observe any changes in $Ca^{2+}$ handling however. This suggests that high levels of αS is not enough to impair calcium handling and normal action potential (AP) firing of neurons is not causing increases in intracellular calcium due to αS, something which could otherwise lead to apoptosis as seen in excitotoxicity from glutamate receptor overactivation (Pivovarova and Andrews, 2010).

αS might cause permeabilization of other membranes than the plasma membrane (PM). Since

αS has been shown to be able to cross the IMM, at least in isolated mitochondria (Devi et al., 2008), it is possible that αS forms a pathological pore in the IMM resembling the mitochondrial permeability transition (MPT) pore. I did not see any changes in mitochondrial membrane potential however, suggesting that this is not the case. But in contrast to elevated ROS production and its apoptotic response which can be assumed to be slower, the release of even very small amounts of cytochrome *c* is known to initiate apoptosis and it is possible that this is what leads to the toxicity of αS observed in cell culture.

It has been shown that αS prefers binding to membranes with high curvature. Middleton and Rhoades (2010) found a 10x stronger binding to vesicles with 46 nm than 77 nm. This is interesting since it fits with preferential binding to small synaptic vesicles in dopaminergic neurons which have similar size (~30-60 nm) (Rayport et al., 1992; Nirenberg et al., 1996). The PM and OMM (~0.5-1 µm) have significantly lower curvature (Frey and Mannella, 2000). The IMM however, have invaginations forming the cristae and these have much higher curvature. Cristae junctions for example have a reported diameter of 12-40 nm (Rabl et al., 2009) and tubular cristae 30-40 nm (Frey and Mannella, 2000). These dimensions are similar to those of small synaptic vesicles, and the diameters reportedly preferred by αS. In PD, perhaps αS looses its binding to synaptic vesicles, either due to crowding from too high concentration of αS or from some yet unknown mechanism, thus becoming present at higher levels close to mitochondria where it crosses the OMM. In the intermembrane space it could associate with the IMM at regions of high curvature, causing swelling and eventual release of cytochrome *c* through a MPT like mechanism. In this scenario, no reduced mitochondrial function or impaired mitochondrial membrane potential is necessary until cytochrome *c* is released, at which moment apoptosis might occur rapidly.

A role for αS in complex I impairment has been suggested from studies on isolated mitochondria. Such an impairment would reduce the ability of the mitochondria to produce ATP and lower the $\Delta\Psi_m$ but none of these changes were measured. This suggests that complex I inhibition is not the primary cause of toxicity from αS in neurons.
Pore formation in the IMM is another possible cause of toxicity. If these pores exists, they are either not permeable to calcium or they are transient enough to not cause any impaired calcium handling. It is possible however, that the loss of neurons observed in the cell cultures occur through apoptosis from cytochrome *c* release in response to MPT induced by αS mediated permeability.

## 4.3 Conclusion and perspectives

The results presented in this thesis demonstrate that αS overexpression does not affect mitochondrial function in primary neuronal cell culture, neither that of calcium handling or ATP production through oxidative phosphorylation. A functional mitochondria was also supported by the presence of an intact mitochondrial membrane potential. But this does not mean that αS is in no way affecting or contributing to pathology through a mechanism involving the mitochondria. In fact, I found that αS overexpression does affect both mitochondrial morphology and motility. Since mitochondrial morphology, integrity and fission especially, is related to mitochondrially regulated apoptosis, this suggests a connection between αS and cell death, which requires further study.

The really surprising finding however, was that βS, previously thought to protect against αS toxicity, is toxic by itself and that it too, leads to fragmentation of mitochondria. But as for αS, no other impairment of mitochondrial function was found.

It was also interesting to discover that calcium influx in response to depolarization, something previously found to be greatly increased for the SH-SY5Y cell line when expressing αS, was hardly affected in primary cortical neurons. This reveals the difficulties and risks of misinterpretation when working *in vitro* and shows the importance of taking these experiments to *in vivo* studies in the future. Our lab has developed and adapted methods for *in vivo* imaging in live animals using two-photon microscopy. The intention is to transfer the methods from primary cell culture to the intact animal and assess the effects of the synucleins there.

Preliminary experiments by our lab show that the loss of neurons by αS and βS can be prevented or reduced by co-expressing mitochondrial anti-apoptotic proteins such as B-cell lymphoma-extra large (Bcl-xl). The immediate work which will be carried out upon the completion of this thesis is the examination of what effects this has on mitochondrial morphology as well as if these "protected" neurons show signs of mitochondrial dysfunction.

The present study also shows that GES hold great potential for use in research on neurodegenerative diseases. AAV vectors coding for the expression of several additional GESs than those covered in this thesis have already been generated. A mitochondrially targeted version of ATeam1.03 is ready and I hope that this can be used to further examine effects on ATP turnover in the mitochondria by the synucleins. Both cytosolic and mitochondrial ROS sensors are also available and it will be interesting to see if these can show increased oxidative state of the cell due to overexpression of αS.

# 5 Summary

Parkinson's disease (PD) is the second most common neurodegenerative disease and it affects more than 1% of the worlds population over the age of 65. A hallmark of PD is the appearance of Lewy bodies (LBs) throughout the brain and a major component of these intracellular inclusions is the small soluble protein α-Synuclein (αS). Rare familial mutations as well as duplications and triplications of the gene coding for αS leads to early onset PD and this makes a role for αS in the etiology of PD likely but exactly how αS contributes to the disease is still unknown. No genetic link to PD has so far been described for the other two members of the synuclein family, β-Synuclein (βS) and γ-Synuclein (γS) but βS has recently been suggested to have neuroprotective properties, evidence of which comes from experiments showing that it reduces αS induced neurotoxicity. However, a mutation in βS is linked to dementia with Lewy bodies (DLB) and has been shown to cause neurodegeneration in transgenic (TG) mice. For this thesis, the effects of overexpression of the synucleins in primary cortical neurons were examined. Because αS has been shown to reduce the activity of complex I of the electron transport chain (ETC) in mitochondria isolated from patients, a special interest was the effects on the mitochondria, its function and morphology. Overexpression of αS as well as βS but not γS led to degeneration of neurons. The mitochondria was also affected, αS and βS both led to a fragmented morphology that worsened with time whereas the mitochondria in γS overexpressing neurons were unaffected. Nevertheless, these mitochondria were still functionally intact. Not only were they able to handle influx of calcium, they were also able to regenerate ATP after depletion at the same rate as control. This suggests that oxidative phosphorylation and as a consequence complex I is not significantly impaired in these neurons. Therefor, the toxicity of αS is not likely to be due to a direct impairment of mitochondrial function. The fact that βS has similar effects as those of αS in terms of toxicity and mitochondrial morphology was new and suggests a role for βS in PD that will require further study.

# Glossary

**DDC** DOPA decarboxylase. 106

**VMAT** vesicular monoamine transporter. 4, 106

*A. victoria* A bioluminescent hydrozoan jellyfish from which GFP was first isolated. 18

**aa** amino acid. 3, 5–7, 17

**AAV** adeno-associated virus. 27–30, 35, 36, 44, 45, 49–58, 61, 63–66, 68, 70, 71, 73–82, 84–89, 91–93, 95, 99, 100, 106, 113, 117, 119

**AB** antibody. 14, 37, 77

**AD** Alzheimer's disease. 1, 5

**AFM** atomic force microscopy. 13

**ANOVA** analysis of variance. 43, 80, 82, 84, 87–89, 91, 95

**AP** action potential. 46, 53, 54, 57–59, 85, 90, 111

**Aβ** amyloid-beta. 5

**BAD** Bcl-2-associated death promoter. 9

**BAX** Bcl-2-associated X protein. 9

**Bcl-xl** B-cell lymphoma-extra large. 113

**BFP** Engineered variant of GFP for blue shifted excitation and emission. 19

**BiFC** bimolecular fluorescence complementation. 105

**BSA** bovine serum albumin. 25

*C. elegans* A transparent nematode extensively used as a model organism in biological research. 109

**CaM** A calcium binding messenger protein. 28, 102

**CCD** charge-coupled device. 56

**CFP** Engineered variant of GFP for blue shifted excitation and emission. 20, 21, 60, 69–72, 100, 102, 103

**CK-1** casein kinase 1. 9

**CK-2** casein kinase 2. 9

**CMV** cytomegalovirus. 100

**COX** cytochrome *c* oxidase. 28, 29, 45, 46, 49, 100

**CSPα** cysteine string protein α. 8

**cytochrome** *c* A small heme protein associated with the inner mitochondrial membrane. Responsible for the transfer of electrons between complex III and complex IV in the electron transport chain. 16, 17, 28, 45, 97, 100, 110, 112, 116

**DAT** dopamine active transporter. 4

**DIV** days *in vitro*. 75, 76, 78, 80, 81

**DJ-1** PARK7 is the gene coding for the human DJ-1 protein. 2, 3, 17

**DLB** dementia with Lewy bodies. 10, 11, 107, 114

**DMSO** dimethyl sulfoxide. 25

**DNA** deoxyribonucleic acid. 17, 32–35, 117

**DPT** days post transduction. 49, 50, 52, 53, 55, 56, 61, 66, 68, 75–79, 81–84, 87–94, 97, 110

*Drosophila* A species of fly in the *Drosophilidae* family commonly known as fruit fly. Used extensively as a model organism in biological research. 17

**Drp1** dynamin related protein 1. 15, 17, 109

**EDTA** ethylenediaminetetraacetic acid. 25

**EGFP** enhanced green fluorescent protein. 19

**EGTA** ethylene glycol tetraacetic acid. 101

**EM** electron microscopy. 13, 14

**ER** endoplasmic reticulum. 67

**ETC** electron transport chain. 4, 16, 23, 73, 92, 110, 111, 114

**FCCP** carbonyl cyanide 4-(trifluoromethoxy)phenylhydrazone. 25, 63–69, 93–95, 97, 98

**FCS** fetal calf serum. 24, 25

**FP** fluorescent protein. 19–22, 45–47, 49, 51, 56, 58, 100, 103–105

**FPLC** fast protein liquid chromatography. 36

**FPS** frames per second. 54

**FRET** Förster resonance energy transfer. 20–22, 27, 42, 43, 46, 49, 51, 53, 55, 59, 60, 62–66, 72, 100, 102–105

**FS** field stimulation. 51, 53, 54, 57–59, 68–71, 85–87, 90, 92, 93, 101–104, 106, 111

**GECI** genetically encoded calcium indicator. 20, 21, 28, 45, 46, 49, 51, 56, 71, 72, 85, 86, 101, 102, 106

**GES** genetically encoded sensor. 19–23, 27, 37, 44, 45, 47, 49, 69, 70, 73, 99, 100, 102, 103, 105, 113

**GFP** A fluorescent protein originally isolated in 1962 from the jellyfish Aequorea victoria. Absorption peak 395 nm and emission peak at 509 nm. Most common engineered form is EGFP which has a red-shifted excitation peak at 488 nm. 18–20, 27, 29, 30, 45–47, 49, 56, 69–72, 74–84, 87–92, 96–98, 105–107, 119

**GPCR** G protein-coupled receptor. 9, 117

**GRK** G protein-coupled receptor (GPCR) kinase. 9

**GWAS** genome-wide association study. 12

**HCV** hepatitis C virus. 104

**HEPES** 4-(2-hydroxyethyl)-1-piperazineethanesulfonic acid. 25

**hSyn** The promoter region from the human synapsin gene. 27, 45, 73, 74, 99, 100, 105

**IMM** inner mitochondrial membrane. 16, 110, 112

**IMPDH2** inosine monophosphate dehydrogenase type II. 104

*in vitro* Designation for experiments on components of a biological system that has been isolated from its original surrounding such as a dissociated and cultured neuron or purified mitochondria. 11–13, 43, 102–104, 109–111, 113

*in vivo* Designation for experiments on a complete living organism such as animal testing. 4, 9, 11, 16, 20, 113

**ITR** Parts of the adeno-associated virus (AAV) genome. Forms hairpins that contribute to self priming for the synthesis of the second deoxyribonucleic acid (DNA) strand. The only sequences required in the plasmid for packaging of AAV when the structural (cap) and packaging (rep) genes are delivered by co-transfection. 27, 34, 35

**KO** knock out. 8, 11, 14

**LB** Lewy body. 2–4, 9–12, 114

**LN** Lewy neurite. 2, 10, 11

**LRRK2** leucine-rich repeat kinase 2. 2, 3, 17

**LUT** lookup table. 66

**MAO** monoamine oxidase. 4, 110

**MCS** multiple cloning site. 30, 45

**Mfn1** mitofusin 1. 15, 109

**Mfn2** mitofusin 2. 15, 109

**$MgCl_2$** magnesium chloride. 31

**MOI** A physical quantity for viral infection defined as vector genomes divided by the number of cells being infected.. 37, 47, 49, 50, 52, 53, 55–58, 61, 66, 68, 75–79, 81, 82, 84–89, 91–93, 95, 97, 98, 106, 108

**$MPDP^+$** 1-methyl-4-phenyl-2,3-dihydropyridinium. 4

**$MPP^+$** 1-methyl-4-phenylpyridinium. 4

**MPPP** 1-methyl-4-phenyl-4-propionoxypiperidine. 3, 4

**MPT** mitochondrial permeability transition. 16, 17, 23, 112

**MPTP** 1-methyl-4-phenyl-1,2,3,6-tetrahydropyridine. 4, 14, 16, 110

**MTS** mitochondrial targeting sequence. 28, 29, 45–47, 49, 54, 58, 59, 99, 100

**MW** molecular weight. 45, 46

**NAC** non-Aβ component. 5, 118

**NACP** non-Aβ component (NAC) protein. 5

**NBM** neurobasal medium. 24

**NSF** N-ethylmaleimide sensitive fusion protein. 8, 119

**OMM** outer mitochondrial membrane. 14–17, 111, 112

**parkin** PARK2 is the gene coding for the human Parkin protein. 2, 3, 17, 108

**PCD** programmed cell death. 1, 9, 15, 16

**PCR** polymerase chain reaction. 30–32, 35, 36

**PD** Parkinson's disease. 1–5, 10–14, 16, 18, 21, 73, 79, 84, 99, 105, 107, 108, 110, 112, 114

**PINK1** P-TEN-induced putative kinase 1. 2, 3, 17, 108

**PLK** polo-like kinase. 9

**PM** plasma membrane. 67, 111, 112

**PMCA** plasma membrane $Ca^{2+}$-ATPase. 67

**PTFE** polytetrafluoroethylene. 38

**RNA** ribonucleic acid. 9, 104

**ROI** region of interest. 42, 46, 48

**ROS** reactive oxygen species. 14, 16, 17, 47, 110, 112, 113

**SD** standard deviation. 43, 52, 55

**SDS** sodium dodecyl sulfate. 25, 36

**SERCA** sarco/endoplasmic reticulum $Ca^{2+}$-ATPase. 67

**SH-SY5Y** Human derived cell line isolated from bone marrow biopsy from patient with neuroblastoma. 13, 14, 85, 109, 111, 113

**SNAP** soluble N-ethylmaleimide sensitive fusion protein (NSF) attachment protein. 8, 119

**SNARE** soluble NSF attachment protein (SNAP) receptor. 8, 9, 15

**SNCA** The gene coding for α-Synuclein.. 2, 3, 6, 10, 73, 105, 119

**SNCB** The gene coding for β-Synuclein.. 6, 11, 73, 107, 119

**SNCG** The gene coding for γ-Synuclein.. 6, 119

**SNpc** A part of the substantia nigra, a region of the midbrain. 1–3, 18, 107, 110

**sph1** synphilin-1. 17

**SURE** electroporation-competent cells, "stop unwanted rearrangement events". 34

**αS** α-Synuclein is a small soluble protein implicated as the toxic entity in Parkinson's diseases. Coded for in humans by the SNCA (PARK1) gene. For the AAV vector used for expression see AAV6-s-aSynWT-WB under the "Vectors" heading or for the bicistronic variant with green fluorescent protein (GFP) expression see AAV6-s-aSynWT-SEIS-WB. 2, 4–16, 21, 23, 44, 73–99, 105–114

**βS** β-Synuclein is a small soluble protein in the synuclein family coded for by the SNCB gene.. 5, 6, 9, 11, 21, 44, 73–75, 79–84, 87–96, 98, 99, 106–110, 113, 114

**γS** γ-Synuclein is a small soluble protein in the synuclein family coded for by the SNCG gene.. 5, 6, 8, 9, 11, 21, 23, 44, 73–75, 79–84, 87–96, 98, 99, 107–109, 114

**TB** transcription blocker. 27

**TG** transgenic. 11, 14, 15, 21, 107, 114

**TH** tyrosine hydroxylase. 105

**TMRM** tetramethylrhodamine-methylester. 25, 97, 98

**TOM** transport outer membrane. 111

**TTL** transistor–transistor logic. 41

**UPS** ubiquitin proteasome system. 3

**vehicle** Refers to the non-expressing vector control used throughout the experiments. See AAV6-3TB-EWB under the “Vectors” heading. 85

**WHP** woodchuck hepatitis virus. 27, 74, 120

**WPRE** woodchuck hepatitis virus (WHP) posttranscriptional regulatory element. 27, 74–76, 80

**WT** wild type. 6, 8, 9, 12–14, 74, 75, 77, 85, 107

**YFP** Engineered variant of GFP for red shifted excitation and emission. 19–21, 69–72, 100, 102, 103

# References


Abeliovich, A, Y Schmitz, I Fariñas, D Choi-Lundberg, WH Ho, et al. (2000). "Mice Lacking α-Synuclein Display Functional Deficits in the Nigrostriatal Dopamine System". In: *Neuron* 25.1, pp. 239–252. ISSN: 0896-6273. DOI: 10.1016/S0896-6273(00)80886-7.

Ainscow, EK, S Mirshamsi, T Tang, MLJ Ashford, and GA Rutter (2002). "Dynamic imaging of free cytosolic ATP concentration during fuel sensing by rat hypothalamic neurones: evidence for ATP-independent control of ATP-sensitive K+ channels". In: *The Journal of Physiology* 544.2, pp. 429–445. ISSN: 0022-3751, 1469-7793. DOI: 10.1113/jphysiol.2002.022434.

Akerboom, J, TW Chen, TJ Wardill, L Tian, JS Marvin, et al. (2012). "Optimization of a GCaMP Calcium Indicator for Neural Activity Imaging". In: *The Journal of Neuroscience* 32.40, pp. 13819–13840. ISSN: 0270-6474, 1529-2401. DOI: 10.1523/JNEUROSCI.2601-12.2012.

Akerboom, J, JDV Rivera, MMR Guilbe, ECA Malavé, HH Hernandez, et al. (2009). "Crystal Structures of the GCaMP Calcium Sensor Reveal the Mechanism of Fluorescence Signal Change and Aid Rational Design". In: *Journal of Biological Chemistry* 284.10, pp. 6455–6464. ISSN: 0021-9258, 1083-351X. DOI: 10.1074/jbc.M807657200.

Ali, SF, SN David, GD Newport, JL Cadet, and W Slikker (1994). "MPTP-induced oxidative stress and neurotoxicity are age-dependent: Evidence from measures of reactive oxygen species and striatal dopamine levels". In: *Synapse* 18.1, pp. 27–34. ISSN: 1098-2396. DOI: 10.1002/syn.890180105.

Amat, A, J Rigau, RW Waynant, IK Ilev, J Tomas, and JJ Anders (2005). "Modification of the intrinsic fluorescence and the biochemical behavior of ATP after irradiation with visible and near-infrared laser light". In: *Journal of Photochemistry and Photobiology B: Biology* 81.1, pp. 26–32. ISSN: 1011-1344. DOI: 10.1016/j.jphotobiol.2005.05.012.

Anderson, JP, DE Walker, JM Goldstein, Rd Laat, K Banducci, et al. (2006). "Phosphorylation of Ser-129 Is the Dominant Pathological Modification of α-Synuclein in Familial and Sporadic Lewy Body Disease". In: *Journal of Biological Chemistry* 281.40, pp. 29739–29752. ISSN: 0021-9258, 1083-351X. DOI: 10.1074/jbc.M600933200.

Ando, T, H Imamura, R Suzuki, H Aizaki, T Watanabe, T Wakita, and T Suzuki (2012). "Visualization and Measurement of ATP Levels in Living Cells Replicating Hepatitis C Virus Genome RNA". In: *PLoS Pathog* 8.3, e1002561. DOI: 10.1371/journal.ppat.1002561.

Arnold, AS, V Laporte, S Dumont, A Appert-Collin, P Erbacher, et al. (2006). "Comparing reagents for efficient transfection of human primary myoblasts: FuGENE 6, Effectene and ExGen 500". In: *Fundamental & Clinical Pharmacology* 20.1, pp. 81–89. ISSN: 1472-8206. DOI: 10.1111/j.1472-8206.2005.00344.x.

Baird, GS, DA Zacharias, and RY Tsien (1999). "Circular permutation and receptor insertion within green fluorescent proteins". In: *Proceedings of the National Academy of Sciences* 96.20, pp. 11241–11246. ISSN: 0027-8424, 1091-6490. DOI: 10.1073/pnas.96.20.11241.

Bartels, T, JG Choi, and DJ Selkoe (2011). "α-Synuclein occurs physiologically as a helically folded tetramer that resists aggregation". In: *Nature* 477.7362, pp. 107–110. ISSN: 0028-0836. DOI: 10.1038/nature10324.

Becker, PL and FS Fay (1987). "Photobleaching of fura-2 and its effect on determination of calcium concentrations". In: *The American journal of physiology* 253.4, pp. C613–618. ISSN: 0002-9513.

Benz, R and S McLaughlin (1983). "The molecular mechanism of action of the proton ionophore FCCP (carbonylcyanide p-trifluoromethoxyphenylhydrazone)." In: *Biophysical Journal* 41.3, pp. 381–398. ISSN: 0006-3495.

Bliek, AMvd, Q Shen, and S Kawajiri (2013). "Mechanisms of Mitochondrial Fission and Fusion". In: *Cold Spring Harbor Perspectives in Biology* 5.6, a011072. ISSN: , 1943-0264. DOI: 10.1101/cshperspect.a011072.

Borbat, P, TF Ramlall, JH Freed, and D Eliezer (2006). "Inter-Helix Distances in Lysophospholipid Micelle-Bound α-Synuclein from Pulsed ESR Measurements". In: *Journal of the American Chemical Society* 128.31, pp. 10004–10005. ISSN: 0002-7863. DOI: 10.1021/ja0631221.

Bove, J, D Prou, C Perier, and S Przedborski (2005). "Toxin-Induced Models of Parkinson's Disease". In: *NeuroRx* 2.3, pp. 484–494. ISSN: 1545-5343.

Braak, H, KD Tredici, U Rüb, RA de Vos, EN Jansen Steur, and E Braak (2003). "Staging of brain pathology related to sporadic Parkinson's disease". In: *Neurobiology of Aging* 24.2, pp. 197–211. ISSN: 0197-4580. DOI: 10.1016/S0197-4580(02)00065-9.

Braithwaite, SP, JB Stock, and MM Mouradian (2012). "α-Synuclein phosphorylation as a therapeutic target in Parkinson's disease". In: *Reviews in the Neurosciences* 23.2, pp. 191–198.

Bredesen, DE, RV Rao, and P Mehlen (2006). "Cell death in the nervous system". In: *Nature* 443.7113, pp. 796–802. ISSN: 0028-0836. DOI: 10.1038/nature05293.

Büki, A, DO Okonkwo, KKW Wang, and JT Povlishock (2000). "Cytochrome c Release and Caspase Activation in Traumatic Axonal Injury". In: *The Journal of Neuroscience* 20.8, pp. 2825–2834. ISSN: 0270-6474, 1529-2401.

Bunt, G and FS Wouters (2004). "Visualization of Molecular Activities Inside Living Cells with Fluorescent Labels". In: *International Review of Cytology*. Vol. Volume 237. Academic Press, pp. 205–277. ISBN: 0074-7696.

Burkhard, P, P Dominici, C Borri-Voltattorni, JN Jansonius, and VN Malashkevich (2001). "Structural insight into Parkinson's disease treatment from drug-inhibited DOPA decarboxylase". In: *Nature Structural & Molecular Biology* 8.11, pp. 963–967. ISSN: 1072-8368. DOI: 10.1038/nsb1101-963.

Burnette, WN (1981). ""Western blotting": electrophoretic transfer of proteins from sodium dodecyl sulfate–polyacrylamide gels to unmodified nitrocellulose and radiographic detection with antibody and radioiodinated protein A". In: *Analytical biochemistry* 112.2, pp. 195–203. ISSN: 0003-2697.

Bussell, R and D Eliezer (2001). "Residual Structure and Dynamics in Parkinson's Disease-associated Mutants of α-Synuclein". In: *Journal of Biological Chemistry* 276.49, pp. 45996–46003. ISSN: 0021-9258, 1083-351X. DOI: 10.1074/jbc.M106777200.

Camilleri, A, C Zarb, M Caruana, U Ostermeier, S Ghio, et al. (2013). "Mitochondrial membrane permeabilisation by amyloid aggregates and protection by polyphenols". In: *Biochimica et Biophysica Acta (BBA) - Biomembranes* 1828.11, pp. 2532–2543. ISSN: 0005-2736. DOI: 10.1016/j.bbamem.2013.06.026.

Canet-Aviles, RM, MA Wilson, DW Miller, R Ahmad, C McLendon, et al. (2004). "The Parkinson's disease protein DJ-1 is neuroprotective due to cysteine-sulfinic acid-driven mitochondrial localization". In: *Proceedings of the National Academy of Sciences of the United States of America* 101.24, pp. 9103–9108. ISSN: 0027-8424. DOI: 10.1073/pnas.0402959101.

Chan, DC (2012). "Fusion and Fission: Interlinked Processes Critical for Mitochondrial Health". In: *Annual Review of Genetics* 46.1, pp. 265–287. DOI: 10.1146/annurev-genet-110410-132529.

Chance, B, H Sies, and A Boveris (1979). "Hydroperoxide metabolism in mammalian organs." In: *Physiological Reviews* 59.3, pp. 527–605. ISSN: 0031-9333, 1522-1210.

Chandra, S, X Chen, J Rizo, R Jahn, and TC Südhof (2003). "A Broken α-Helix in Folded α-Synuclein". In: *Journal of Biological Chemistry* 278.17, pp. 15313–15318. ISSN: 0021-9258, 1083-351X. DOI: 10.1074/jbc.M213128200.

Chandra, S, G Gallardo, R Fernández-Chacón, OM Schlüter, and TC Südhof (2005). "Alpha-synuclein cooperates with CSPalpha in preventing neurodegeneration". In: *Cell* 123.3, pp. 383–396. ISSN: 0092-8674. DOI: 10.1016/j.cell.2005.09.028.

Chartier-Harlin, MC, J Kachergus, C Roumier, V Mouroux, X Douay, et al. (2004). "α-synuclein locus duplication as a cause of familial Parkinson's disease". In: *The Lancet* 364.9440, pp. 1167–1169. ISSN: 0140-6736. DOI: 10.1016/S0140-6736(04)17103-1.

Chen, H and DC Chan (2009). "Mitochondrial dynamics-fusion, fission, movement, and mitophagy-in neurodegenerative diseases". In: *Human Molecular Genetics* 18 (R2), R169–R176. ISSN: 0964-6906. DOI: 10.1093/hmg/ddp326.

Chen, H, SA Detmer, AJ Ewald, EE Griffin, SE Fraser, and DC Chan (2003). "Mitofusins Mfn1 and Mfn2 coordinately regulate mitochondrial fusion and are essential for embryonic development". In: *The Journal of Cell Biology* 160.2, pp. 189–200. ISSN: 0021-9525. DOI: 10.1083/jcb.200211046.

Chen, L, J Jin, J Davis, Y Zhou, Y Wang, J Liu, PJ Lockhart, and J Zhang (2007). "Oligomeric α-synuclein inhibits tubulin polymerization". In: *Biochemical and Biophysical Research Communications* 356.3, pp. 548–553. ISSN: 0006-291X. DOI: 10.1016/j.bbrc.2007.02.163.

Chinta, SJ, JK Mallajosyula, A Rane, and JK Andersen (2010). "Mitochondrial alpha-synuclein accumulation impairs complex I function in dopaminergic neurons and results in increased mitophagy in vivo". In: *Neuroscience Letters* 486.3, pp. 235–239. ISSN: 0304-3940. DOI: 10.1016/j.neulet.2010.09.061.

Chung, CY, JB Koprich, H Siddiqi, and O Isacson (2009). "Dynamic Changes in Presynaptic and Axonal Transport Proteins Combined with Striatal Neuroinflammation Precede Dopaminergic Neuronal Loss in a Rat Model of AAV α-Synucleinopathy". In: *The Jour-*

*nal of Neuroscience* 29.11, pp. 3365–3373. ISSN: 0270-6474, 1529-2401. DOI: 10.1523/JNEUROSCI.5427-08.2009.

Clayton, DF and JM George (1998). "The synucleins: a family of proteins involved in synaptic function, plasticity, neurodegeneration and disease". In: *Trends in Neurosciences* 21.6, pp. 249–254. ISSN: 0166-2236. DOI: 10.1016/S0166-2236(97)01213-7.

Conway, KA, SJ Lee, JC Rochet, TT Ding, RE Williamson, and PT Lansbury (2000). "Acceleration of oligomerization, not fibrillization, is a shared property of both α-synuclein mutations linked to early-onset Parkinson's disease: Implications for pathogenesis and therapy". In: *Proceedings of the National Academy of Sciences of the United States of America* 97.2, pp. 571–576. ISSN: 0027-8424.

Cribbs, JT and S Strack (2007). "Reversible phosphorylation of Drp1 by cyclic AMP-dependent protein kinase and calcineurin regulates mitochondrial fission and cell death". In: *EMBO Reports* 8.10, pp. 939–944. ISSN: 1469-221X. DOI: 10.1038/sj.embor.7401062.

Culvenor, JG, CA McLean, S Cutt, BCV Campbell, F Maher, et al. (1999). "Non-Aβ Component of Alzheimer's Disease Amyloid (NAC) Revisited". In: *The American Journal of Pathology* 155.4, pp. 1173–1181. ISSN: 0002-9440.

Danzer, KM, D Haasen, AR Karow, S Moussaud, M Habeck, et al. (2007). "Different Species of α-Synuclein Oligomers Induce Calcium Influx and Seeding". In: *The Journal of Neuroscience* 27.34, pp. 9220–9232. ISSN: 0270-6474, 1529-2401. DOI: 10.1523/JNEUROSCI.2617-07.2007.

Datta, SR, A Katsov, L Hu, A Petros, SW Fesik, MB Yaffe, and ME Greenberg (2000). "14-3-3 Proteins and Survival Kinases Cooperate to Inactivate BAD by BH3 Domain Phosphorylation". In: *Molecular Cell* 6.1, pp. 41–51. ISSN: 1097-2765. DOI: 10.1016/S1097-2765(05)00012-2.

Dauer, W, N Kholodilov, M Vila, AC Trillat, R Goodchild, et al. (2002). "Resistance of α-synuclein null mice to the parkinsonian neurotoxin MPTP". In: *Proceedings of the National Academy of Sciences of the United States of America* 99.22, pp. 14524–14529. ISSN: 0027-8424. DOI: 10.1073/pnas.172514599.

Davidson, WS, A Jonas, DF Clayton, and JM George (1998). "Stabilization of α-Synuclein Secondary Structure upon Binding to Synthetic Membranes". In: *Journal of Biological Chemistry* 273.16, pp. 9443–9449. ISSN: 0021-9258, 1083-351X. DOI: 10.1074/jbc.273.16.9443.

De Vos, KJ, J Sable, KE Miller, and MP Sheetz (2003). "Expression of Phosphatidylinositol (4,5) Bisphosphate-specific Pleckstrin Homology Domains Alters Direction But Not the Level of Axonal Transport of Mitochondria". In: *Molecular Biology of the Cell* 14.9, pp. 3636–3649. ISSN: 1059-1524. DOI: 10.1091/mbc.E02-10-0638.

Devi, L, V Raghavendran, BM Prabhu, NG Avadhani, and HK Anandatheerthavarada (2008). "Mitochondrial Import and Accumulation of α-Synuclein Impair Complex I in Human Dopaminergic Neuronal Cultures and Parkinson Disease Brain". In: *Journal of Biological Chemistry* 283.14, pp. 9089–9100. ISSN: 0021-9258, 1083-351X. DOI: 10.1074/jbc.M710012200.

Ding, TT, SJ Lee, JC Rochet, and PT Lansbury (2002). "Annular α-Synuclein Protofibrils Are Produced When Spherical Protofibrils Are Incubated in Solution or Bound to Brain-

Derived Membranes". In: *Biochemistry* 41.32, pp. 10209–10217. ISSN: 0006-2960. DOI: 10.1021/bi020139h.

Dittmer, PJ, JG Miranda, JA Gorski, and AE Palmer (2009). "Genetically Encoded Sensors to Elucidate Spatial Distribution of Cellular Zinc". In: *Journal of Biological Chemistry* 284.24, pp. 16289–16297. ISSN: 0021-9258, 1083-351X. DOI: 10.1074/jbc.M900501200.

Dixit, R and R Cyr (2003). "Cell damage and reactive oxygen species production induced by fluorescence microscopy: effect on mitosis and guidelines for non-invasive fluorescence microscopy". In: *The Plant Journal* 36.2, pp. 280–290. ISSN: 1365-313X. DOI: 10.1046/j.1365-313X.2003.01868.x.

Djurovic, S, N Iversen, S Jeansson, F Hoover, and G Christensen (2004). "Comparison of nonviral transfection and adeno-associated viral transduction on cardiomyocytes". In: *Molecular Biotechnology* 28.1, pp. 21–31. ISSN: 1073-6085, 1559-0305. DOI: 10.1385/MB:28:1:21.

Dodiya, HB, T Bjorklund, J Stansell Iii, RJ Mandel, D Kirik, and JH Kordower (2010). "Differential Transduction Following Basal Ganglia Administration of Distinct Pseudotyped AAV Capsid Serotypes in Nonhuman Primates". In: *Molecular Therapy* 18.3, pp. 579–587. ISSN: 1525-0016. DOI: 10.1038/mt.2009.216.

Dong, Z, B Ferger, J Feldon, and H Büeler (2002). "Overexpression of Parkinson's disease-associated α-SynucleinA53T by recombinant adeno-associated virus in mice does not increase the vulnerability of dopaminergic neurons to MPTP". In: *Journal of Neurobiology* 53.1, pp. 1–10. ISSN: 1097-4695. DOI: 10.1002/neu.10094.

Ducas, VC and E Rhoades (2012). "Quantifying Interactions of β-Synuclein and γ-Synuclein with Model Membranes". In: *Journal of molecular biology* 423.4, pp. 528–539. ISSN: 0022-2836. DOI: 10.1016/j.jmb.2012.08.008.

Eiden, LE, MKH Schäfer, E Weihe, and B Schütz (2004). "The vesicular amine transporter family (SLC18): amine/proton antiporters required for vesicular accumulation and regulated exocytotic secretion of monoamines and acetylcholine". In: *Pflügers Archiv* 447.5, pp. 636–640. ISSN: 0031-6768, 1432-2013. DOI: 10.1007/s00424-003-1100-5.

Engelender, S, Z Kaminsky, X Guo, AH Sharp, RK Amaravi, et al. (1999). "Synphilin-1 associates with α-synuclein and promotes the formation of cytosolic inclusions". In: *Nature Genetics* 22.1, pp. 110–114. ISSN: 1061-4036. DOI: 10.1038/8820.

Erdahl, WL, CJ Chapman, RW Taylor, and DR Pfeiffer (1994). "Ca2+ transport properties of ionophores A23187, ionomycin, and 4-BrA23187 in a well defined model system". In: *Biophysical Journal* 66.5, pp. 1678–1693. ISSN: 0006-3495. DOI: 10.1016/S0006-3495(94)80959-2.

Eschbach, J and KM Danzer (2013). "α-Synuclein in Parkinson's Disease: Pathogenic Function and Translation into Animal Models". In: *Neurodegenerative Diseases*. ISSN: 1660-2862, 1660-2854. DOI: 10.1159/000354615.

et al., Gv (2013). *Python library reference*.

Fahn, S (2008). "The history of dopamine and levodopa in the treatment of Parkinson's disease". In: *Movement Disorders* 23 (S3), S497–S508. ISSN: 1531-8257. DOI: 10.1002/mds.22028.

Fan, Y, P Limprasert, IVJ Murray, AC Smith, VMY Lee, JQ Trojanowski, BL Sopher, and ARL Spada (2006). "β-synuclein modulates α-synuclein neurotoxicity by reducing α-synuclein

protein expression". In: *Human Molecular Genetics* 15.20, pp. 3002–3011. ISSN: 0964-6906, 1460-2083. DOI: 10.1093/hmg/ddl242.

Fauvet, B, MK Mbefo, MB Fares, C Desobry, S Michael, et al. (2012). "α-Synuclein in Central Nervous System and from Erythrocytes, Mammalian Cells, and Escherichia coli Exists Predominantly as Disordered Monomer". In: *Journal of Biological Chemistry* 287.19, pp. 15345–15364. ISSN: 0021-9258, 1083-351X. DOI: 10.1074/jbc.M111.318949.

Feng, LR, HJ Federoff, S Vicini, and KA Maguire-Zeiss (2010). "α-Synuclein mediates alterations in membrane conductance: a potential role for α-synuclein oligomers in cell vulnerability". In: *The European journal of neuroscience* 32.1, pp. 10–17. ISSN: 0953-816X. DOI: 10.1111/j.1460-9568.2010.07266.x.

Filippin, L, MC Abad, S Gastaldello, PJ Magalhães, D Sandonà, and T Pozzan (2005). "Improved strategies for the delivery of GFP-based Ca2+ sensors into the mitochondrial matrix". In: *Cell Calcium* 37.2, pp. 129–136. ISSN: 0143-4160. DOI: 10.1016/j.ceca.2004.08.002.

Fink, AL (1998). "Protein aggregation: folding aggregates, inclusion bodies and amyloid". In: *Folding and Design* 3.1, R9–R23. ISSN: 1359-0278. DOI: 10.1016/S1359-0278(98)00002-9.

Fink, AL (2006). "The Aggregation and Fibrillation of α-Synuclein". In: *Accounts of Chemical Research* 39.9, pp. 628–634. ISSN: 0001-4842. DOI: 10.1021/ar050073t.

Forno, LS, LE DeLanney, I Irwin, and JW Langston (1993). "Similarities and differences between MPTP-induced parkinsonsim and Parkinson's disease. Neuropathologic considerations". In: *Advances in neurology* 60, pp. 600–608. ISSN: 0091-3952.

Főrster, T (1959). "10th Spiers Memorial Lecture. Transfer mechanisms of electronic excitation". In: *Discussions of the Faraday Society* 27, pp. 7–17. ISSN: 0366-9033. DOI: 10.1039/DF9592700007.

Fowler, CJ and G Tiger (1997). "Calibration of Fura-2 signals introduces errors into measurement of thrombin-stimulated calcium mobilisation in human platelets". In: *Clinica Chimica Acta* 265.2, pp. 247–261. ISSN: 0009-8981. DOI: 10.1016/S0009-8981(97)00139-3.

Fox, J and S Weisberg (2011). *An R Companion to Applied Regression*. Second. Thousand Oaks CA: Sage.

Frank, M, S Duvezin-Caubet, S Koob, A Occhipinti, R Jagasia, et al. (2012). "Mitophagy is triggered by mild oxidative stress in a mitochondrial fission dependent manner". In: *Biochimica et biophysica acta* 1823.12, pp. 2297–2310. ISSN: 0006-3002. DOI: 10.1016/j.bbamcr.2012.08.007.

Fredenburg, RA, C Rospigliosi, RK Meray, JC Kessler, HA Lashuel, D Eliezer, and J Lansbury Peter T (2007). "The impact of the E46K mutation on the properties of alpha-synuclein in its monomeric and oligomeric states". In: *Biochemistry* 46.24, pp. 7107–7118. ISSN: 0006-2960. DOI: 10.1021/bi7000246.

Frey, TG and CA Mannella (2000). "The internal structure of mitochondria". In: *Trends in Biochemical Sciences* 25.7, pp. 319–324. ISSN: 0968-0004. DOI: 10.1016/S0968-0004(00)01609-1.

Fujita, M, S Sugama, K Sekiyama, A Sekigawa, T Tsukui, et al. (2010). "A β-synuclein mutation linked to dementia produces neurodegeneration when expressed in mouse brain". In: *Nature Communications* 1, p. 110. ISSN: 2041-1723. DOI: 10.1038/ncomms1101.

Fujiwara, H, M Hasegawa, N Dohmae, A Kawashima, E Masliah, et al. (2002). "α-Synuclein is phosphorylated in synucleinopathy lesions". In: *Nature Cell Biology* 4.2, pp. 160–164. ISSN: 1465-7392. DOI: 10.1038/ncb748.

Fukuda, J, Y Fujita, and K Ohsawa (1983). "ATP content in isolated mammalian nerve cells assayed by a modified luciferin-luciferase method". In: *Journal of neuroscience methods* 8.3, pp. 295–302. ISSN: 0165-0270.

Furukawa, K, M Matsuzaki-Kobayashi, T Hasegawa, A Kikuchi, N Sugeno, et al. (2006). "Plasma membrane ion permeability induced by mutant α-synuclein contributes to the degeneration of neural cells". In: *Journal of Neurochemistry* 97.4, pp. 1071–1077. ISSN: 1471-4159. DOI: 10.1111/j.1471-4159.2006.03803.x.

Galvin, JE, K Uryu, VMY Lee, and JQ Trojanowski (1999). "Axon pathology in Parkinson's disease and Lewy body dementia hippocampus contains α-, β-, and γ-synuclein". In: *Proceedings of the National Academy of Sciences of the United States of America* 96.23, pp. 13450–13455. ISSN: 0027-8424.

Gandhi, S, A Wood-Kaczmar, Z Yao, H Plun-Favreau, E Deas, et al. (2009). "PINK1-Associated Parkinson's Disease Is Caused by Neuronal Vulnerability to Calcium-Induced Cell Death". In: *Molecular Cell* 33.5, pp. 627–638. ISSN: 1097-2765. DOI: 10.1016/j.molcel.2009.02.013.

George, JM (2002). "The synucleins". In: *Genome Biology* 3.1, reviews3002.1–reviews3002.6. ISSN: 1465-6906.

George, JM, H Jin, WS Woods, and DF Clayton (1995). "Characterization of a novel protein regulated during the critical period for song learning in the zebra finch". In: *Neuron* 15.2, pp. 361–372. ISSN: 0896-6273. DOI: 10.1016/0896-6273(95)90040-3.

Georgieva, ER, TF Ramlall, PP Borbat, JH Freed, and D Eliezer (2008). "Membrane-Bound Alpha-Synuclein Forms an Extended Helix: Long-Distance Pulsed ESR Measurements Using Vesicles, Bicelles, and Rod-Like Micelles". In: *Journal of the American Chemical Society* 130.39, pp. 12856–12857. ISSN: 0002-7863. DOI: 10.1021/ja804517m.

Giasson, BI, MS Forman, M Higuchi, LI Golbe, CL Graves, PT Kotzbauer, JQ Trojanowski, and VMY Lee (2003). "Initiation and Synergistic Fibrillization of Tau and Alpha-Synuclein". In: *Science* 300.5619, pp. 636–640. ISSN: 0036-8075, 1095-9203. DOI: 10.1126/science.1082324.

Golbe, LI, AM Lazzarini, RC Duvoisin, GD Iorio, G Sanges, V Bonavita, and S la Sala (1996). "Clinical genetic analysis of Parkinson's disease in the contursi kindred". In: *Annals of Neurology* 40.5, pp. 767–775. ISSN: 1531-8249. DOI: 10.1002/ana.410400513.

Gottlieb, E, SM Armour, MH Harris, and CB Thompson (2003). "Mitochondrial membrane potential regulates matrix configuration and cytochrome c release during apoptosis". In: *Cell Death & Differentiation* 10.6, pp. 709–717. ISSN: 1350-9047. DOI: 10.1038/sj.cdd.4401231.

Greenbaum, L, C Rothmann, R Lavie, and Z Malik (2000). "Green Fluorescent Protein Photobleaching: a Model for Protein Damage by Endogenous and Exogenous Singlet Oxygen". In: *Biological Chemistry* 381.12, pp. 1251–1258.

Griesbeck, O (2004). "Fluorescent proteins as sensors for cellular functions". In: *Current Opinion in Neurobiology* 14.5, pp. 636–641. ISSN: 0959-4388. DOI: 10.1016/j.conb.2004.08.002.

Grynkiewicz, G, M Poenie, and RY Tsien (1985). "A new generation of Ca2+ indicators with greatly improved fluorescence properties." In: *Journal of Biological Chemistry* 260.6, pp. 3440–3450. ISSN: 0021-9258, 1083-351X.

Guerrero, G and EY Isacoff (2001). "Genetically encoded optical sensors of neuronal activity and cellular function". In: *Current Opinion in Neurobiology* 11.5, pp. 601–607. ISSN: 0959-4388. DOI: 10.1016/S0959-4388(00)00256-7.

Haggerty, T, J Credle, O Rodriguez, J Wills, AW Oaks, E Masliah, and A Sidhu (2011). "Hyperphosphorylated Tau in an α-synuclein overexpressing transgenic model of Parkinson's disease". In: *The European journal of neuroscience* 33.9, pp. 1598–1610. ISSN: 0953-816X. DOI: 10.1111/j.1460-9568.2011.07660.x.

Hashimoto, M, E Rockenstein, M Mante, L Crews, P Bar-On, FH Gage, R Marr, and E Masliah (2004). "An antiaggregation gene therapy strategy for Lewy body disease utilizing β-synuclein lentivirus in a transgenic model". In: *Gene Therapy* 11.23, pp. 1713–1723. ISSN: 0969-7128. DOI: 10.1038/sj.gt.3302349.

Hashimoto, M, E Rockenstein, M Mante, M Mallory, and E Masliah (2001). "beta-Synuclein inhibits alpha-synuclein aggregation: a possible role as an anti-parkinsonian factor". In: *Neuron* 32.2, pp. 213–223. ISSN: 0896-6273.

Hauptmann, N, J Grimsby, JC Shih, and E Cadenas (1996). "The Metabolism of Tyramine by Monoamine Oxidase A/B Causes Oxidative Damage to Mitochondrial DNA". In: *Archives of Biochemistry and Biophysics* 335.2, pp. 295–304. ISSN: 0003-9861. DOI: 10.1006/abbi.1996.0510.

Heikkila, RE, WJ Nicklas, I Vyas, and RC Duvoisin (1985). "Dopaminergic toxicity of rotenone and the 1-methyl-4-phenylpyridinium ion after their stereotaxic administration to rats: Implication for the mechanism of 1-methyl-4-phenyl-1,2,3,6-tetrahydropyridine toxicity". In: *Neuroscience Letters* 62.3, pp. 389–394. ISSN: 0304-3940. DOI: 10.1016/0304-3940(85)90580-4.

Heim, R and RY Tsien (1996). "Engineering green fluorescent protein for improved brightness, longer wavelengths and fluorescence resonance energy transfer". In: *Current Biology* 6.2, pp. 178–182. ISSN: 0960-9822. DOI: 10.1016/S0960-9822(02)00450-5.

Hettiarachchi, NT, A Parker, ML Dallas, K Pennington, C Hung, et al. (2009). "α-Synuclein modulation of Ca2+ signaling in human neuroblastoma (SH-SY5Y) cells". In: *Journal of Neurochemistry* 111.5, pp. 1192–1201. ISSN: 1471-4159. DOI: 10.1111/j.1471-4159.2009.06411.x.

Hires, SA, L Tian, and LL Looger (2008). "Reporting neural activity with genetically encoded calcium indicators". In: *Brain cell biology* 36.1, pp. 69–86. ISSN: 1559-7105. DOI: 10.1007/s11068-008-9029-4.

Hisata, JS (2001). *Lake and Stream Rehabilitation: Rotenone Use and Health Risks : Final Supplemental Environmental Impact Statement*. Washington Department of Fish and Wildlife. 34 pp.

Hlavaty, J, M Schittmayer, A Stracke, G Jandl, E Knapp, et al. (2005). "Effect of posttranscriptional regulatory elements on transgene expression and virus production in the context of retrovirus vectors". In: *Virology* 341.1, pp. 1–11. ISSN: 0042-6822. DOI: 10.1016/j.virol.2005.06.037.

Hollenbeck, PJ and WM Saxton (2005). "The axonal transport of mitochondria". In: *Journal of cell science* 118 (Pt 23), pp. 5411–5419. ISSN: 0021-9533. DOI: 10.1242/jcs.02745.

Hothorn, T, F Bretz, and P Westfall (2008). "Simultaneous Inference in General Parametric Models". In: *Biometrical Journal* 50.3, pp. 346–363.

Howarth, C, P Gleeson, and D Attwell (2012). "Updated energy budgets for neural computation in the neocortex and cerebellum". In: *Journal of Cerebral Blood Flow & Metabolism* 32.7, pp. 1222–1232. ISSN: 0271-678X. DOI: 10.1038/jcbfm.2012.35.

Hsu, LJ, Y Sagara, A Arroyo, E Rockenstein, A Sisk, et al. (2000). "α-Synuclein Promotes Mitochondrial Deficit and Oxidative Stress". In: *The American Journal of Pathology* 157.2, pp. 401–410. ISSN: 0002-9440. DOI: 10.1016/S0002-9440(10)64553-1.

Huettner, JE (2003). "Kainate receptors and synaptic transmission". In: *Progress in Neurobiology* 70.5, pp. 387–407. ISSN: 0301-0082. DOI: 10.1016/S0301-0082(03)00122-9.

Ibáñez, P, AM Bonnet, B Débarges, E Lohmann, F Tison, et al. (2004). "Causal relation between α-synuclein locus duplication as a cause of familial Parkinson's disease". In: *The Lancet* 364.9440, pp. 1169–1171. ISSN: 0140-6736. DOI: 10.1016/S0140-6736(04)17104-3.

Imamura, H, KP Huynh Nhat, H Togawa, K Saito, R Iino, Y Kato-Yamada, T Nagai, and H Noji (2009). "Visualization of ATP levels inside single living cells with fluorescence resonance energy transfer-based genetically encoded indicators". In: *Proceedings of the National Academy of Sciences of the United States of America* 106.37, pp. 15651–15656. ISSN: 0027-8424. DOI: 10.1073/pnas.0904764106.

Iwai, A, E Masliah, M Yoshimoto, N Ge, L Flanagan, HA de Silva, A Kittel, and T Saitoh (1995). "The precursor protein of non-A beta component of Alzheimer's disease amyloid is a presynaptic protein of the central nervous system". In: *Neuron* 14.2, pp. 467–475. ISSN: 0896-6273.

Jakes, R, MG Spillantini, and M Goedert (1994). "Identification of two distinct synucleins from human brain". In: *FEBS Letters* 345.1, pp. 27–32. ISSN: 0014-5793. DOI: 10.1016/0014-5793(94)00395-5.

Jankovic, J (2008). "Parkinson's disease: clinical features and diagnosis". In: *Journal of Neurology, Neurosurgery & Psychiatry* 79.4, pp. 368–376. ISSN: , 1468-330X. DOI: 10.1136/jnnp.2007.131045.

Jao, CC, A Der-Sarkissian, J Chen, and R Langen (2004). "Structure of membrane-bound α-synuclein studied by site-directed spin labeling". In: *Proceedings of the National Academy of Sciences of the United States of America* 101.22, pp. 8331–8336. ISSN: 0027-8424. DOI: 10.1073/pnas.0400553101.

Jenco, JM, A Rawlingson, B Daniels, and AJ Morris (1998). "Regulation of Phospholipase D2: Selective Inhibition of Mammalian Phospholipase D Isoenzymes by α- and β-Synucleins†". In: *Biochemistry* 37.14, pp. 4901–4909. ISSN: 0006-2960. DOI: 10.1021/bi972776r.

Jensen, PH, MS Nielsen, R Jakes, CG Dotti, and M Goedert (1998). "Binding of alpha-synuclein to brain vesicles is abolished by familial Parkinson's disease mutation". In: *The Journal of biological chemistry* 273.41, pp. 26292–26294. ISSN: 0021-9258.

Jensen, PH, H Hager, MS Nielsen, P Højrup, J Gliemann, and R Jakes (1999). "α-Synuclein Binds to Tau and Stimulates the Protein Kinase A-catalyzed Tau Phosphorylation of Serine Residues 262 and 356". In: *Journal of Biological Chemistry* 274.36, pp. 25481–25489. ISSN: 0021-9258, 1083-351X. DOI: 10.1074/jbc.274.36.25481.

Ji, H, YE Liu, T Jia, M Wang, J Liu, et al. (1997). "Identification of a Breast Cancer-specific Gene, BCSG1, by Direct Differential cDNA Sequencing". In: *Cancer Research* 57.4, pp. 759–764. ISSN: 0008-5472, 1538-7445.

Junn, E and M Mouradian (2002). "Human α-Synuclein over-expression increases intracellular reactive oxygen species levels and susceptibility to dopamine". In: *Neuroscience Letters* 320.3, pp. 146–150. ISSN: 0304-3940. DOI: 10.1016/S0304-3940(02)00016-2.

Kamp, F, N Exner, AK Lutz, N Wender, J Hegermann, et al. (2010). "Inhibition of mitochondrial fusion by α-synuclein is rescued by PINK1, Parkin and DJ-1". In: *The EMBO Journal* 29.20, pp. 3571–3589. ISSN: 0261-4189. DOI: 10.1038/emboj.2010.223.

Karpinar, DP, MBG Balija, S Kügler, F Opazo, N Rezaei-Ghaleh, et al. (2009). "Pre-fibrillar α-synuclein variants with impaired β-structure increase neurotoxicity in Parkinson's disease models". In: *The EMBO Journal* 28.20, pp. 3256–3268. ISSN: 0261-4189. DOI: 10.1038/emboj.2009.257.

Kerppola, TK (2006). "Design and implementation of bimolecular fluorescence complementation (BiFC) assays for the visualization of protein interactions in living cells". In: *Nature Protocols* 1.3, pp. 1278–1286. ISSN: 1754-2189. DOI: 10.1038/nprot.2006.201.

Kim, HY, MK Cho, A Kumar, E Maier, C Siebenhaar, et al. (2009). "Structural Properties of Pore-Forming Oligomers of α-Synuclein". In: *Journal of the American Chemical Society* 131.47, pp. 17482–17489. ISSN: 0002-7863. DOI: 10.1021/ja9077599.

Klivenyi, P, D Siwek, G Gardian, L Yang, A Starkov, et al. (2006). "Mice lacking alpha-synuclein are resistant to mitochondrial toxins". In: *Neurobiology of Disease* 21.3, pp. 541–548. ISSN: 0969-9961. DOI: 10.1016/j.nbd.2005.08.018.

Kneen, M, J Farinas, Y Li, and A Verkman (1998). "Green Fluorescent Protein as a Noninvasive Intracellular pH Indicator". In: *Biophysical Journal* 74.3, pp. 1591–1599. ISSN: 0006-3495. DOI: 10.1016/S0006-3495(98)77870-1.

Knott, AB, G Perkins, R Schwarzenbacher, and E Bossy-Wetzel (2008). "Mitochondrial fragmentation in neurodegeneration". In: *Nature Reviews Neuroscience* 9.7, pp. 505–518. ISSN: 1471-003X. DOI: 10.1038/nrn2417.

Koshiba, T, SA Detmer, JT Kaiser, H Chen, JM McCaffery, and DC Chan (2004). "Structural Basis of Mitochondrial Tethering by Mitofusin Complexes". In: *Science* 305.5685, pp. 858–862. ISSN: 0036-8075, 1095-9203. DOI: 10.1126/science.1099793.

Kozak, M (1986). "Point mutations define a sequence flanking the AUG initiator codon that modulates translation by eukaryotic ribosomes". In: *Cell* 44.2, pp. 283–292. ISSN: 0092-8674.

Krüger, R, W Kuhn, T Müller, D Woitalla, M Graeber, et al. (1998). "Ala30Pro mutation in the gene encoding α-synuclein in Parkinson's disease". In: *Nature Genetics* 18.2, pp. 106–108. DOI: 10.1038/ng0298-106.

Kubli, DA and ÅB Gustafsson (2012). "Mitochondria and Mitophagy The Yin and Yang of Cell Death Control". In: *Circulation Research* 111.9, pp. 1208–1221. ISSN: 0009-7330, 1524-4571. DOI: 10.1161/CIRCRESAHA.112.265819.

Kugler, S, R Hahnewald, M Garrido, and J Reiss (2007). "Long-Term Rescue of a Lethal Inherited Disease by Adeno-Associated Virus-Mediated Gene Transfer in a Mouse Model of Molybdenum-Cofactor Deficiency". In: *American Journal of Human Genetics* 80.2, pp. 291–297. ISSN: 0002-9297.

Kügler, S, E Kilic, and M Bähr (2003). "Human synapsin 1 gene promoter confers highly neuron-specific long-term transgene expression from an adenoviral vector in the adult rat brain depending on the transduced area". In: *Gene Therapy* 10.4, pp. 337–347. ISSN: 0969-7128. DOI: 10.1038/sj.gt.3301905.

Langston, JW, P Ballard, JW Tetrud, and I Irwin (1983). "Chronic Parkinsonism in humans due to a product of meperidine-analog synthesis". In: *Science (New York, N.Y.)* 219.4587, pp. 979–980. ISSN: 0036-8075.

Lashuel, HA, BM Petre, J Wall, M Simon, RJ Nowak, T Walz, and PT Lansbury Jr (2002). "α-Synuclein, Especially the Parkinson's Disease-associated Mutants, Forms Pore-like Annular and Tubular Protofibrils". In: *Journal of Molecular Biology* 322.5, pp. 1089–1102. ISSN: 0022-2836. DOI: 10.1016/S0022-2836(02)00735-0.

Lavedan, C, E Leroy, A Dehejia, S Buchholtz, A Dutra, RL Nussbaum, and MH Polymeropoulos (1998). "Identification, localization and characterization of the human gamma-synuclein gene". In: *Human genetics* 103.1, pp. 106–112. ISSN: 0340-6717.

Lavedan, C (1998). "The Synuclein Family". In: *Genome Research* 8.9, pp. 871–880. ISSN: 1088-9051, 1549-5469. DOI: 10.1101/gr.8.9.871.

Lazarou, M, DP Narendra, SM Jin, E Tekle, S Banerjee, and RJ Youle (2013). "PINK1 drives Parkin self-association and HECT-like E3 activity upstream of mitochondrial binding". In: *The Journal of Cell Biology* 200.2, pp. 163–172. ISSN: 0021-9525. DOI: 10.1083/jcb.201210111.

Lee, HJ, F Khoshaghideh, S Lee, and SJ Lee (2006). "Impairment of microtubule-dependent trafficking by overexpression of α-synuclein". In: *European Journal of Neuroscience* 24.11, pp. 3153–3162. ISSN: 1460-9568. DOI: 10.1111/j.1460-9568.2006.05210.x.

Legros, F, A Lombès, P Frachon, and M Rojo (2002). "Mitochondrial Fusion in Human Cells Is Efficient, Requires the Inner Membrane Potential, and Is Mediated by Mitofusins". In: *Molecular Biology of the Cell* 13.12, pp. 4343–4354. ISSN: 1059-1524, 1939-4586. DOI: 10.1091/mbc.E02-06-0330.

Lerma, J, AV Paternain, A Rodríguez-Moreno, and JC López-García (2001). "Molecular Physiology of Kainate Receptors". In: *Physiological Reviews* 81.3, pp. 971–998. ISSN: 0031-9333, 1522-1210.

Li, C, M Numata, M Takeuchi, and S Shinkai (2005). "A Sensitive Colorimetric and Fluorescent Probe Based on a Polythiophene Derivative for the Detection of ATP". In: *Angewandte Chemie International Edition* 44.39, pp. 6371–6374. ISSN: 1521-3773. DOI: 10.1002/anie.200501823.

Li, J, VN Uversky, and AL Fink (2001). "Effect of Familial Parkinson's Disease Point Mutations A30P and A53T on the Structural Properties, Aggregation, and Fibrillation of Human α-Synuclein†". In: *Biochemistry* 40.38, pp. 11604–11613. ISSN: 0006-2960. DOI: 10.1021/bi010616g.

Li, N, K Ragheb, G Lawler, J Sturgis, B Rajwa, JA Melendez, and JP Robinson (2003). "Mitochondrial Complex I Inhibitor Rotenone Induces Apoptosis through Enhancing Mitochondrial Reactive Oxygen Species Production". In: *Journal of Biological Chemistry* 278.10, pp. 8516–8525. ISSN: 0021-9258, 1083-351X. DOI: 10.1074/jbc.M210432200.

Li, WW, R Yang, JC Guo, HM Ren, XL Zha, JS Cheng, and DF Cai (2007). "Localization of alpha-synuclein to mitochondria within midbrain of mice". In: *Neuroreport* 18.15, pp. 1543–1546. ISSN: 0959-4965. DOI: 10.1097/WNR.0b013e3282f03db4.

Lim, GE, M Piske, and JD Johnson (2013). "14-3-3 proteins are essential signalling hubs for beta cell survival". In: *Diabetologia* 56.4, pp. 825–837. ISSN: 0012-186X, 1432-0428. DOI: 10.1007/s00125-012-2820-x.

Linkert, M, CT Rueden, C Allan, JM Burel, W Moore, et al. (2010). "Metadata matters: access to image data in the real world". In: *The Journal of Cell Biology* 189.5, pp. 777–782. ISSN: 0021-9525, 1540-8140. DOI: 10.1083/jcb.201004104.

Linse, S, A Helmersson, and S Forsén (1991). "Calcium binding to calmodulin and its globular domains." In: *Journal of Biological Chemistry* 266.13, pp. 8050–8054. ISSN: 0021-9258, 1083-351X.

Liu, C and TE Hermann (1978). "Characterization of ionomycin as a calcium ionophore." In: *Journal of Biological Chemistry* 253.17, pp. 5892–5894. ISSN: 0021-9258, 1083-351X.

Liu, G, C Zhang, J Yin, X Li, F Cheng, et al. (2009). "α-Synuclein is differentially expressed in mitochondria from different rat brain regions and dose-dependently down-regulates complex I activity". In: *Neuroscience Letters* 454.3, pp. 187–192. ISSN: 0304-3940. DOI: 10.1016/j.neulet.2009.02.056.

Liu, HS, MS Jan, CK Chou, PH Chen, and NJ Ke (1999). "Is Green Fluorescent Protein Toxic to the Living Cells?" In: *Biochemical and Biophysical Research Communications* 260.3, pp. 712–717. ISSN: 0006-291X. DOI: 10.1006/bbrc.1999.0954.

Liu, Y, A Roghani, and RH Edwards (1992). "Gene transfer of a reserpine-sensitive mechanism of resistance to N-methyl-4-phenylpyridinium." In: *Proceedings of the National Academy of Sciences of the United States of America* 89.19, pp. 9074–9078. ISSN: 0027-8424.

Loeb, V, E Yakunin, A Saada, and R Sharon (2010). "The Transgenic Overexpression of α-Synuclein and Not Its Related Pathology Associates with Complex I Inhibition". In: *Journal of Biological Chemistry* 285.10, pp. 7334–7343. ISSN: 0021-9258, 1083-351X. DOI: 10.1074/jbc.M109.061051.

Lotharius, J, S Barg, P Wiekop, C Lundberg, HK Raymon, and P Brundin (2002). "Effect of Mutant α-Synuclein on Dopamine Homeostasis in a New Human Mesencephalic Cell Line". In: *Journal of Biological Chemistry* 277.41, pp. 38884–38894. ISSN: 0021-9258, 1083-351X. DOI: 10.1074/jbc.M205518200.

MacAskill, AF and JT Kittler (2010). "Control of mitochondrial transport and localization in neurons". In: *Trends in Cell Biology* 20.2, pp. 102–112. ISSN: 0962-8924. DOI: 10.1016/j.tcb.2009.11.002.

Maddalena, A (2012). "A mifepristone-regulated adeno-associated viral vector system for regulated neurotrophic factor expression in the central nervous system". PhD thesis. Faculty of Biology: Georg August University Göttingen.

Mandemakers, W, A Snellinx, MJ O'Neill, and B de Strooper (2012). "LRRK2 expression is enriched in the striosomal compartment of mouse striatum". In: *Neurobiology of Disease* 48.3, pp. 582–593. ISSN: 0969-9961. DOI: 10.1016/j.nbd.2012.07.017.

Marambaud, P, U Dreses-Werringloer, and V Vingtdeux (2009). "Calcium signaling in neurodegeneration". In: *Molecular Neurodegeneration* 4, p. 20. ISSN: 1750-1326. DOI: 10.1186/1750-1326-4-20.

Maroteaux, L, JT Campanelli, and RH Scheller (1988). "Synuclein: a neuron-specific protein localized to the nucleus and presynaptic nerve terminal". In: *The Journal of Neuroscience* 8.8, pp. 2804–2815. ISSN: 0270-6474, 1529-2401.

Martin, LJ, Y Pan, AC Price, W Sterling, NG Copeland, NA Jenkins, DL Price, and MK Lee (2006). "Parkinson's Disease α-Synuclein Transgenic Mice Develop Neuronal Mitochondrial Degeneration and Cell Death". In: *The Journal of Neuroscience* 26.1, pp. 41–50. ISSN: 0270-6474, 1529-2401. DOI: 10.1523/JNEUROSCI.4308-05.2006.

Matsushita, N, H Okada, Y Yasoshima, K Takahashi, K Kiuchi, and K Kobayashi (2002). "Dynamics of tyrosine hydroxylase promoter activity during midbrain dopaminergic neuron development". In: *Journal of Neurochemistry* 82.2, pp. 295–304. ISSN: 1471-4159. DOI: 10.1046/j.1471-4159.2002.00972.x.

Maurel, A, C Hernandez, O Kunduzova, G Bompart, C Cambon, A Parini, and B Francés (2003). "Age-dependent increase in hydrogen peroxide production by cardiac monoamine oxidase A in rats". In: *American Journal of Physiology - Heart and Circulatory Physiology* 284.4, H1460–H1467. DOI: 10.1152/ajpheart.00700.2002.

Mayer, RA, MV Kindt, and RE Heikkila (1986). "Prevention of the Nigrostriatal Toxicity of 1-Methyl-4-Phenyl-1,2,3,6-Tetrahydropyridine by Inhibitors of 3,4-Dihydroxyphenylethylamine Transport". In: *Journal of Neurochemistry* 47.4, pp. 1073–1079. ISSN: 1471-4159. DOI: 10.1111/j.1471-4159.1986.tb00722.x.

Mbefo, MK, KE Paleologou, A Boucharaba, A Oueslati, H Schell, et al. (2010). "Phosphorylation of Synucleins by Members of the Polo-like Kinase Family". In: *The Journal of Biological Chemistry* 285.4, pp. 2807–2822. ISSN: 0021-9258. DOI: 10.1074/jbc.M109.081950.

Middleton, ER and E Rhoades (2010). "Effects of Curvature and Composition on α-Synuclein Binding to Lipid Vesicles". In: *Biophysical Journal* 99.7, pp. 2279–2288. ISSN: 0006-3495. DOI: 10.1016/j.bpj.2010.07.056.

Miesenböck, G, DA De Angelis, and JE Rothman (1998). "Visualizing secretion and synaptic transmission with pH-sensitive green fluorescent proteins". In: *Nature* 394.6689, pp. 192–195. ISSN: 0028-0836. DOI: 10.1038/28190.

Mironov, SL (2007). "ADP Regulates Movements of Mitochondria in Neurons". In: *Biophysical Journal* 92.8, pp. 2944–2952. ISSN: 0006-3495. DOI: 10.1529/biophysj.106.092981.

Mitsumoto, A and Y Nakagawa (2001). "DJ-1 is an indicator for endogenous reactive oxygen species elicited by endotoxin". In: *Free Radical Research* 35.6, pp. 885–893. ISSN: 1071-5762, 1029-2470. DOI: 10.1080/10715760100301381.

Miyawaki, A, J Llopis, R Heim, JM McCaffery, JA Adams, M Ikura, and RY Tsien (1997). "Fluorescent indicators for Ca2+based on green fluorescent proteins and calmodulin". In: *Nature* 388.6645, pp. 882–887. ISSN: 0028-0836. DOI: 10.1038/42264.

Mizuno, Y, S Ohta, M Tanaka, S Takamiya, K Suzuki, et al. (1989). "Deficiencies in Complex I subunits of the respiratory chain in Parkinson's disease". In: *Biochemical and Biophysical Research Communications* 163.3, pp. 1450–1455. ISSN: 0006-291X. DOI: 10.1016/0006-291X(89)91141-8.

Morell, M, P Czihal, R Hoffmann, L Otvos, FX Avilés, and S Ventura (2008). "Monitoring the interference of protein-protein interactions in vivo by bimolecular fluorescence complementation: the DnaK case". In: *PROTEOMICS* 8.17, pp. 3433–3442. ISSN: 1615-9861. DOI: 10.1002/pmic.200700739.

Mukhopadhyay, A, P Hammen, M Waltner-Law, and H Weiner (2002). "Timing and structural consideration for the processing of mitochondrial matrix space proteins by the mitochondrial processing peptidase (MPP)". In: *Protein Science : A Publication of the Protein Society* 11.5, pp. 1026–1035. ISSN: 0961-8368.

Murphy, DD, SM Rueter, JQ Trojanowski, and VMY Lee (2000). "Synucleins Are Developmentally Expressed, and α-Synuclein Regulates the Size of the Presynaptic Vesicular Pool in Primary Hippocampal Neurons". In: *The Journal of Neuroscience* 20.9, pp. 3214–3220. ISSN: 0270-6474, 1529-2401.

Nagai, T, A Sawano, ES Park, and A Miyawaki (2001). "Circularly permuted green fluorescent proteins engineered to sense Ca2+". In: *Proceedings of the National Academy of Sciences* 98.6, pp. 3197–3202. ISSN: 0027-8424, 1091-6490. DOI: 10.1073/pnas.051636098.

Nakai, J, M Ohkura, and K Imoto (2001). "A high signal-to-noise Ca2+ probe composed of a single green fluorescent protein". In: *Nature Biotechnology* 19.2, pp. 137–141. ISSN: 1087-0156. DOI: 10.1038/84397.

Nakajo, S, K Omata, T Aiuchi, T Shibayama, I Okahashi, et al. (1990). "Purification and Characterization of a Novel Brain-Specific 14-kDa Protein". In: *Journal of Neurochemistry* 55.6, pp. 2031–2038. ISSN: 1471-4159. DOI: 10.1111/j.1471-4159.1990.tb05792.x.

Nakamura, K, VM Nemani, F Azarbal, G Skibinski, JM Levy, et al. (2011). "Direct Membrane Association Drives Mitochondrial Fission by the Parkinson Disease-associated Protein α-Synuclein". In: *Journal of Biological Chemistry* 286.23, pp. 20710–20726. DOI: 10.1074/jbc.M110.213538.

Nakamura, K, VM Nemani, EK Wallender, K Kaehlcke, M Ott, and RH Edwards (2008). "Optical Reporters for the Conformation of α-Synuclein Reveal a Specific Interaction with Mitochondria". In: *The Journal of Neuroscience* 28.47, pp. 12305–12317. ISSN: 0270-6474, 1529-2401. DOI: 10.1523/JNEUROSCI.3088-08.2008.

Nakano, M, H Imamura, T Nagai, and H Noji (2011). "Ca2+ Regulation of Mitochondrial ATP Synthesis Visualized at the Single Cell Level". In: *ACS Chemical Biology* 6.7, pp. 709–715. ISSN: 1554-8929. DOI: 10.1021/cb100313n.

Nalls, MA, V Plagnol, and J Simón-Sánchez (2011). "Imputation of sequence variants for identification of genetic risks for Parkinson's disease: a meta-analysis of genome-wide association studies". In: *Lancet* 377.9766, pp. 641–649. ISSN: 0140-6736. DOI: 10.1016/S0140-6736(10)62345-8.

Narendra, DP, SM Jin, A Tanaka, DF Suen, CA Gautier, J Shen, MR Cookson, and RJ Youle (2010). "PINK1 Is Selectively Stabilized on Impaired Mitochondria to Activate Parkin". In: *PLoS Biology* 8.1. ISSN: 1544-9173. DOI: 10.1371/journal.pbio.1000298.

Negro, A, AM Brunati, A Donella-Deana, ML Massimino, and LA Pinna (2001). "Multiple phosphorylation of a-synuclein by protein tyrosine kinase Syk prevents eosin-induced aggregation". In: *The FASEB Journal.* ISSN: 0892-6638, 1530-6860. DOI: 10.1096/fj.01-0517fje.

Nemani, VM, W Lu, V Berge, K Nakamura, B Onoa, et al. (2010). "Increased Expression of α-Synuclein Reduces Neurotransmitter Release by Inhibiting Synaptic Vesicle Reclustering after Endocytosis". In: *Neuron* 65.1, pp. 66–79. ISSN: 0896-6273. DOI: 10.1016/j.neuron.2009.12.023.

Nicholls, DG (1986). "Intracellular Calcium Homeostasis". In: *British Medical Bulletin* 42.4, pp. 353–358. ISSN: 0007-1420, 1471-8391.

Nieto, M, FJ Gil-Bea, E Dalfó, M Cuadrado, F Cabodevilla, et al. (2006). "Increased sensitivity to MPTP in human α-synuclein A30P transgenic mice". In: *Neurobiology of Aging* 27.6, pp. 848–856. ISSN: 0197-4580. DOI: 10.1016/j.neurobiolaging.2005.04.010.

Ninkina, N, OM Peters, N Connor-Robson, O Lytkina, E Sharfeddin, and VL Buchman (2012). "Contrasting Effects of ?-Synuclein and ?-Synuclein on the Phenotype of Cysteine String Protein ? (CSP?) Null Mutant Mice Suggest Distinct Function of these Proteins in Neuronal Synapses". In: *The Journal of Biological Chemistry* 287.53, pp. 44471–44477. ISSN: 0021-9258. DOI: 10.1074/jbc.M112.422402.

Ninkina, N, O Peters, S Millership, H Salem, H van der Putten, and VL Buchman (2009). "γ-Synucleinopathy: neurodegeneration associated with overexpression of the mouse protein". In: *Human Molecular Genetics* 18.10, pp. 1779–1794. ISSN: 0964-6906. DOI: 10.1093/hmg/ddp090.

Nirenberg, MJ, J Chan, Y Liu, RH Edwards, and VM Pickel (1996). "Ultrastructural Localization of the Vesicular Monoamine Transporter-2 in Midbrain Dopaminergic Neurons: Potential Sites for Somatodendritic Storage and Release of Dopamine". In: *The Journal of Neuroscience* 16.13, pp. 4135–4145. ISSN: 0270-6474, 1529-2401.

Nuytemans, K, J Theuns, M Cruts, and C Van Broeckhoven (2010). "Genetic etiology of Parkinson disease associated with mutations in the SNCA, PARK2, PINK1, PARK7, and LRRK2 genes: a mutation update". In: *Human Mutation* 31.7, pp. 763–780. ISSN: 1098-1004. DOI: 10.1002/humu.21277.

Ogawa, Y and M Tanokura (1984). "Calcium Binding to Calmodulin: Effects of Ionic Strength, $Mg^{2+}$, pH and Temperature". In: *The Journal of Biochemistry* 95.1, pp. 19–28.

Oh, MS, SJ Hong, Y Huh, and KS Kim (2009). "Expression of transgenes in midbrain dopamine neurons using the tyrosine hydroxylase promoter". In: *Gene therapy* 16.3, pp. 437–440. ISSN: 0969-7128. DOI: 10.1038/gt.2008.148.

Okochi, M, J Walter, A Koyama, S Nakajo, M Baba, et al. (2000). "Constitutive Phosphorylation of the Parkinson's Disease Associated α-Synuclein". In: *Journal of Biological Chemistry* 275.1, pp. 390–397. ISSN: 0021-9258, 1083-351X. DOI: 10.1074/jbc.275.1.390.

Orrenius, S, V Gogvadze, and B Zhivotovsky (2007). "Mitochondrial Oxidative Stress: Implications for Cell Death". In: *Annual Review of Pharmacology and Toxicology* 47.1, pp. 143–183. DOI: 10.1146/annurev.pharmtox.47.120505.105122.

Ostrerova, N, L Petrucelli, M Farrer, N Mehta, P Choi, J Hardy, and B Wolozin (1999). "α-Synuclein Shares Physical and Functional Homology with 14-3-3 Proteins". In: *The Journal of Neuroscience* 19.14, pp. 5782–5791. ISSN: 0270-6474, 1529-2401.

O'Sullivan, SS, DR Williams, DA Gallagher, LA Massey, L Silveira-Moriyama, and AJ Lees (2008). "Nonmotor symptoms as presenting complaints in Parkinson's disease: A clinicopathological study". In: *Movement Disorders* 23.1, pp. 101–106. ISSN: 1531-8257. DOI: 10.1002/mds.21813.

Ott, M, B Zhivotovsky, and S Orrenius (2007). "Role of cardiolipin in cytochrome c release from mitochondria". In: *Cell Death & Differentiation* 14.7, pp. 1243–1247. ISSN: 1350-9047. DOI: 10.1038/sj.cdd.4402135.

Outeiro, TF, P Putcha, JE Tetzlaff, R Spoelgen, M Koker, F Carvalho, BT Hyman, and PJ McLean (2008). "Formation of Toxic Oligomeric α-Synuclein Species in Living Cells". In: *PLoS ONE* 3.4, e1867. DOI: 10.1371/journal.pone.0001867.

Paisán-Ruíz, C, S Jain, EW Evans, WP Gilks, J Simón, et al. (2004). "Cloning of the gene containing mutations that cause PARK8-linked Parkinson's disease". In: *Neuron* 44.4, pp. 595–600. ISSN: 0896-6273. DOI: 10.1016/j.neuron.2004.10.023.

Palmer, AE, M Giacomello, T Kortemme, SA Hires, V Lev-Ram, D Baker, and RY Tsien (2006). "Ca2+ Indicators Based on Computationally Redesigned Calmodulin-Peptide Pairs". In: *Chemistry & Biology* 13.5, pp. 521–530. ISSN: 1074-5521. DOI: 10.1016/j.chembiol.2006.03.007.

Palmer, AE, Y Qin, JG Park, and JE McCombs (2011). "Design and application of genetically encoded biosensors". In: *Trends in biotechnology* 29.3, pp. 144–152. ISSN: 0167-7799. DOI: 10.1016/j.tibtech.2010.12.004.

Papapetropoulos, S, J Ellul, C Paschalis, A Athanassiadou, A Papadimitriou, and T Papapetropoulos (2003). "Clinical characteristics of the alpha-synuclein mutation (G209A)-associated Parkinson's disease in comparison with other forms of familial Parkinson's disease in Greece". In: *European Journal of Neurology* 10.3, pp. 281–286. ISSN: 1468-1331. DOI: 10.1046/j.1468-1331.2003.00576.x.

Parihar, MS, A Parihar, M Fujita, M Hashimoto, and P Ghafourifar (2008). "Mitochondrial association of alpha-synuclein causes oxidative stress". In: *Cellular and Molecular Life Sciences* 65.7, pp. 1272–1284. ISSN: 1420-682X, 1420-9071. DOI: 10.1007/s00018-008-7589-1.

Parkinson, J (2002). "An Essay on the Shaking Palsy". In: *The Journal of Neuropsychiatry and Clinical Neurosciences* 14.2, pp. 223–236. ISSN: 0895-0172. DOI: 10.1176/appi.neuropsych.14.2.223.

Perez, RG, JC Waymire, E Lin, JJ Liu, F Guo, and MJ Zigmond (2002). "A Role for α-Synuclein in the Regulation of Dopamine Biosynthesis". In: *The Journal of Neuroscience* 22.8, pp. 3090–3099. ISSN: 0270-6474, 1529-2401.

Pérez-Sánchez, F, M Milán, P Buendía, M Cano-Jaimez, S Ambrosio, A Rosenthal, and I Fariñas (2010). "Prosurvival effect of human wild-type α-synuclein on MPTP-induced toxicity to central but not peripheral catecholaminergic neurons isolated from transgenic mice". In: *Neuroscience* 167.2, pp. 261–276. ISSN: 0306-4522. DOI: 10.1016/j.neuroscience.2010.02.016.

Petit, PX, M Goubern, P Diolez, SA Susin, N Zamzami, and G Kroemer (1998). "Disruption of the outer mitochondrial membrane as a result of large amplitude swelling: the impact of irreversible permeability transition". In: *FEBS Letters* 426.1, pp. 111–116. ISSN: 0014-5793. DOI: 10.1016/S0014-5793(98)00318-4.

Pinheiro, J, D Bates, S DebRoy, D Sarkar, and R Core Team (2013). *nlme: Linear and Nonlinear Mixed Effects Models*.

Pivovarova, NB and SB Andrews (2010). "Calcium-dependent mitochondrial function and dysfunction in neurons". In: *The FEBS journal* 277.18, pp. 3622–3636. ISSN: 1742-464X. DOI: 10.1111/j.1742-4658.2010.07754.x.

Polymeropoulos, MH, C Lavedan, E Leroy, SE Ide, A Dehejia, et al. (1997). "Mutation in the α-Synuclein Gene Identified in Families with Parkinson's Disease". In: *Science* 276.5321, pp. 2045–2047. ISSN: 0036-8075, 1095-9203. DOI: 10.1126/science.276.5321.2045.

Prasher, DC, VK Eckenrode, WW Ward, FG Prendergast, and MJ Cormier (1992). "Primary structure of the Aequorea victoria green-fluorescent protein". In: *Gene* 111.2, pp. 229–233. ISSN: 0378-1119. DOI: 10.1016/0378-1119(92)90691-H.

Pronin, AN, AJ Morris, A Surguchov, and JL Benovic (2000). "Synucleins Are a Novel Class of Substrates for G Protein-coupled Receptor Kinases". In: *Journal of Biological Chemistry* 275.34, pp. 26515–26522. ISSN: 0021-9258, 1083-351X. DOI: 10.1074/jbc.M003542200.

Przedborski, S and M Vila (2001). "MPTP: a review of its mechanisms of neurotoxicity". In: *Clinical Neuroscience Research* 1.6, pp. 407–418. ISSN: 1566-2772. DOI: 10.1016/S1566-2772(01)00019-6.

Puschmann, A (2013). "Monogenic Parkinson's disease and parkinsonism: Clinical phenotypes and frequencies of known mutations". In: *Parkinsonism & Related Disorders* 19.4, pp. 407–415. ISSN: 1353-8020. DOI: 10.1016/j.parkreldis.2013.01.020.

Qian, JJ, YB Cheng, YP Yang, CJ Mao, ZH Qin, K Li, and CF Liu (2008). "Differential effects of overexpression of wild-type and mutant human α-synuclein on MPP+-induced neurotoxicity in PC12 cells". In: *Neuroscience Letters* 435.2, pp. 142–146. ISSN: 0304-3940. DOI: 10.1016/j.neulet.2008.02.021.

R Development Core Team (2011). *R: A Language and Environment for Statistical Computing*. R Foundation for Statistical Computing. Vienna, Austria.

Rabl, R, V Soubannier, R Scholz, F Vogel, N Mendl, et al. (2009). "Formation of cristae and crista junctions in mitochondria depends on antagonism between Fcj1 and Su e/g". In: *The Journal of Cell Biology* 185.6, pp. 1047–1063. ISSN: 0021-9525, 1540-8140. DOI: 10.1083/jcb.200811099.

Ramsay, RR and TP Singer (1986). "Energy-dependent uptake of N-methyl-4-phenylpyridinium, the neurotoxic metabolite of 1-methyl-4-phenyl-1,2,3,6-tetrahydropyridine, by mitochondria." In: *Journal of Biological Chemistry* 261.17, pp. 7585–7587. ISSN: 0021-9258, 1083-351X.

Rappley, I, AD Gitler, PE Selvy, MJ LaVoie, BD Levy, HA Brown, S Lindquist, and DJ Selkoe (2009). "Evidence that α-Synuclein Does Not Inhibit Phospholipase D". In: *Biochemistry* 48.5, pp. 1077–1083. ISSN: 0006-2960. DOI: 10.1021/bi801871h.

Rathke-Hartlieb, S, PJ Kahle, M Neumann, L Ozmen, S Haid, M Okochi, C Haass, and JB Schulz (2001). "Sensitivity to MPTP is not increased in Parkinson's disease-associated mutant α-synuclein transgenic mice". In: *Journal of Neurochemistry* 77.4, pp. 1181–1184. ISSN: 1471-4159. DOI: 10.1046/j.1471-4159.2001.00366.x.

Rayport, S, D Sulzer, WX Shi, S Sawasdikosol, J Monaco, D Batson, and G Rajendran (1992). "Identified postnatal mesolimbic dopamine neurons in culture: morphology and electrophysiology". In: *The Journal of Neuroscience* 12.11, pp. 4264–4280. ISSN: 0270-6474, 1529-2401.

Reis, K, Å Fransson, and P Aspenström (2009). "The Miro GTPases: At the heart of the mitochondrial transport machinery". In: *FEBS Letters* 583.9, pp. 1391–1398. ISSN: 0014-5793. DOI: 10.1016/j.febslet.2009.04.015.

Ricci, C, V Pastukh, J Leonard, J Turrens, G Wilson, D Schaffer, and SW Schaffer (2008). "Mitochondrial DNA damage triggers mitochondrial-superoxide generation and apoptosis".

In: *American journal of physiology. Cell physiology* 294.2, pp. C413–422. ISSN: 0363-6143. DOI: 10.1152/ajpcell.00362.2007.

Rintoul, GL, AJ Filiano, JB Brocard, GJ Kress, and IJ Reynolds (2003). "Glutamate Decreases Mitochondrial Size and Movement in Primary Forebrain Neurons". In: *The Journal of Neuroscience* 23.21, pp. 7881–7888. ISSN: 0270-6474, 1529-2401.

Rizzuto, R, M Brini, P Pizzo, M Murgia, and T Pozzan (1995). "Chimeric green fluorescent protein as a tool for visualizing subcellular organelles in living cells". In: *Current Biology* 5.6, pp. 635–642. ISSN: 0960-9822. DOI: 10.1016/S0960-9822(95)00128-X.

Robertson, DC, O Schmidt, N Ninkina, PA Jones, J Sharkey, and VL Buchman (2004). "Developmental loss and resistance to MPTP toxicity of dopaminergic neurones in substantia nigra pars compacta of γ-synuclein, α-synuclein and double α/γ-synuclein null mutant mice". In: *Journal of Neurochemistry* 89.5, pp. 1126–1136. ISSN: 1471-4159. DOI: 10.1111/j.1471-4159.2004.02378.x.

Ross, WN (1989). "Changes in Intracellular Calcium During Neuron Activity". In: *Annual Review of Physiology* 51.1, pp. 491–506. DOI: 10.1146/annurev.ph.51.030189.002423.

Rubinsztein, DC (2006). "The roles of intracellular protein-degradation pathways in neurodegeneration". In: *Nature* 443.7113, pp. 780–786. ISSN: 0028-0836. DOI: 10.1038/nature05291.

Sambrook, J and DW Russell (2001). *Molecular Cloning: A Laboratory Manual*. Third. Cold Spring Harbor Laboratory Press. ISBN: 0879695773.

Sawamoto, K, N Nakao, K Kobayashi, N Matsushita, H Takahashi, et al. (2001). "Visualization, direct isolation, and transplantation of midbrain dopaminergic neurons". In: *Proceedings of the National Academy of Sciences of the United States of America* 98.11, pp. 6423–6428. ISSN: 0027-8424. DOI: 10.1073/pnas.111152398.

Scaduto, RC and LW Grotyohann (1999). "Measurement of mitochondrial membrane potential using fluorescent rhodamine derivatives." In: *Biophysical Journal* 76.1, pp. 469–477. ISSN: 0006-3495.

Schapira, A, J Cooper, D Dexter, P Jenner, J Clark, and C Marsden (1989). "Mitochondrial complex I deficiency in Parkinson's disease". In: *The Lancet* 333.8649, p. 1269. ISSN: 0140-6736. DOI: 10.1016/S0140-6736(89)92366-0.

Schapira, AHV and M Gegg (2011). "Mitochondrial Contribution to Parkinson's Disease Pathogenesis". In: *Parkinson's Disease* 2011. ISSN: 2042-0080. DOI: 10.4061/2011/159160.

Seidel, K, L Schöls, S Nuber, E Petrasch-Parwez, K Gierga, et al. (2010). "First appraisal of brain pathology owing to A30P mutant alpha-synuclein". In: *Annals of Neurology* 67.5, pp. 684–689. ISSN: 1531-8249. DOI: 10.1002/ana.21966.

Selvin, PR (2000). "The renaissance of fluorescence resonance energy transfer". In: *Nature Structural & Molecular Biology* 7.9, pp. 730–734. ISSN: 1072-8368. DOI: 10.1038/78948.

Shagin, DA, EV Barsova, YG Yanushevich, AF Fradkov, KA Lukyanov, et al. (2004). "GFP-like Proteins as Ubiquitous Metazoan Superfamily: Evolution of Functional Features and Structural Complexity". In: *Molecular Biology and Evolution* 21.5, pp. 841–850. ISSN: 0737-4038, 1537-1719. DOI: 10.1093/molbev/msh079.

Sherer, TB, JH Kim, R Betarbet, and J Greenamyre (2003). "Subcutaneous Rotenone Exposure Causes Highly Selective Dopaminergic Degeneration and α-Synuclein Aggregation". In:

*Experimental Neurology* 179.1, pp. 9–16. ISSN: 0014-4886. DOI: 10.1006/exnr.2002.8072.

Shimomura, O, FH Johnson, and Y Saiga (1962). "Extraction, Purification and Properties of Aequorin, a Bioluminescent Protein from the Luminous Hydromedusan, Aequorea". In: *Journal of Cellular and Comparative Physiology* 59.3, pp. 223–239. ISSN: 1553-0809. DOI: 10.1002/jcp.1030590302.

Shimura, H, N Hattori, Si Kubo, Y Mizuno, S Asakawa, et al. (2000). "Familial Parkinson disease gene product, parkin, is a ubiquitin-protein ligase". In: *Nature Genetics* 25.3, pp. 302–305. ISSN: 1061-4036. DOI: 10.1038/77060.

Shoffner, JM, RL Watts, JL Juncos, A Torroni, and DC Wallace (1991). "Mitochondrial oxidative phosphorylation defects in Parkinson's disease". In: *Annals of neurology* 30.3, pp. 332–339. ISSN: 0364-5134. DOI: 10.1002/ana.410300304.

Singleton, AB, M Farrer, J Johnson, A Singleton, S Hague, et al. (2003). "α-Synuclein Locus Triplication Causes Parkinson's Disease". In: *Science* 302.5646, pp. 841–841. ISSN: 0036-8075, 1095-9203. DOI: 10.1126/science.1090278.

Singleton, AB, MJ Farrer, and V Bonifati (2013). "The genetics of Parkinson's disease: Progress and therapeutic implications". In: *Movement Disorders* 28.1, pp. 14–23. ISSN: 1531-8257. DOI: 10.1002/mds.25249.

Sinha, K, J Das, PB Pal, and PC Sil (2013). "Oxidative stress: the mitochondria-dependent and mitochondria-independent pathways of apoptosis". In: *Archives of Toxicology* 87.7, pp. 1157–1180. ISSN: 0340-5761, 1432-0738. DOI: 10.1007/s00204-013-1034-4.

Skulachev, VP (2001). "Mitochondrial filaments and clusters as intracellular power-transmitting cables". In: *Trends in Biochemical Sciences* 26.1, pp. 23–29. ISSN: 0968-0004. DOI: 10.1016/S0968-0004(00)01735-7.

Smith, WW, Z Pei, H Jiang, DJ Moore, Y Liang, et al. (2005). "Leucine-rich repeat kinase 2 (LRRK2) interacts with parkin, and mutant LRRK2 induces neuronal degeneration". In: *Proceedings of the National Academy of Sciences of the United States of America* 102.51, pp. 18676–18681. ISSN: 0027-8424, 1091-6490. DOI: 10.1073/pnas.0508052102.

Somme, JH, JC Gomez-Esteban, A Molano, B Tijero, E Lezcano, and JJ Zarranz (2011). "Initial neuropsychological impairments in patients with the E46K mutation of the α-synuclein gene (PARK 1)". In: *Journal of the Neurological Sciences* 310.1, pp. 86–89. ISSN: 0022-510X. DOI: 10.1016/j.jns.2011.07.047.

Song, DD, CW Shults, A Sisk, E Rockenstein, and E Masliah (2004). "Enhanced substantia nigra mitochondrial pathology in human α-synuclein transgenic mice after treatment with MPTP". In: *Experimental Neurology* 186.2, pp. 158–172. ISSN: 0014-4886. DOI: 10.1016/S0014-4886(03)00342-X.

Spillantini, MG, ML Schmidt, VMY Lee, JQ Trojanowski, R Jakes, and M Goedert (1997). "α-Synuclein in Lewy bodies". In: *Nature* 388.6645, pp. 839–840. ISSN: 0028-0836. DOI: 10.1038/42166.

Stefanis, L (2012). "α-Synuclein in Parkinson's Disease". In: *Cold Spring Harbor Perspectives in Medicine* 2.2. ISSN: 2157-1422. DOI: 10.1101/cshperspect.a009399.

Stöckl, MT, N Zijlstra, and V Subramaniam (2013). "α-Synuclein Oligomers: an Amyloid Pore?" In: *Molecular Neurobiology* 47.2, pp. 613–621. ISSN: 0893-7648, 1559-1182. DOI: 10.1007/s12035-012-8331-4.

Strack, RL, DE Strongin, D Bhattacharyya, W Tao, A Berman, HE Broxmeyer, RJ Keenan, and BS Glick (2008). "A noncytotoxic DsRed variant for whole-cell labeling". In: *Nature Methods* 5.11, pp. 955–957. ISSN: 1548-7091. DOI: 10.1038/nmeth.1264.

Surguchov, A (2013). "Synucleins: Are they two-edged swords?" In: *Journal of Neuroscience Research* 91.2, pp. 161–166. ISSN: 1097-4547. DOI: 10.1002/jnr.23149.

Szabadkai, G and MR Duchen (2008). "Mitochondria: The Hub of Cellular Ca2+ Signaling". In: *Physiology* 23.2, pp. 84–94. ISSN: 1548-9213, 1548-9221. DOI: 10.1152/physiol.00046.2007.

Takahashi, A, P Camacho, JD Lechleiter, and B Herman (1999). "Measurement of Intracellular Calcium". In: *Physiological Reviews* 79.4, pp. 1089–1125. ISSN: 0031-9333, 1522-1210.

Takahashi, N, LL Miner, I Sora, H Ujike, RS Revay, et al. (1997). "VMAT2 knockout mice: Heterozygotes display reduced amphetamine-conditioned reward, enhanced amphetamine locomotion, and enhanced MPTP toxicity". In: *Proceedings of the National Academy of Sciences of the United States of America* 94.18, pp. 9938–9943. ISSN: 0027-8424.

Takao, K, KI Okamoto, T Nakagawa, RL Neve, T Nagai, et al. (2005). "Visualization of Synaptic Ca2+ /Calmodulin-Dependent Protein Kinase II Activity in Living Neurons". In: *The Journal of Neuroscience* 25.12, pp. 3107–3112. ISSN: 0270-6474, 1529-2401. DOI: 10.1523/JNEUROSCI.0085-05.2005.

Taschenberger, G, J Toloe, J Tereshchenko, J Akerboom, P Wales, et al. (2013). "β-synuclein aggregates and induces neurodegeneration in dopaminergic neurons". In: *Annals of Neurology*, n/a–n/a. ISSN: 1531-8249. DOI: 10.1002/ana.23905.

Towbin, H, T Staehelin, and J Gordon (1979). "Electrophoretic transfer of proteins from polyacrylamide gels to nitrocellulose sheets: procedure and some applications." In: *Proceedings of the National Academy of Sciences of the United States of America* 76.9, pp. 4350–4354. ISSN: 0027-8424.

Tsien, RY (1998). "The Green Fluorescent Protein". In: *Annual Review of Biochemistry* 67.1, pp. 509–544. DOI: 10.1146/annurev.biochem.67.1.509.

Tsigelny, IF, Y Sharikov, W Wrasidlo, T Gonzalez, PA Desplats, L Crews, B Spencer, and E Masliah (2012). "Role of α-synuclein penetration into the membrane in the mechanisms of oligomer pore formation". In: *FEBS Journal* 279.6, pp. 1000–1013. ISSN: 1742-4658. DOI: 10.1111/j.1742-4658.2012.08489.x.

Tyas, L, VA Brophy, A Pope, AJ Rivett, and JM Tavaré (2000). "Rapid caspase-3 activation during apoptosis revealed using fluorescence-resonance energy transfer". In: *EMBO reports* 1.3, pp. 266–270. ISSN: 1469-221X. DOI: 10.1093/embo-reports/kvd050.

Uéda, K, H Fukushima, E Masliah, Y Xia, A Iwai, et al. (1993). "Molecular cloning of cDNA encoding an unrecognized component of amyloid in Alzheimer disease". In: *Proceedings of the National Academy of Sciences* 90.23, pp. 11282–11286. ISSN: 0027-8424, 1091-6490.

Unoki, M and Y Nakamura (2001). "Growth-suppressive effects of BPOZ and EGR2, two genes involved in the PTEN signaling pathway". In: *, Published online: 25 July 2001; | doi:10.1038/sj.onc.1204608* 20.33. DOI: 10.1038/sj.onc.1204608.

Uversky, VN and D Eliezer (2009). "Biophysics of Parkinson's Disease: Structure and Aggregation of α-Synuclein". In: *Current protein & peptide science* 10.5, pp. 483–499. ISSN: 1389-2037.

Uversky, VN, J Li, and AL Fink (2001). "Evidence for a Partially Folded Intermediate in α-Synuclein Fibril Formation". In: *Journal of Biological Chemistry* 276.14, pp. 10737–10744. ISSN: 0021-9258, 1083-351X. DOI: 10.1074/jbc.M010907200.

Uversky, VN, J Li, P Souillac, IS Millett, S Doniach, R Jakes, M Goedert, and AL Fink (2002). "Biophysical Properties of the Synucleins and Their Propensities to Fibrillate INHIBITION OF α-SYNUCLEIN ASSEMBLY BY β- AND γ-SYNUCLEINS". In: *Journal of Biological Chemistry* 277.14, pp. 11970–11978. ISSN: 0021-9258, 1083-351X. DOI: 10.1074/jbc.M109541200.

Valente, EM, PM Abou-Sleiman, V Caputo, MMK Muqit, K Harvey, et al. (2004). "Hereditary Early-Onset Parkinson's Disease Caused by Mutations in PINK1". In: *Science* 304.5674, pp. 1158–1160. ISSN: 0036-8075, 1095-9203. DOI: 10.1126/science.1096284.

Van Kuilenburg, AB, AO Muijsers, H Demol, HL Dekker, and JJ Van Beeumen (1988). "Human heart cytochrome c oxidase subunit VIII Purification and determination of the complete amino acid sequence". In: *FEBS Letters* 240.1, pp. 127–132. ISSN: 0014-5793. DOI: 10.1016/0014-5793(88)80353-3.

Varon, S and C Raiborn Jr. (1969). "Dissociation, fractionation, and culture of embryonic brain cells". In: *Brain Research* 12.1, pp. 180–199. ISSN: 0006-8993. DOI: 10.1016/0006-8993(69)90065-1.

Veech, RL, JW Lawson, NW Cornell, and HA Krebs (1979). "Cytosolic phosphorylation potential." In: *Journal of Biological Chemistry* 254.14, pp. 6538–6547. ISSN: 0021-9258, 1083-351X.

Venderova, K and DS Park (2012). "Programmed Cell Death in Parkinson's Disease". In: *Cold Spring Harbor Perspectives in Medicine* 2.8, a009365. ISSN: , 2157-1422. DOI: 10.1101/cshperspect.a009365.

Visanji, NP, S Wislet-Gendebien, LW Oschipok, G Zhang, I Aubert, PE Fraser, and A Tandon (2011). "The effect of S129 phosphorylation on the interaction of α-synuclein with synaptic and cellular membranes". In: *Journal of Biological Chemistry*, jbc.M111.253450. ISSN: 0021-9258, 1083-351X. DOI: 10.1074/jbc.M111.253450.

Volles, MJ and PT Lansbury (2002). "Vesicle Permeabilization by Protofibrillar α-Synuclein Is Sensitive to Parkinson's Disease-Linked Mutations and Occurs by a Pore-like Mechanism†". In: *Biochemistry* 41.14, pp. 4595–4602. ISSN: 0006-2960. DOI: 10.1021/bi0121353.

Volles, MJ, SJ Lee, JC Rochet, MD Shtilerman, TT Ding, JC Kessler, and PT Lansbury (2001). "Vesicle Permeabilization by Protofibrillar α-Synuclein: Implications for the Pathogenesis and Treatment of Parkinson's Disease". In: *Biochemistry* 40.26, pp. 7812–7819. ISSN: 0006-2960. DOI: 10.1021/bi0102398.

Wallace, AJ, TJ Stillman, A Atkins, SJ Jamieson, PA Bullough, J Green, and PJ Artymiuk (2000). "E. coli Hemolysin E (HlyE, ClyA, SheA): X-Ray Crystal Structure of the Toxin and Observation of Membrane Pores by Electron Microscopy". In: *Cell* 100.2, pp. 265–276. ISSN: 0092-8674. DOI: 10.1016/S0092-8674(00)81564-0.

Wang, W, I Perovic, J Chittuluru, A Kaganovich, LTT Nguyen, et al. (2011). "A soluble α-synuclein construct forms a dynamic tetramer". In: *Proceedings of the National Academy of Sciences* 108.43, pp. 17797–17802. DOI: 10.1073/pnas.1113260108.

Wang, X and TL Schwarz (2009). "The Mechanism of Kinesin Regulation by Ca++ for Control of Mitochondrial Motility". In: *Cell* 136.1, pp. 163–174. ISSN: 0092-8674. DOI: 10.1016/j.cell.2008.11.046.

Weinberg, MS, RJ Samulski, and TJ McCown (2013). "Adeno-associated virus (AAV) gene therapy for neurological disease". In: *Neuropharmacology* 69, pp. 82–88. ISSN: 0028-3908. DOI: 10.1016/j.neuropharm.2012.03.004.

Weinreb, PH, W Zhen, AW Poon, KA Conway, and PT Lansbury (1996). "NACP, A Protein Implicated in Alzheimer's Disease and Learning, Is Natively Unfolded†". In: *Biochemistry* 35.43, pp. 13709–13715. ISSN: 0006-2960. DOI: 10.1021/bi961799n.

Weiss, JH (2011). "Ca2+ permeable AMPA channels in diseases of the nervous system". In: *Frontiers in Molecular Neuroscience* 4, p. 42. DOI: 10.3389/fnmol.2011.00042.

West, AB, DJ Moore, S Biskup, A Bugayenko, WW Smith, CA Ross, VL Dawson, and TM Dawson (2005). "Parkinson's disease-associated mutations in leucine-rich repeat kinase 2 augment kinase activity". In: *Proceedings of the National Academy of Sciences of the United States of America* 102.46, pp. 16842–16847. ISSN: 0027-8424, 1091-6490. DOI: 10.1073/pnas.0507360102.

Westermann, B (2010). "Mitochondrial fusion and fission in cell life and death". In: *Nature Reviews Molecular Cell Biology* 11.12, pp. 872–884. ISSN: 1471-0072. DOI: 10.1038/nrm3013.

Willemse, M, E Janssen, Fd Lange, B Wieringa, and J Fransen (2007). "ATP and FRET—a cautionary note". In: *Nature Biotechnology* 25.2, pp. 170–172. ISSN: 1087-0156. DOI: 10.1038/nbt0207-170.

Winner, B, R Jappelli, SK Maji, PA Desplats, L Boyer, et al. (2011). "In vivo demonstration that α-synuclein oligomers are toxic". In: *Proceedings of the National Academy of Sciences of the United States of America* 108.10, pp. 4194–4199. ISSN: 0027-8424. DOI: 10.1073/pnas.1100976108.

Wislet-Gendebien, S, NP Visanji, SN Whitehead, D Marsilio, W Hou, et al. (2008). "Differential regulation of wild-type and mutant alpha-synuclein binding to synaptic membranes by cytosolic factors". In: *BMC Neuroscience* 9, p. 92. ISSN: 1471-2202. DOI: 10.1186/1471-2202-9-92.

Xiong, H, D Wang, L Chen, YS Choo, H Ma, et al. (2009). "Parkin, PINK1, and DJ-1 form a ubiquitin E3 ligase complex promoting unfolded protein degradation". In: *The Journal of Clinical Investigation* 119.3, pp. 650–660. ISSN: 0021-9738. DOI: 10.1172/JCI37617.

Yavin, E and JH Menkes (1973). "The Culture of Dissociated Cells from Rat Cerebral Cortex". In: *The Journal of Cell Biology* 57.1, pp. 232–237. ISSN: 0021-9525, 1540-8140. DOI: 10.1083/jcb.57.1.232.

Yoshino, H, Y Nakagawa-Hattori, T Kondo, and PY Mizuno (1992). "Mitochondrial complex I and II activities of lymphocytes and platelets in Parkinson's disease". In: *Journal of Neural Transmission - Parkinson's Disease and Dementia Section* 4.1, pp. 27–34. ISSN: 0936-3076, 1435-1463. DOI: 10.1007/BF02257619.

Youle, RJ and DP Narendra (2011). "Mechanisms of mitophagy". In: *Nature Reviews Molecular Cell Biology* 12.1, pp. 9–14. ISSN: 1471-0072. DOI: 10.1038/nrm3028.

Yu, WH, Y Matsuoka, I Sziráki, A Hashim, J LaFrancois, H Sershen, and KE Duff (2008). "Increased Dopaminergic Neuron Sensitivity to 1-Methyl-4-Phenyl-1,2,3,6-Tetrahydropyridine (MPTP) in Transgenic Mice Expressing Mutant A53T α-Synuclein". In: *Neurochemical Research* 33.5, pp. 902–911. ISSN: 0364-3190, 1573-6903. DOI: 10.1007/s11064-007-9533-4.

Zakharov, SD, JD Hulleman, EA Dutseva, YN Antonenko, JC Rochet, and WA Cramer (2007). "Helical α-Synuclein Forms Highly Conductive Ion Channels". In: *Biochemistry* 46.50, pp. 14369–14379. ISSN: 0006-2960. DOI: 10.1021/bi701275p.

Zarranz, JJ, J Alegre, JC Gómez-Esteban, E Lezcano, R Ros, et al. (2004). "The new mutation, E46K, of α-synuclein causes parkinson and Lewy body dementia". In: *Annals of Neurology* 55.2, pp. 164–173. ISSN: 1531-8249. DOI: 10.1002/ana.10795.

Zhao, Y, S Araki, J Wu, T Teramoto, YF Chang, et al. (2011). "An Expanded Palette of Genetically Encoded Ca2+ Indicators". In: *Science* 333.6051, pp. 1888–1891. DOI: 10.1126/science.1208592.

Zhou, RM, YX Huang, XL Li, C Chen, Q Shi, et al. (2010). "Molecular interaction of α-synuclein with tubulin influences on the polymerization of microtubule in vitro and structure of microtubule in cells". In: *Molecular Biology Reports* 37.7, pp. 3183–3192. ISSN: 0301-4851, 1573-4978. DOI: 10.1007/s11033-009-9899-2.

Zimmermann, T, J Rietdorf, and R Pepperkok (2003). "Spectral imaging and its applications in live cell microscopy". In: *FEBS Letters* 546.1, pp. 87–92. ISSN: 0014-5793. DOI: 10.1016/S0014-5793(03)00521-0.

# Acknowledgments

I would like to take this opportunity to thank all of the people who have been with me for the last four years in one way or another.

I am especially grateful to:

My supervisor Dr. Sebastian Kügler for his great support, interesting discussions (also beyond science) and last but not least, patience.
My second supervisor PD. Dr. Sergej L. Mironov for many very interesting discussions that always motivated me to continue and to try new approaches.

Andrea Maddalena, with whom I shared lots of fun moments and who was always ready for a coffee (as long as its Italian) or lunch at the mensa.
Another thank you to Rustam Mollajew for all the interesting moments in and out of the lab.
All the rest of my coworkers, especially Ulrike Schöll, Monika Zebski, Lisa Barski, Nicole Hartelt, Dr. Grit Taschenberger and Dr. Julia Tereshchenko.

My parents, my sister and my brother whom I all miss very much, living abroad.

The Kaufmanns, for helping out whenever necessary.

My parents-in-law for taking such great care of our children when we needed it.

Last but not least, my wife Esther Tolö, thank you for all of your patience, love and for being a truly awesome mother to our two children! I might as well thank them too, Iris and Frieda, for making life so beautiful!

# *Curriculum vitae*

Contents removed from published electronic version.

Contents removed from published electronic version.

# 2 Publications

Akerboom, J, NC Calderón, L Tian, M Prigge, J Tolö, et al. (2013). "Genetically encoded calcium indicators for multi-color neural activity imaging and combination with optogenetics". In: *Frontiers in Molecular Neuroscience* 6, p. 2. DOI: 10.3389/fnmol.2013.00002.

Mollajew, R, J Toloe, and SL Mironov (2013). "Single KATP channel opening in response to stimulation of AMPA/kainate receptors is mediated by Na+ accumulation and submembrane ATP and ADP changes". In: *The Journal of Physiology*. ISSN: 00223751. DOI: 10.1113/jphysiol.2012.248369.

Taschenberger*, G, J Toloe*, J Tereshchenko*, J Akerboom, P Wales, et al. (2013). "β-synuclein aggregates and induces neurodegeneration in dopaminergic neurons". In: *Annals of Neurology*. ISSN: 1531-8249. DOI: 10.1002/ana.23905.

Toloe, J, R Mollajew, S Kügler, and SL Mironov (2014). "Metabolic differences in hippocampal 'Rett' neurons revealed by ATP imaging". In: *Molecular and Cellular Neuroscience*. ISSN: 1044-7431. DOI: 10.1016/j.mcn.2013.12.008.

* equal contribution